1125

UNIVERSITÉ DE NEUCHÂTEL
INSTITUT DE MICROTECHNIQUE
Switzerland

MICROCRYSTALLINE SILICON (μc-Si:H) PREPARED WITH VERY HIGH FREQUENCY GLOW DISCHARGE (VHF-GD) PROCESS

KSHEM PRASAD

UNIVERSITÉ DE NEUCHATEL
INSTITUT DE MICROTECHNIQUE
Switzerland

MICROCRYSTALLINE SILICON (μc-Si:H) PREPARED WITH VERY HIGH FREQUENCY GLOW DISCHARGE (VHF-GD) PROCESS

KSHEM PRASAD

A THESIS
SUBMITTED TO THE FACULTY OF SCIENCE
FOR THE DEGREE OF DOCTOR OF PHILOSOPHY

Discoveries of Science III

Our science is an abstract cold and brief
That cuts in formulas the living whole.
It has a brain and head but not a soul:
It sees all things in outward carved relief.

But how without its depths can the world be known?
The visible has its roots in the unseen
And each invisible hides what it can mean
In a yet deeper invisible, unshown.

The objects that you probe are not their form.
Each is a mass of forces thrown in shape.
The forces caught, their inner lines escape
In a fathomless consciousness beyond mind's norm.

Probe it and you shall meet a ***BEING*** *still*
Infinite, nameless, mute, unknowable.

Sri Aurobindo

offered to The ***BEING***

IMPRIMATUR POUR LA THÈSE

Microcrystalline silicon (μc-Si:H) prepared with very high frequency glow discharge (VHF-GD) process

de Monsieur Kshem Prasad

UNIVERSITÉ DE NEUCHÂTEL

FACULTÉ DES SCIENCES

La Faculté des sciences de l'Université de Neuchâtel sur le rapport des membres du jury,

Messieurs A. Shah, N. de Rooij, F. Finger (Jülich) et G. Willeke (Constance)

autorise l'impression de la présente thèse.

Neuchâtel, le 18 décembre 1991

Le doyen :

A. Robert

MICROCRYSTALLINE SILICON (μc-Si:H) PREPARED WITH VERY HIGH FREQUENCY GLOW DISCHARGE (VHF-GD) PROCESS

SUMMARY

The very high frequency glow discharge (VHF-GD) technique using a discharge frequency of 70 MHz has been explored for the preparation of microcrystalline silicon (μc-Si:H). Investigation of the influence of silane concentration in hydrogen and the discharge power level have been extensively carried out for the formation of undoped and doped μc-Si:H films. Detailed study of the influence of phosphorus and boron doping is also performed. The electrical, optical and structural properties of these specimens are correlated with the deposition parameters in order to identify the optimal preparation conditions.

As compared to other preparation techniques, using VHF-GD good quality μc-Si:H is obtained at very low power levels (23 mW/cm^2 for the undoped and n-type material and 75 mW/cm^2 for the p-type material) at substrate temperatures well below 200 °C. Conductivities of 130 S/cm and 30 S/cm have been achieved in n- and p-type μc-Si:H, respectively. High resolution TEM micrographs and Raman scattering results indicate that structurally these specimen resemble closely poly-silicon (poly-Si). The latter are usually prepared by low pressure chemical vapour deposition (LPCVD) technique at temperatures above 550 °C and contain negligible amount of amorphous tissue. Conductivities of ultra thin films having thicknesses ranging between 100 and 500 Å are also high as compared to those reported earlier. With these promising results μc-Si:H could become an interesting candidate for device applications.

TABLE OF CONTENTS

1. INTRODUCTION

The past decade has seen a rapid development of hydrogenated amorphous and microcrystalline silicon (a-Si:H and μc-Si:H) as new thin film semiconductors. Since the discovery of successful doping of a-Si:H [Spear, 1975] at low temperatures (200-350 °C) using the plasma enhanced chemical vapour deposition (PE-CVD) this material has attracted attention as candidate for low cost solar cell fabrication [Carlson, 1977]. For the growing interest in μc-Si:H two main factors can be mentioned: 1) the possibility to produce μc-Si:H simply by modifying some of the deposition parameters used for the preparation of a-Si:H is attractive from the application point of view , and 2) as its structure lies between purely amorphous and polycrystalline phases, the material is interesting from the physicist's point of view. Hand in hand, a-Si:H and μc-Si:H are fast growing as potential new materials for opto-electronic devices such as solar cells, flat panel displays and large area microelectronics (macroelectronics) [Kanicki, 1991]. The high conductivities reached in μc-Si:H material have motivated many research groups to substitute it for the doped amorphous layers, in p-i-n solar cells, which has conductivities lower by 3 to 4 orders of magnitude [Willeke, 1991]. Some improvements in solar cell efficiency has been reported as early as 1981 [Uchida, 1981].

μc-Si:H was first prepared by chemical vapour transport in 1968 (Veprek, 1968) at substrate temperatures of 600°C. In 1979 Usui and Kikuchi reported on μc-Si:H prepared by inductive glow-discharge (PE-CVD) of silane using high input power levels of 100 W [Usui, 1979]. Since then, many research groups have carried out extensive investigation on the preparation and characterization of this material [Matsuda, 1987 and references therein]. Three important conditions are said to be necessary for the formation of microcrystalline silicon (μc-Si:H) using the glow discharge process. These are (1) high dilution of silane in hydrogen, (2) high discharge power and (3) a high substrate temperature. The first two enrich the plasma with atomic hydrogen and the interface between the plasma and the film growth surface approaches partial chemical equilibrium (PCE) [Veprek, 1988]. Under these conditions a balance is reached between the deposition of silicon atoms and radicals and erosion of weak and disordered bonds, promoting microcrystalline growth. The atomic hydrogen is understood to play a predominant role in the preferential elimination of the weak and disordered bonds by a chemical etching mechanism [Tsai, 1988] opening the way for tetrahedral configuration. Along with the first two, the high substrate temperature provides the necessary energy, to enhance surface mobility of the oncoming reactive species and for the desorption of surplus hydrogen [Matsuda, 1989]. Atomic hydrogen is also claimed to perform 'chemical annealing' i.e. interact with the weak silicon bonds and dangling bonds under the growth zone to induce energetic relaxation and restructure the silicon network [Shimizu, 1989; Street, 1991].

The structure of μc-Si:H is understood to be composed of small crystallites embedded in an amorphous matrix. It is characterised by the average crystallite size ∂ and the relative amount of crystalline phase X_c contained in the volume of the film. These are a function of various parameters such as the deposition parameters mentioned earlier, the substrate bias, etc [Veprek, 1981; Matsuda, 1983; Nakatani, 1983]. The average crystallite size ∂ is determined from X-ray or electron diffraction measurements and lies between 30 and 350 Å. X_c is evaluated from Raman scattering studies, and has values between a few percent to almost 100 % in the volume. The remaining fraction of the volume is occupied by amorphous tissues or grain boundaries depending on whether X_c is low or high, respectively. These amorphous zones or grain boundaries are defect rich regions which introduce high density of states which trap charge carriers; although the hydrogen contained within the μc-Si:H (5 to 15 atomic%) passivates some of these defects. The high conductivity reached in this material is attributed to the four fold doping within the crystallites as found in c-Si and the high free carrier concentration in the conduction or valence bands, as compared to in a-Si:H [Le Comber, 1983; Willeke, 1991]. Besides, the long range order (100 to 250 Å) in the crystallites also improves the mobility of these carriers as compared to in a-Si:H. In poor μc-Si:H, i.e. having a crystallite volume fraction X_c below the percolation threshold value of about 20 %, the transport is dominated by the amorphous phase [Komuro, 1984].

The techniques used for the preparation of both a-Si:H and μc-Si:H are based on technologies using the standard industrial frequencies - namely DC, 13.56 MHz [Matsuda, 1987] and 2.54 GHz (microwave) [Hattori, 1987], except for limited number of laboratories which are working at other frequencies like 27.12 MHz [Kausche, 1989], 40.68 MHz [Spear, 1981], 110 MHz [Chatham, 1989], and 140 MHz [Oda, 1988].

In our laboratory the very high frequency (VHF) of 70 MHz has been established as the standard frequency for our work. This frequency was found to be the optimum frequency from our investigation on the influence of discharge frequency on the deposition rate and film properties of a-Si:H, carried out in the range of 25 to 150 MHz [Curtins, 1987]. In view of developing solar cells based on both a-Si:H and μc-Si:H prepared at this same frequency we have carried out extensive research on the preparation and optimisation of μc-Si:H using the 70 MHz as the discharge frequency. The influence of different deposition parameters, namely the hydrogen dilution, discharge power and doping concentrations, on the optical, electrical and structural properties of these μc-Si:H films have been investigated in detail. This is the subject of the work presented here. Influence of substrate temperature is reported elsewhere [Prasad, 1991a & b].

Note that due to the lack of any data on material prepared at this same frequency elsewhere, all comparisons and references mentioned in this thesis are pertaining to the results obtained at the frequencies mentioned above and reported elsewhere by others.

The layout of the present thesis is as follows: Chapter 2 describes the VHF-GD deposition system and the deposition process used for the preparation of our specimens. Chapter 3 gives details on the various techniques used for the electrical, optical and structural characterization of our specimens. Some details on the kind of information expected from these techniques and its interpretation are also given. Chapter 4 treats the results concerning the influence of the hydrogen dilution of silane and the discharge power on the formation of undoped, phosphorus and boron doped μc-Si:H. The electrical, optical and structural properties of the μc-Si:H films are discussed as a function of these two variables. The influence of phosphorus and boron doping, on the film properties, at high doping levels is presented in chapter 5. These studies have been performed for films having a thickness of about 5000 Å. For device applications one requires films having thicknesses in the range of 100 to 500 Å. Chapter 6 presents our study on the influence of film thickness for both phosphorus and boron doped μc-Si:H. Finally chapter 7 summarises some important conclusions and suggestions for possible future work.

Parts of the results contained in the present thesis have been reported earlier in the following publications. Details of the influence of the substrate temperature is also reported there:

K. Prasad, F. Finger, H. Curtins, A. Shah, J. Bauman "Preparation and Characterization of Highly Conductive (100 S/cm) Phosphorus Doped μc-Si:H Films deposited using the VHF-GD Technique", Proceedings of the MRS Symp. Vol. 164, 27-32 (1989)

K. Prasad, U. Kroll, F. Finger, A. Shah, J-L. Dorier, A. Howling, J. R. Baumann, M. Schubert. "Highly conductive μc-Si:H layers for tunnel junctions in stacked silicon based solar cells", MRS Symp. Proc. 219, 469 (1991)

F.Finger, K. Prasad, A. Shah, X. M. Tang, J, Weber, W. Beyer, "Influence of Doping on the Structural Properties of Microcrystalline Silicon Prepared with the VHF-GD Technique at Low Deposition Temperatures", MRS Symp. Proc. 219, 383 (1991)

K. Prasad, F. Finger, A. Shah, M. Schubert, "Deposition of Doped Microcrystalline Silicon Below 70°C at 70 MHz", Proc. of ICAS-14, Garmisch-Partenkirchen, August 1991.

References

D. E. Carlson, IEEE Trans. Elec. Dev. 24, 449 (1977)

H. Chatham, P. K. Bhat, MRS Symp. Proc. 149, 4477 (1989)

H. Curtins, N. Wyrsch, A. Shah, Elec. Lett. 23, 228 (1987)

H. Curtins, N. Wyrsch, M. Favre, K. Prasad, M. Brechet, A. V. Shah, MRS Symp. Proc. 95, 249 (1987)

Y. Hattori, D. Kruangam, K. Katoh, Y. Nitta, H. Okamoto, Y. Hamakawa, 19th IEEE PV-SEC, New Orleans (1987)

J. Kanicki, Ch. 1 in ' Amorphous and Microcrystalline Semiconductor Devices: Optoelectronic Devices', Ed. J. Kanicki, Artech House, London (1991)

H. Kausche, K. Prasad, R. Plättner, Proc. of 9th EC.PVSEC, 595, Freiburg (1989)

S. Komuro, Y. Aoyagi, Y. Segawa, S. Namba, J. Appl. Phys. 56, 1658 (1984)

P. G. Lecomber, G. Willeke W. E. Spear, J. Non-Cryst. Sol. 59&60, 795 (1983)

A. Matsuda, J. Non-Cryst. Sol. 59&60, 767 (1983)

A. Matsuda, JARECT 22, Amorphous Semiconductor Technologies and Devices, Ed. Y. Hamakawa, OHMSHA LTD and North-Holland (1987)

A. Matsuda, T. Goto, MRS Symt. Proc. 164, 3 (1989)

K. Nakatani, M. Yano, K. Suzuki, H. Okaniwa, J. Non-Cryst. Sol. 59&60, 827 (1983)

S. Oda, J. Noda, M. Matsumura, MRS Symp. Proc. 118, 117 (1988)

K. Prasad, U. Kroll, F. Finger, A. Shah, J-L. Dorier, A. Howling, J. Baumann, M. Schubert, MRS Symp. Proc. 219, 469 (1991a)

K. Prasad, F. Finger, S. Dubail, A. Shah, M. Schubert, Proc. of ICAS-14, Garmisch-Partenkirchen (1991b)

I. Shimizu, J. Non-Cryst. Sol. 114, 145 (1989)

W. E. Spear, P. G. Le Comber, Sol. St. Comm. 17, 1193 (1975)

W. E. Spear, G. Willeke, P. G. Le Comber, A. G. Fitzgerald, J. de Phys. 42, C4-257 (1981)

R. A. Street, Proc. of ICAS-14, Garmisch-Partenkirchen (1991)

C. C. Tsai, pp 123 in 'Amorphous Silicon and Related Materials' Ed. H. Fritzsche, World Scientific Publ. Co, (1988)

G. Willeke, in ' Amorphous and Microcrystalline Semiconductor Devices: Materials and Device Physics', Ed. J. Kanicki, Artech House, Norwood (in Press) (1991)

Y. Uchida, T. Ichimura, A. Ueno, M. Ohsawa, J. de Phys. 42 - Suppl., C4-265 (1981)

S. Usui, M. Kikuchi, J. Non-Cryst. Sol. 34, 1 (1979)

S. Veprek, V. Marecek, Sol. St. Elec. 11, 683 (1968)

S. Veprek, Z. Iqbal, H. R. Oswald, A. P. Webb, J. Phys. C: Sol. St. Phys. 14, 295 (1981)

S. Veprek, M. Heintze, S. A. Sarott, M. Jurcik-Rajman, P. Willmot, MRS Symp. Proc. 118, 3 (1988)

2. VERY HIGH FREQUENCY GLOW-DISCHARGE (VHF-GD) DEPOSITION PROCESS

2.1 Introduction

The past decade has seen an important growth of amorphous silicon technology. Numerous techniques have been developed and perfected for the deposition of hydrogenated amorphous silicon (a-Si:H) thin films. Most of these techniques are also used to deposit microcrystalline silicon (μc-Si:H) thin films simply by tuning a few of the deposition parameters. Amongst these techniques, the plasma enhanced chemical vapour deposition (PE-CVD) is the most popular and commonly used. Often referred to as the glow discharge (GD) it uses a DC or AC electrical energy source for the dissociation of the source gases. The DC and 13.56 MHz sources and their accessories are easily available off the shelf as these frequencies are authorised industrial frequencies and are widely used for industrial applications. Very little work at higher frequencies has been reported upto now. In the interest to investigate the influence of discharge frequency on the deposition rate and material quality of a-Si:H, our group explored the frequencies in the range 25 to 150 MHz. This was done using a conventional capacitively coupled diode reactor and an adapted matching network [Curtins,1987a & b].

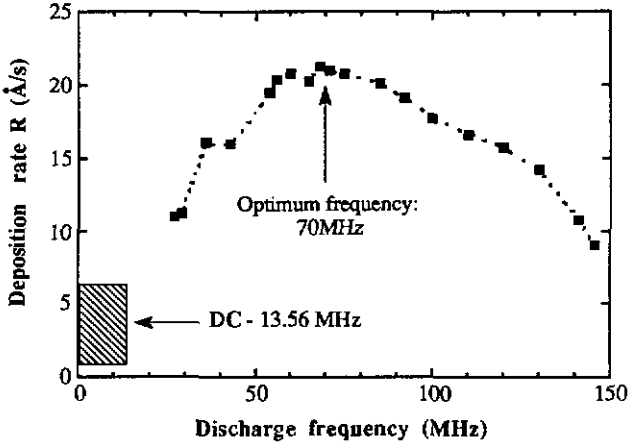

Figure 2.1 Deposition rate of a-Si:H as a function of plasma excitation frequency [H. Curtins, 1987]. The deposition parameters are: substrate temperature T_s=220°C, discharge power P=150 mW/cm^2, total gas pressure p=0.28 mbar and silane flow ϕ_{SiH4}=20 sccm.

It was found that, for our reactor geometry and the selected set of process parameters, the deposition rate increases with increasing frequency up to an optimum frequency of 70 MHz (figure 2.1). Opto-electronic properties such as the dark conductivity, photoconductivity, optical gap and the density of defects in the gap as determined by photothermal deflection spectroscopy (PDS) were comparable with those of a-Si:H prepared at 13.56 MHz [Curtins, 1987c]. This increase in the deposition rate with frequency has been explained by a higher power transfer efficiency into the plasma and a higher decomposition of silane at higher frequencies [Howling, 1991]. The higher decomposition of silane may also be influenced by changes in the electron energy distribution function (EEDF) which would be influenced by the higher excitation frequency. Beyond the optimum frequency the deposition rate is observed to decrease. Possible reasons for this decrease can be parasitic capacitive losses or internal resonant behaviours due to the reactor configuration. The high deposition rate obtained at 70 MHz can be of advantage to reduce production cost of a-Si:H based solar cells by achieving a higher throughput. In view of investigating such a possibility, this frequency has been used as the standard source frequency for our Very High Frequency Glow Discharge (VHF-GD) in our laboratory for both a-Si:H and μc-Si:H depositions [Prasad, 1989, Fischer, 1991]. The tendency of the high deposition rate was also observed in the study of μc-Si:H as well and shall be discussed in the present work.

2.2 Deposition System

Figure 2.2 illustrates the deposition set up. It consists of a cubic stainless steel reactor (A) containing two stainless steel electrodes (B and C). The reactor has a total volume of 15 l. Both electrodes are 13 cm in diameter and are separated by 15 mm. The lower electrode (C) is coupled to the high frequency source (F) and an amplifier (G) by means of a power meter (H) and an intermediate impedance matching L-C network (I). The upper grounded electrode (B), which can be heated using a coaxial heating coil integrated into it, is used to fix the substrate (D) on which the film is deposited. The assembly (J and K) consisting of pressurised gas bottles, pressure reducers, mass flow controllers and control electronics enables to introduce the source gases in a well controlled manner into the reactor (A). The Butterfly valve (N) in conjunction with the capacitive manometer (L) and the required electronic control regulate the total gas pressure within the reactor during the deposition process. The gases are constantly pumped out using a pumping stand comprising of a roots blower (P) and primary pump (Q1). They are then totally consumed at the outlet of the pumps in a burner (R) held above 700 °C before letting them out in the air. A higher throughput is obtained using a roots blower and it prevents the oil vapours from the primary pump diffusing back into the reactor and contaminating the process.

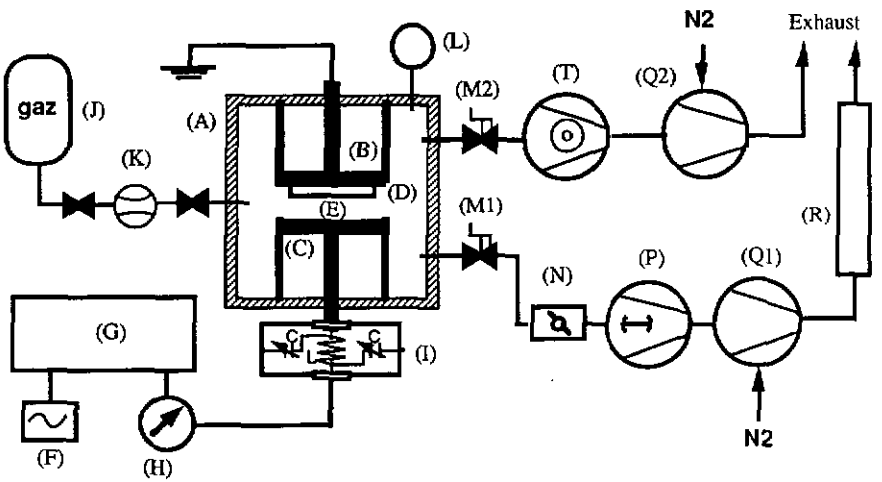

Figure 2.2 VHF-GD deposition system comprising of stainless steel reactor(A), grounded electrode and susbstrate holder (B), cathode (C) , substrate (D), plasma zone (E), high frequency generator (F), wide band amplifier (G), power meter (H), matching network (I), assembly of gas supplies (J) and mass flow meters (K), capacitive manometer (L), outlet valves (M1 and M2), butterfly valve (N), roots blower (P), two stage primary pumps (Q1 and Q2), silane burner (R) and turbomolecular pump (T). The electronic controls are not shown.

Prior to a deposition, the chamber is pumped out to reach a maximum vacuum possible with the help of the turbomolecular pump (T) backed by another primary pump (Q2). To enhance the elimination of impurities, especially water vapours, the walls of the reactor are baked constantly at about 80 °C. Due to the non-bakable nature of the viton o-rings it is not possible, under the present system configuration, to reach higher temperatures which would be, in fact, more beneficial. A base pressure of $2x10^{-6}$ mbars is reached under these conditions after an overnight pumping. The outgassing from the wall then is typically about $1.5x10^{-5}$ mbarl/s. As 1 mbarl/s equals a flow of 60 sccm, this corresponds to a flow of $9x10^{-4}$ sccm of mixed gases coming from the chamber walls. For a typical total flow of about 100 sccm used during the process, this corresponds to a contamination by a factor of 9.0 ppm. This is an important contamination in the case of intrinsic film deposition but can be neglected for the doped films since we are mostly using impurity doping concentrations greater than 1000 ppm.

For the doping purpose, phosphine (PH_3) and diborane (B_2H_6) gases diluted to 500 or 1000 ppm in hydrogen are used. The doping ratio is determined as the flow ratio of the dopant gas

to that of silane. Using the present concentration of doping gases and the range of flow meters (0-100 sccm) it was only possible to span doping ratios between 100 and 50000 ppm (10^{-4} and 5 %). To span lower doping levels the best way would be to connect a mixing bottle between the gas supplies and the deposition chamber. This would allow one to prepare a desired dopant concentration directly in the bottle prior to deposition. Such a system has not been used for our work.

The outgassing was calculated frora the rise in the system pressure, with all its valves closed, for a given time interval. Both, long and short time intervals were used to assure that there was no leakage in the system.

2.3 Temperature Calibration

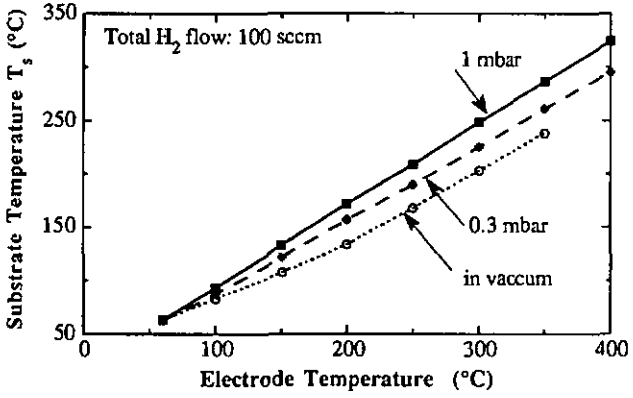

Figure 2.3 Calibration curve for substrate temperature at different gas pressures.

The substrate temperature during the deposition is controlled using a coaxial heating coil and a PT 100 sensor incorporated in the grounded electrode ((B) in figure 2.2). Due to the poor thermal conductivity between the substrate and the heating block, the thermal inertia of the electrode base plate, and the losses by radiation and convection, the effective temperature at the substrate needs to be calibrated for various temperature set points under different deposition conditions. This was performed using another PT 100 fixed on the substrate during trial runs in the absence of any plasma. Figure 2.3 illustrates the results which were used to determine the precise substrate temperature during the deposition. The effective substrate temperature is lowest under vacuum. As the gas pressure increases the difference between the effective substrate temperature and the electrode temperature decreases. This is due to heating of the substrate surface by the surrounding gas which absorbs heat from the hot surfaces of the

electrode and releases it at the cooler substrate surface. In comparison, estimates of temperature measurements at the substrate before and after a plasma indicated an increase of temperature of about 20 °C with a hydrogen discharge at 20 W (150 mW/cm^2). Such a high power was used only for the preparation of p-type specimens. In this case, the plasma will increase the effective substrate temperature by about 20 °C, reducing thereby the offset between the effective substrate temperature and the set point. As undoped and n-type specimens were deposited using a lower discharge power of 23 mW/cm^2, the modifications of the substrate temperature from the plasma and the ion bombardment at the substrate can be considered to be negligible. Due to the system limitations it was not possible to raise the substrate temperature beyond 300 °C.

2.4 Substrates

8.3 x 8.3 cm^2 alkali free glass substrates (7059) from Dow-Corning are used as substrates for most of the electrical, optical and structural studies. A small piece of resistive (1 Ω/cm) crystalline silicon with <100> orientation is also used for infrared transmission studies. The latter is fixed on the glass substrate with the help of silver paste. All substrates are cut, cleaned and dried using our standard processes (Annexe A & B).

2.5 *Deposition Parameters*

Table 2.1. Deposition parameters and their ranges:

Parameter	Scan range	(units)
Substrate temperature	150-200	°C
Input discharge power	3 - 50	W
(Input power density)	20 - 375	mW/cm^2
Working pressure	0.4 or 0.8	mbars
Silane concentration in hydrogen	1 - 10	%
Doping gas/silane	0.01 - 5	%
Electrode spacing (with substrate)	15	mm
Electrode area	133	cm^2
Discharge frequency	70	MHz

The experimental parameters required for the deposition of highly conductive μc-Si:H films using 13.56 MHz have been defined as low concentration of silane in hydrogen (1-10 %), a high discharge power (>150 mW/cm^2) and a high substrate temperature (>200 °C) [A. Matsuda, 1987 and references therein]. Best conductivity results for doped films have been

reported for gas phase doping levels around 1%. In contrast, pure silane and low discharge powers are recommended to produce quality a-Si:H films. For our investigations and optimisation of thin films, deposited using 70 MHZ-GD, we have scanned the deposition parameters over a wide range. Table 2.1 gives an overview. More details related to individual parametric study are provided in the corresponding sections.

2.6 Deposition Process

A typical deposition cycle consists of the following steps: First, the substrates are loaded onto the grounded electrode using a stainless steel holder. The chamber is then closed and pumped down overnight, or at least for four hours, during which the chamber walls are heated to the maximum of 80 °C. Before beginning the deposition run the base pressure and outgassing rates are recorded. This allows a quick check of the system and detection of leakage if any is present. Then a 150 mW/cm^2 argon plasma at 0.4 mbar is performed for five minutes, in the aim of cleaning the cold substrate surface. Following this, the substrate electrode is heated up to the deposition temperature under a constant hydrogen flow of 100 sccm at 1 mbar for 30 to 45 minutes. Such a flushing allows further cleaning of the chamber walls and electrodes while stabilising the temperature conditions for the deposition. Next, another 150 mW/cm^2 plasma for five minutes, with hydrogen this time, is produced. This allows a final surface cleaning of the substrate before the deposition of the film. We are of the opinion that it also produces a hydrogen coverage at the surface of the substrate which possibly plays a role in the initial nucleation process and adhesion of the film to the substrate. Then the gas flows and the operating pressure are set and let to stabilise for a couple of minutes, the deposition plasma is ignited and the input power is carefully adjusted using the matching network so as to have a minimum power loss by reflection. The deposition time is estimated so as to obtain the required film thickness, which in most cases was selected as 5000 Å. After the estimated time, the plasma and substrate heating is switched off. The gas flow rates are then systematically calibrated by measuring the rise in chamber pressure over a measured time and used to readjust the set points on the flow meters. This also allows a more precise determination of the silane concentration and the doping ratios which are quite critical in our work. The gas flows are then switched off and the chamber is pumped down using the turbomolecular pump. The substrate is allowed to cool down to around room temperature before unloading. Upon unloading the substrate holder and the plate situated over the cathode are cleaned chemically before reloading (Annexe C).

The plasma ignition itself is performed manually, in each case, by first raising the discharge power to just a few Watts but less than the operating level, and then introducing an electric spark through an electrical feed through of the chamber with the help of a conventional gas

flame igniter based on piezoelectric quartz. This is a very simple and efficient technique which allows plasma ignition at very low power levels. This is of importance since it eliminates the undesirable transients caused otherwise during the switching on of plasmas by raising the power much beyond the operational value. Such transients can result in undefined interface layers deposited between the substrate and the required film.

References

H. Curtins, N. Wyrsch, A. Shah, Elec. Lett. 23, 228 (1987a)

H. Curtins, N. Wyrsch, M. Favre, K. Prasad, M. Brechet, A. V. Shah, MRS Symp. Proc. 95, 249 (1987b)

H. Curtins, N. Wyrsch, M. Favre, A. V. Shah, Plasma Chem. and Plasma Process. 7, 267 (1987c)

D. Fischer, H. Keppner, F. Finger, K. Prasad, A. Shah, Proc. of EC-PVSEC-10, Lisbon, 201 (1991)

A. Howling, J.-L. Dorier, Ch. Hollenstein, U. Kroll, F. finger, to be published in J. Vac. Sci. Techn. (1991)

A. Matsuda, JARECT 22, Amorphous Semiconductor Technologies and Devices, Ed. Y. Hamakawa, OHMSHA LTD and North-Holland (1987)

K. Prasad, F. Finger, H. Curtins, A. Shah, J. Baumann, MRS Symp. Proc. 164, 27 (1989)

3. CHARACTERIZATION TECHNIQUES

This chapter describes the different methods which have been used for the characterization of electrical, optical and structural properties of our films. In addition methods used to diagnose the electrical properties of the plasma and the kinetics of deposition are also included in brief. Table 3.I enumerates these techniques and the information they provide.

Table 3.I List of characterization techniques used in this work:

Characterization Technique	Information
Stylus step profiling	Film thickness
Electrical conductivity	*Conductivity and activation energy*
Ultra Violet-Visible transmission	Optical absorption ($\alpha = 10^6$ to 10^3 cm^{-1})
PDS	Subgap optical absorption ($\alpha = 10^4$ to 1 cm^{-1})
IR transmission	Hydrogen bonding
Raman Scattering	Crystalline volume fraction, bond angle disorder
X-ray Diffraction	Average crystallite grain size and orientation
TEM	Details of crystallites and grain boundaries
SIMS	Dopant concentrations
OES	Intensities of SiH and atomic H radicals in the plasma
Electrical measurements on the reactor electrodes	Electrode, sheath and plasma voltages

3.1 Stylus Step Profiling

The evaluation of the film thickness with precision is of importance as it is used for determining most of the other film properties. The thickness is measured using a stylus profiling over a step etched out on the glass substrate (Tencor: Alpha Step 200). The step is produced very close to the area used for other measurements so that errors due to the film non-uniformity are minimised.

To create the step, first the entire specimen except the area to be etched out is covered with a protective lacquer (PLASTIK 70). Once it is dried in ambient air, the sample is dipped in hot

diluted KOH solution which is at 60 to 70 °C. The KOH attacks and etches out the exposed part of the film. As the etch rate for the silicon film is much faster than for the glass or the protective lacquer, one obtains with care a very neat step. The lacquer is then removed and the specimen cleaned by rinsing with Acetone and Isopropyl Alcohol (IPA). The stylus profiling is carried out across the step over a range of 2 mm. The precise film thickness is obtained by applying standard leveling procedures.

3.2 Electrical Conductivity

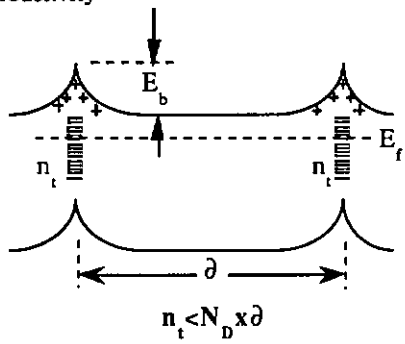

Fig. 3.1 Suggested energy band profile through crystallites in pc-Si [Le Comber, 1983].

The electrical conductivity is an important and useful parameter which is measured to evaluate and optimise our films. Electronic transport in μc-Si:H has been successfully interpreted using the well established model for polycrystalline silicon (pc-Si) [Seto, 1975], although the size of the crystallite grains is larger than 400 Å in pc-Si as compared to less than 300 Å in μc-Si:H [Le Comber, 1983]. Figure 3.1 illustrates the energy band model across the crystallite of size ∂, for n-type specimen, bordered by the influence of the grain boundary containing states in the gap. Amongst these states, a certain amount n_t per unit area is filled by some of the free electrons supplied by the active dopant concentration causing a depletion of charges near the grain boundary. This results in a potential barrier having a height E_b. E_b represents the activation energy of the carrier mobility as it is the potential which the free carriers need to overcome while crossing over from one crystallite to another. Note that for dopant concentrations greater than 10^{17} cm^{-3} the space charge region is localised to a few atomic spacing since $n_t << N_D x \partial$. N_D defines the bulk doping concentration in the crystallites. The activation energy E_a of the conductivity also equals E_b under this condition [Le Comber, 1983]. In our case the above condition is satisfied even in undoped specimens which have impurity concentrations in the range of 5-8x10^{17} cm^{-3} as measured by SIMS. This is

attributed to stray doping coming from the walls of the reactor. In doped specimens the dopant concentration is still higher.

For the above model the dark conductivity σ is expressed as:

$$\sigma = \sigma_0 \exp(-E_a/kT) \qquad [S/cm] \qquad (3.1)$$

where σ_0 is the conductivity prefactor, E_a the activation energy, k the Boltzmann constant and T is the temperature given in Kelvin. This equation is also used to determine the activation energy E_a which is related to the potential barrier E_b seen by the carriers at the grain boundaries [G.Willeke, 1991].

The measurement is performed using a coplanar configuration in vacuum under darkness.

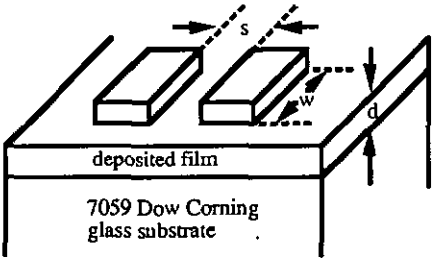

Fig. 3.2 Electrode contact geometry used for conductivity measurements.

Two parallel aluminium electrodes, as described in figure 3.2, having a thickness of 100 nm are evaporated on the film. The specimen is then mounted on the temperature controlled sample holder and loaded into the measurement chamber. The chamber is pumped down using a turbomolecular pump backed by a primary pump. When the pressure falls below 10^{-3} mbar the following thermal cycle is initiated on the sample: First the sample is heated rapidly up to the temperature used during the deposition, which is 150 °C in most cases. It is then maintained at this temperature for 90 minutes and then cooled down slowly to room temperature at a rate of 0.8 °C/min. The importance of the thermal cycle lies in having the specimen in a reproducible state before measuring the dark conductivity.

In most cases the electrical measurements are performed continuously during the entire thermal cycle using the Keithley Electrometer 617. The voltage drop across the two electrodes is measured by introducing a known current in the constant current mode. The current level is

automatically selected by the electrometer based on the resistance of the film so as to generate a maximum voltage drop less than 2 V across the two electrodes. The Ohmic behaviour of the aluminium contacts was verified in the range of 0.2 to 2 V, for both low and high conductive films.

The resistance R [Ω] obtained in this manner is then converted to the dark conductivity σ by the relation:

$$\sigma = s / Rdw \qquad [S/cm] \qquad (3.2)$$

where: s is the electrode spacing, w the width of the electrode and d the film thickness. w and d are expressed in cm.

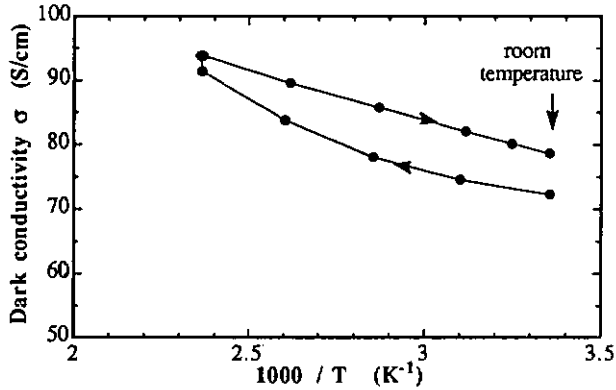

Figure 3.3. Conductivity as a function of inverse temperature.

The electrical measurements are plotted as conductivity vs 1/T (σ_d vs 1000/T), where the temperature T is expressed in Kelvin. Figure 3.3 illustrates a typical measurement. The variation of conductivity with temperature, during the cooling cycle, is well fitted for our temperature range using the standard transport equation 3.1 and is used to determine the activation energy E_a. The room temperature conductivity is indicated by the value at 1000/T = 3.35. The small increase in conductivity at room temperature after the annealing cycle is suspected to result from effusion of hydrogen, occuring at the annealing temperature of 150°C, which results in the depassivation of previously passivated dopants [Finger, 1991].

In some cases the conductivity is measured in air at the end of the thermal cycle when the sample is back to room temperature. No difference is observed in the conductivity of the heavily doped n and p-type films when measured in air or in vacuum. The undoped specimens were always measured in vacuum.

3.3 Optical Absorption

The optical absorption behaviour in the range of 400 to 1400 nm (3 to 0.8 eV) provides information on the electronic transitions occuring between energy bands. Figure 3.4 illustrates a typical spectrum of an undoped μc-Si:H film. Absorption characteristics of a typical undoped a-Si, a-Si:H and c-Si are also given for comparison [Godet, 1987]. Data reported for undoped and phosphorus doped polysilicon [Lubberts, 1981] are also illustrated.

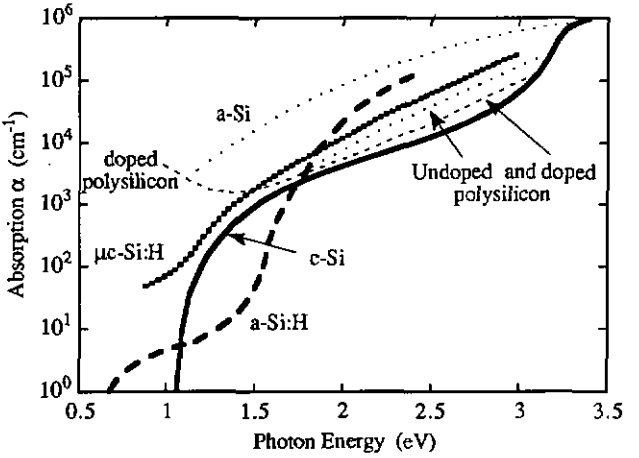

Fig. 3.4 Absorption behaviour of undoped c-Si, a-Si, a-Si:H, μc-Si:H [Godet, 1987] and LPCVD deposited doped and undoped poly-Si [Lubberts, 1981].

As a reminder, in c-Si the direct transitions from the valence band to the conduction band occurs for photon energies greater than 3.2 eV and results in a high absorption coefficient. At lower energies the absorption is reduced due to the indirect transitions and the phonon conservation. It then drops to zero at 1.12 eV marking the energy of the band gap. As the density of states (DOS) in the band gap is insignificantly low, no transitions occur for lower energies and the optical absorption remains zero.

The energy band diagram is very different in a-Si:H. The important consequence of the disordered network is that there is a quasi continuum of DOS over a wide energy range, although hydrogen saturates many of the silicon dangling bonds. Therefore, one cannot strictly speak of a gap as in the case of c-Si. A common practice is to associate energy levels based on the values of mobility, corresponding to the bottom of the conduction band E_c and the top of the valence band E_v. For states situated at energy levels above E_c and below E_v one refers

to as extended states since there the electron or hole states are delocalized, whereas states situated below E_c or above E_v are localized. For the facility of communication, one often refers to the energy band between E_c and E_v levels as the 'mobility gap'. The absence of the long range order also relaxes the phonon conservation rule and one obtains non-direct transitions between the two bands [Cody, 1988]. Between E_c and E_v the DOS extends as decreasing tails deep within the 'mobility gap'. These tail states are produced by the weak and deformed silicon bonds of the network. Finally, in the centre of the 'mobility gap' there exists a high DOS resulting from the unsaturated silicon dangling bonds. All these states participate in electronic transitions and are reflected in the absorption behaviour.

So, one obtains a very high absorption ($>10^4$ cm^{-1}) for photon energies greater than 2.3 eV due to the non-direct transitions. Below this energy level the optical absorption falls off exponentially characteristic of the exponential decrease of the DOS in the band tails. The Urbach energy E_0 determined from the slope is used as a parameter to characterize the width of the valence bandtail of a-Si:H. A smaller E_0 signifies a narrow band tail indicative of a better material. Finally for photon energies less than 1.5 eV the absorption decreases slowly but still retains a finite value due to the transitions occuring between the bands or band tails and the density of states (DOS) in the centre of the gap. The film quality can be evaluated by determining the absorption coefficient $\alpha_{1.2}$ at 1.2 eV which can be then correlated to the defect density [N. Wyrsch, 1991]. A lower value of $\alpha_{1.2}$ is indicative of a lower DOS and a better material. Note that, in comparison, due to the absence of any hydrogen the DOS is much higher in non-hydrogenated amorphous silicon (a-Si) and leads to the very high absorption seen in the low energy range.

For practical purpose, the energy at which the absorption value is 10^4 cm^{-1} is often referred to as the optical gap although a rigourous definition and determination of the 'gap' remains still an open question.

In comparison, the energy bands and especially the band gap is still poorly understood in the μc-Si:H. One can draw some information from the optical absorption behaviour. So far, the μc-Si:H is understood to be, like polysilicon (poly-Si), consisting of a composite of finite size crystallites and a certain amount of disordered/amorphous tissue forming the grain boundaries. Both these components influence the optical absorption property. In the high photon energy range (3 eV > E > 2 eV) the absorption coefficient lies between that of the c-Si and a-Si:H, and in fact resembles quite closely that of undoped poly-Si This can be attributed to the non-direct transitions occuring between the valence and conduction like bands formed by the disordered tissue forming the grain boundaries. The absorption is nevertheless lower than for a-Si:H due to the smaller volume fraction of the amorphous tissue in the μc-Si:H. For energies

below 1.8 eV two factors influence the absorption behaviour: In the case of undoped material, transitions occuring to and from the high DOS created in the middle of the gap due to the dangling bonds at the grain boundaries contribute at least partly to the absorption, as discussed for a-Si:H. However, their contribution is masked by the stronger absorption corresponding to the indirect transitions occuring in the energy states resulting from the crystalline configurations. This is relatively high (10^4-10^2 cm^{-1}) and therefore lies above the exponential tail of the a-Si:H. In doped material, the excitation of free carriers within the conduction band of n-type or valence band of p-type material dominate the absorption behaviour as also observed in doped polysilicon deposited at 620 °C [Mishima, 1980; Lubberts, 1981] and mask out the effects of the indirect transitions and the DOS mentioned earlier. This contribution increases with increasing dc conductivity and shall be treated in some detail in the results. The reasons for the difference in the absorption at high energies between the undoped and doped poly-Si is not clearly identified.

The optical absorption is determined using two different techniques in two separate energy ranges. For energies above 2 eV the standard transmission and reflection spectroscopy is used while for lower energies the Photothermal Deflection Spectroscopy (PDS) is used [Curtins, 1988]. Taking the values of absorption obtained from the PDS and the optical transmission measurements the absorption characteristic is plotted over the energy range from 0.8 eV to 3.1 eV. The two measurement techniques are briefly described below.

Absorption in the Ultra Violet and Visible spectrum

The optical absorption provides information on the electronic transitions between the energy bands. It has been determined from transmission measurements carried out at room temperature using a commercial computer controlled spectrophotometer (model LAMBDA 17 from Perkin Elmer). The transmission of films deposited on 7059 glass substrate was measured for wavelengths ranging from 300 to 700 nm. This corresponds to photon energies in the range of 4.1 eV to 1.8 eV. The film surface was positioned towards the source beam. The spectrometer uses a double beam technique, one of which is used as the reference while the other traverses the specimen. The detection is performed by a photomultiplier and controlled by a computer.

For the evaluation of absorption, the typical reflection R_{af} occuring at the air-film interface is also measured on the same system which uses an Ulbricht's integrating sphere in the reflection mode. In the wavelength range between 400 and 900 nm the reflection coefficient R_{af} is almost constant and has a value of 40%.

The absorption coefficient α is calculated in the range of 400 to 700 nm, using the following standard equation for transmission T:

$$T = (1-R_{af})x\{\exp(-\alpha d) / (1-R_{af} \times R_{fg} \times \exp(-2\alpha d))\}x(1-R_{fg})x(1-R_{ga}) \qquad (3.3)$$

where the subscripts a,f, and g stand for air, film and glass respectively. R_{xy} represents the reflection coefficient at the interface of medium x-y and d is the film thickness. The factors $(1-R_{af})$, $(1-R_{fg})$ and $(1-R_{ga})$ account for the loss due to reflections at the air/film, film/glass and glass/air interfaces, respectively. $\{\exp(-\alpha d) / (1-R_{af} . R_{fg} . \exp(-2\alpha d))\}$ accounts for the total absorption within the film resulting from the multiple reflections at the two interfaces of the film: film-air and film-glass. R_{fg} is determined from the value of transmission at 900 nm for which the absorption is assumed as 0 and considering the refractive index of glass substrate to be 1.51.

The precise value of absorption coefficient is determined by taking the geometric average over the interference fringes of the resulting α vs λ plot which is obtained by using equation 3.3 and the measured transmission values.

Photothermal Deflection Spectroscopy (PDS)

The Photothermal Deflection Spectroscopy (PDS) is used to measure the absorption coefficient in the range of 600 to 1400 nm wavelength (2.07 to 0.89 eV). The system set-up and measurement technique is described in detail elsewhere [Curtins, 1988]. The measurement results provide the relative changes in the absorption coefficient as a function of the wavelength of the incident beam. The data are then calibrated using the absorption coefficient obtained for a wavelength of 600 nm from the previous technique. The error in the measurement of α, estimated from the signal to noise ratio, is less than 10 % at an absorption of 1 cm^{-1} and is expected to be even smaller for higher absorption values.

3.4 Infrared Absorption

The infra-red (IR) absorption gives information on the hydrogen bonding with its surrounding within the films, via excitation of the phonons. The absorption signatures at the different energy positions are associated to the corresponding vibrational modes excited within the material. Figure 3.5 illustrates typical IR transmission spectra of undoped a-Si:H and μc-Si:H. In both cases, the most important absorption signatures are situated at the following energy positions: a) around 630 cm^{-1}, b) between 850 and 900 cm^{-1} and c) around 2000 cm^{-1}.

In a-Si:H, the peak at 630 cm^{-1} is attributed to vibrational excitations of the wagging modes of SiH, and rocking modes of SiH_2, $(SiH_2)_n$ and SiH_3 bonds [Lucovsky,1979]. This peak is usually used to calculate the total hydrogen content within the film [Shanks, 1980]. The signatures situated at 850 cm^{-1} and 890 cm^{-1} are associated with dihydride ($=SiH_2$) and polyhydride ($(=SiH_2)_n$) vibrational modes. These bonds also produce a signature at 2100 cm^{-1}. The presence of a peak at 2100 cm^{-1} in the absence of any signatures between 800 cm^{-1} and 900 cm^{-1} is attributed to SiH bonds situated in the internal surfaces of the voids [Beyer, 1985]. Finally, another peak centred at 2000 cm^{-1} is attributed to the stretching vibrations of isolated monohydrides (Si-H) [Beyer, 1985].

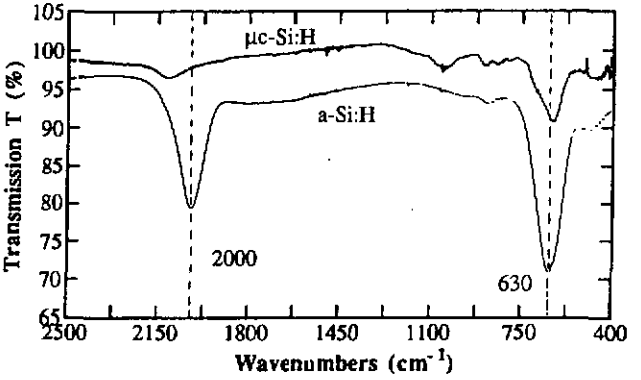

Figure 3.5 IR transmission data of undoped a-Si:H and μc-Si:H.

In the case of μc-Si:H, most of the signatures maintain their energetic positions but their amplitudes and symmetry are modified. Usually the peak at 630 cm^{-1} has a contribution at 590 cm^{-1} which is attributed to SiH_2 rocking modes [Uchida,1981]. In our case, a contribution is observed at 700 cm^{-1} which is not identified. The signature at 2000 cm^{-1} is asymmetric towards or completely shifted to 2100 cm^{-1}. This is attributed to SiH_3 and $(SiH_2)_n$ vibrational modes [Tsai, 1988]. These groups are assumed to be situated at the surfaces of the crystallites and in the disordered tissue forming the grain boundaries. In the case of doped specimens the background transmission is reduced due to the increase in absorption originating from free carriers. This will be discussed in the results. Note that little or no hydrogen is expected within the crystallites except for passivating dopants [Johnson,1991]. The large peak situated between 1000 and 1300 cm^{-1} indicates the presence of oxygen in the form of Si-O bonds situated within the voids and at the grain boundaries [Curtins, 1986].

The measurement of infrared transmission is performed on films deposited on crystalline substrates, using a commercial Fourrier Transform - Infra Red (FT-IR) spectrometer (model 1720 X from Perkin Elmer). The spectrometer has the possibility to scan over wave numbers from 400 to 7900 cm^{-1}. This corresponds to photon energies extending from 0.05 eV to 0.98 eV, although a shorter range from 400 to 5250 cm^{-1} was mostly used in our work. Prior to the measurements, a standard background correction is performed using a piece from the same c-Si wafer, which is used as substrate.

3.5 Raman Scattering

The Raman scattering measurement is useful to determine the structural properties of the material. In this measurement technique the 1st order TO phonon spectrum resulting from the inelastic scattering of the incident beam is measured. During the inelastic collision with the existing phonon bath the incident photons give up some of its energy to excite the vibrational energy levels of the interacting molecules and emerge with a lower energy. These scattered photons constitute the lower-frequency Stokes rays. Other incident photons may collect energy from the molecules and emerge at a higher frequency as anti-Stokes radiation. The shift in frequency gives information on the vibrational energies and structure of the molecules. As the shifts in frequency of the scattered radiation from the incident radiation are very small, one requires very monochromatic incident radiation and a powerful monochromator to detect the shifts. In the present experiment only the Stokes radiation is studied.

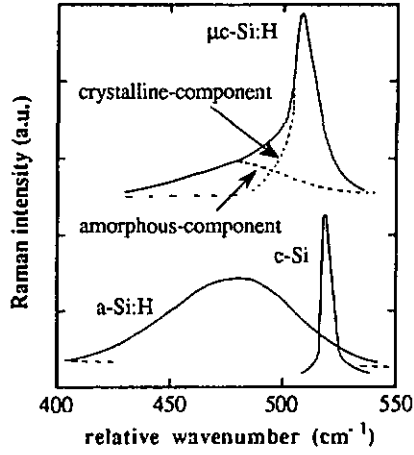

Fig. 3.6 Raman profiles of c-Si, a-Si:H and μc-Si:H [Iqbal, 1982].

Figure 3.6 illustrates typical spectra obtained for crystalline silicon (c-Si), a-Si:H and μc-Si:H. In the case of c-Si only the TO phonon resulting from the vibration of the Si-Si bonds is allowed which produces a sharp peak centered at 522 cm^{-1} and has a full width at half maximum (FWHM) of 3.5 cm^{-1} to which is added the effect due to the thermal broadening. In comparison, due to the disorder in a-Si:H the phonon conservation rule is relaxed and all the modes are Raman active [Shuker, 1970]. This results in a broad Gaussian centered around 480 cm^{-1}. In this case the FWHM of the Gaussian peak is taken as a degree of disorder of the bond angles [Beeman, 1985]. The value of 60 cm^{-1} is obtained for the FWHM for good quality a-Si:H. It is higher for material with poorer quality i.e. poor opto-electronic property and higher density of defects in the gap.

In the case of μc-Si:H one obtains a profile which can be deconvoluted into two components: a sharp peak centered near 515 cm^{-1} called the crystalline component and a broad Gaussian centered near 480 cm^{-1} which is called the amorphous component. The first one is understood to result from the crystallites and the second from the disordered regions of grain boundary like (GBL) zones. A Lorentzian fit works better for the crystalline component when the material has uniform crystallite sizes, whereas the Gaussian fit suits the spectrum obtained from a material having a wide distribution of crystallite sizes [Bustarret, 1991]. The shift of the TO-peak position of the crystalline component to lower wavenumbers, as compared to 522 cm^{-1} in c-Si, is attributed to crystallite size effect and stress within the material [Richter, 1981; Fauchet, 1989].

Using the integrated areas under the crystalline component (I_c) and the amorphous component (I_a) one can determine the volume fraction X_c of the crystallites in the μc-Si:H specimen:

$$X_c = I_c/(I_c+yI_a) \qquad (3.4)$$

Here, y is the ratio of the integrated Raman scattering cross sections Σ_c/Σ_a of the TO band in the crystalline grains and in the amorphous GBL zones. The ratio y has been reported to be from 0.14 for polycrystalline silicon relative to a-Si:H [Brodsky, 1977, and Bermejo, 1979] to 0.88 for microcrystalline silicon relative to a-Si:H specimens [Tsu, 1982]. In the latter evaluation of y, the absorption coefficient α for the two materials was comparable at 2.5 eV, which would be true in the case of very small crystallite sizes or the material containing a large amount of amorphous tissue. In our case, α in μc-Si:H is lower than in a-Si:H at least by a factor three and therefore, it would be incorrect to take the value of y as 0.88. The former value of 0.14 is quite appropriate down to a crystallite size of 400 Å and has been selected for the evaluation in the present work. One should keep in mind that as the crystallite size decreases to 100 Å, y would increase from 0.14 to 0.77, which will in turn influence X_c by

a factor 0.5 [Bustarret, 1988]. Therefore, in less crystalline material, for example in specimens belonging to the microcrystalline to amorphous transition region, X_c will fall off twice as rapidly than as determined by using y=0.14. The crystallite size, its geometry or stress in the film can influence line width, symmetry and the peak positions of the Raman peaks [Richter, 1981; Fauchet, 1989]. However, such influences have been neglected here.

The measurements have been performed by M. Schubert at the Institut für Physikalische Elektronik, Universität Stuttgart. They have been carried out at room temperature in the quasi-backscattering set up. A 100 mW incident beam having a wavelength of 488 nm (2.54 eV) has been used from an Ar laser to illuminate a sample area of 10 x 50 μm^2. As the absorption at this energy is about $5x10^4$ cm^{-1} the probing depth is estimated to be less than 2000 Å. The scattered Stokes lines are recorded in the range of 300 to 600 cm^{-1} with respect to the incident radiation, using a scanning photon counting system attached to a double monochromator. Sampling is averaged over 30 seconds and repeated over 3 times. The resolution is 0.2 cm^{-1} for the system but 4 cm^{-1} for the measurements [Schubert, 1990].

3.6 X-ray Diffraction

The X-ray diffraction technique is also commonly used to obtain structural information of the samples. The diffraction results contain signatures for different crystallographic planes. From these one can derive information on preferential orientations of crystallites and the mean value of the grain sizes.

Table 3.2 Crystallographic parameters for polycrystalline silicon powder where <hkl> are Miller's indices defining the crystallographic plane, d(hkl) is the interplanar distance and 2θ (hkl) is the angular position satisfying Bragg's condition, when Cu-K_α radiation is used.

hkl	d(hkl)[Å]	2θ(hkl)[°]
<111>	3.135	28.45
<220>	1.920	47.31
<311>	1.637	56.14
<400>	1.358	69.11

Figure 3. 7 illustrates a typical diffraction pattern resulting from poly-crystalline silicon powder having random orientation of crystallites. The sharp peaks characteristic of the <111>, <220>, <311> and <400> crystallographic planes are observed at the angular position which satisfies the Bragg condition for the corresponding planes. Table 3.2 gives details of the

different crystallographic orientations <hkl>, their interplanar distance d(hkl) and the angular position 2θ of their peaks, when Cu-K_α radiation is used.

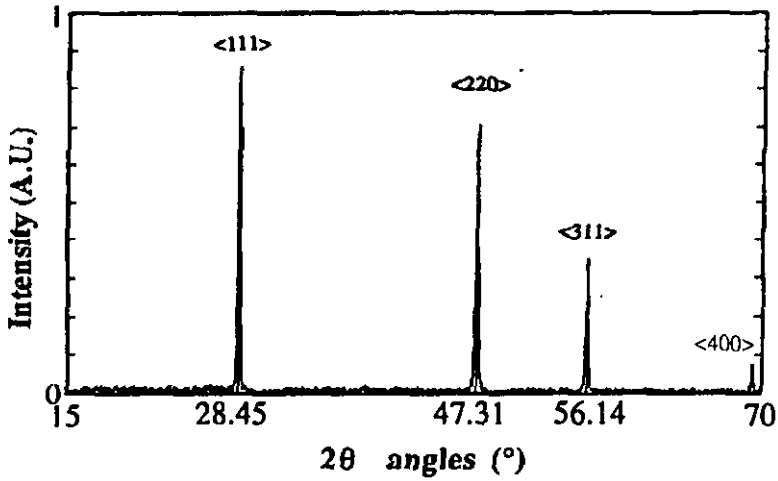

Figure. 3.7 X-Ray spectra of poly-Si powder.

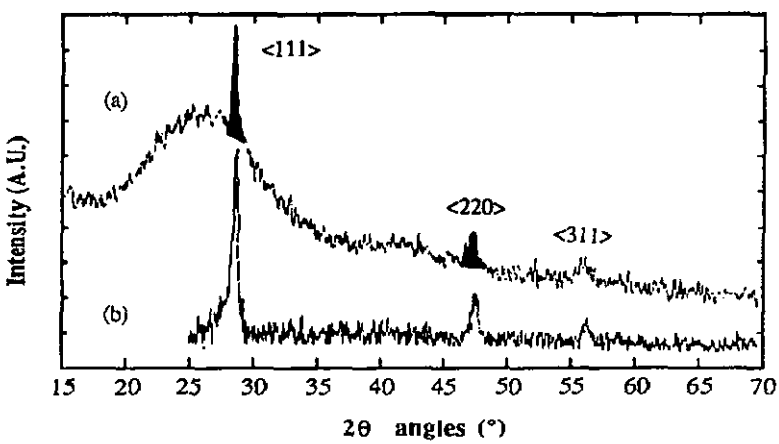

Fig. 3.8 *Diffraction spectra of μc-Si:H* (a) as measured and (b) after backgroung substraction.

When measuring the μc-Si:H samples deposited on glass one encounters some difficulties. As the absorption coefficient of the silicon for the X-rays, having a wavelength of 1.5406 Å (= 8 KeV), is rather low (141 cm^{-1}) and as the sample is rather thin (0.5 μm), the diffracted

signal is rather weak since most of the X-rays are absorbed or scattered by the glass substrate. Fig 3.8 illustrates a typical diffraction spectra (a) as obtained for a μc-Si:H sample prepared on glass substrate and (b) after eliminating the contribution of the substrate and smoothing it. These results are then compared with that of random oriented polycrystalline silicon, to determine the crystallite orientation and whether any preferential orientation in the films is present.

For crystallites having a limited dimension, one can determine the average size ∂ of the grains by using the full width at half maximum (FWHM) β of a selected peak and Scherrer's equation [Klug, 1954].

$$\partial = k\lambda / \beta \cos(2\theta) \quad [\text{Å}] \qquad (3.5)$$

where, 2θ is the angular peak position, λ the wavelength of the X-rays and k a constant determined by the geometry of the crystallite which has a value of 0.89 for an assumed spherical grain structure. This equation is valid for uniform grain sizes larger than 100 Å in our case. For smaller grain sizes the determination of peaks and the FWHM becomes very erronous due to the background noise. For the intrinsic and n-type samples the <111> peaks were used for the above evaluation as they were most prominent while for the p-type films, due to the absence of the <111> peak, <220> peaks were used.

The FWHM is corrected for the peak broadening b due to the system which is of approximately 0.1°. Thus the corrected $\beta = (\beta_{measured}^2 - b^2)^{1/2}$ is used in equation 3.5. Besides, stresses in the film can also contribute to the peak broadening but Scherrer's procedure used in our case does not perform the necessary correction. Further limitations using Scherrer's procedure have been recently reported by Veprek, who suggests instead a complete analysis of the Bragg peak profiles using the Warren-Averbach procedure which takes into account the contribution of mechanical microstress and finite crystallite size on the width of the peaks [Veprek, 1991]. This procedure has not been used in our case as we were unaware of it until now. Therefore, the results obtained in our case, using Scherrer's formula, should be treated with care as they are indicative of the average grain sizes and by no means exact.

X-ray diffraction measurements, in our case, have been performed by J. Baumann at the Physics Institute of Konstanz University using a commercial Siemens D501 X-ray diffractometer. An accelerating voltage of 40 KeV at 30 mA is used to produce Cu-K_α radiation having a wavelength of 1.5406 Å. Specimens having a size of about 4 cm^2 are fixed

on the sample holder, which is rotated by θ during measurements. The diffracted rays are recorded for 2θ angles ranging from 15° to 70°.

In the final phase of this work, due to the necessity of a higher sensitivity, some grazing angle X-ray measurements have been carried out at CNRS -Grenoble. A grazing angle of 0.3° increases the volume of the probed specimen which reacts to the X-rays, increasing the sensitivity of the measurement [Brunel,1989]. In this case the diffracted peaks of the <111>, <220> and <311> planes are obtained at 14.18°, 23.72° and 28.07°, respectively. The detector is scanned in the range of 10 to 30°.

3.7 TEM and Electron Diffraction

High resolution micrographs obtained from transmission electron microscopy (TEM) enables one to have details of the film structure, namely: the crystalline and amorphous zones, crystallographic defects, and grain boundaries. One also obtains details of the structure at the film-substrate interface. The microscope used for the study (Philips CM30; 300 kV) provides a magnification factor of 110000 which gives a point resolution of 1.9 Å.

The selected area electron diffraction (SAED) patterns obtained at the focal plane of microscope provides further information on the film structure. An amorphous structure results in a diffraction pattern with broad diffused haloes, while sharp rings with distinct points are observed in the case of randomly oriented polycrystalline structure [Tsai, 1988]. A pattern exhibiting a periodic structure of bright diffraction spots is characteristic for a large crystalline area with a low-indexed crystallographic orientation parallel to the electron beam.

The specimens on glass and c-Si substrates have been prepared by cleavage. The measurements have been performed by Mrs. E. Müller at the Solid State Physics Laboratory of ETH, Zurich.

3.8 Secondary Ion Mass Spectroscopy (SIMS)

The concentration of dopant atoms have been measured using secondary ion mass spectroscopy (SIMS). A depth profile of the dopant concentration is obtained from the measurements. In the case of a nonuniform depth profile, the concentration is determined by averaging the concentrations of three different depths.

The measurements of phosphorus content in the n-type specimens have been carried out at Charles Evans & Associates, specialists in materials characterization. The measurement is performed using a Cesium ion source against the specimen and counting the negative secondary ion mass as a function of time. The treated data gives the depth profile of the dopant concentration. The resolution of the system is 10^{16} cm^{-3} and the dynamic range is 4 and 1/2 orders of magnitude. The intensity of the secondary ions is proportional to the dopant concentration over the entire dynamic range. The calibration is performed using a P implant silicon standard.

The p-type samples were analysed at the 'Zentrum für Sonnenenergie und Wasserstoff Forschung', Stuttgart. Here a 40 KeV Ar^+ ion source was used. The detection limit in this case was 10^{19} cm^{-3} for phosphorus and 10^{18} cm^{-3} for boron. The calibration is performed using concentrations obtained from XPS and AES on a couple of samples.

Silicon density is assumed to be $5x10^{22}$ cm^{-3} for the calculations in all cases.

3.9 Plasma Characterization

Two different types of measurements have been performed to have a better understanding of the VHF plasma. These are 1) Optical Emission Spectroscopy (OES) and 2) Electrical measurements.These diagnostics have been performed by J.-L. Dorrier, A. Howling and Ch. Hollenstein at the Centre de Recherche de Physique des Plasmas, EPFL for hydrogen diluted silane plasmas [J.-L. Dorrier, 1990]. They are described briefly hereunder.

Optical Emission Spectroscopy (OES)

The optical emission spectroscopy (OES) of the plasma is useful to determine the concentrations of some of the radicals produced in the hydrogen diluted silane plasma. These radicals are recognised by their characteristic emission upon deexcitation. The following two radicals have been observed at their corresponding wavelengths: SiH at 414 nm and atomic H at 656 nm. SiH is often associated with the deposition rate and H is suspected to play a significant role in the surface kinetics during the μc-Si:H film growth [Oda, 1988].

The measurements are performed using an optical multichannel analyser (OMA). No dopant gas was used in this case. The influence of dilution and discharge power was investigated for a discharge frequency of 70 MHz. Some measurements were also performed at 13.56 MHz for comparison.

Electrical measurements

Electrical measurements such as the self bias and the peak to peak voltage present at the RF electrode are useful to determine the voltage profile between the two electrodes. From these, one can also determine the sheath potentials and evaluate the influence of the ion impact at the film growth surface. Details of the technique are given elsewhere [Howling, 1991].

References

D. Beeman, R. Tsu, M. F. Thorpe, Phys. Rev. B 32, 874 (1985)

D. Bermejo, M. Cardona, J. of Non-Cryst. Sol. 32, 405 (1979)

W. Beyer, pp.129 in 'Tetrahedrally Bonded Amorphous Semiconductors', Ed. D. Adler and H. Fritzsche, Plenum Press-New York (1985)

M. H. Brodsky, M. Cardona, J. J. Coumo, Phys. Rev. B 16, 3556 (1977)

M. Brunel, Analusis 17, 125 (1989)

E. Bustarret, M. A. Hachicha, M. Brunel, Appl. Phys. Lett. 52, 1675 (1988)

E. Bustarret, Private communication (1991)

G. D. Cody, Proc. of 2nd Int. Workshop on Physics and Applications of Amorphous Semiconductors, Turin (1988)

H. Curtins and S. Veprek, Solid State Comm. 57, 215 (1986).

H. Curtins, M. Favre, in 'Amorphous Silicon and Related Materials, Ed. H. Fritzsche, World Scientific Co.(1988) p.329

J.-L. Dorrier, Diploma project, CRPP, EPFL (Jan.1991)

P. M. Fauchet, I. H. Cambell, MRS Symp. Proc. 164, 259 (1989)

F. Finger, K. Prasad, S. Dubail, A. Shah, X. M. Tang, J. Weber, W. Beyer, MRS Symp. Proc.219, 383 (1991)

C. Godet, Ph.D. Thesis, Université de Paris-Sud, Centre D'Orsay (1987)

A. A. Howling, Ch. Hollenstein, P. -J. Paris, F. finger, U. Kroll, submitted to 20th Int. Conf. on Phys. of Ionised Gases, Pisa, July 1991.

Z. Iqbal, S. Veprek, J. de Phys. C, 15, 377 (1982)

N. M. Johnson, 'Hydrogen in Semiconductors',Semiconductors and Semimetals Vol 34, Ed. J. I. Pankove, N. M. Johnson, Academic Publ., San Diego (1991)

H. P. Klug and L. E. Alexander, X-ray Diffraction Procedures, John Wiley, New York (1954)

P. G. Le Comber, G. Willeke, W. E. Spear, J. Non-Cryst. Sol. 59&60, 795 (1983)

G. Lubberts, B. C. Burkey, F. Moser, E. A. Trabka, J. Appl. Phys. 52, 6870 (1981)

G. Lucovsky, R. J. Nemanich, J. C. Knights, Phys. Rev. B19, 2064 (1979)

Y. Mishima, M. Hirose, Y. Osaka, J. Appl. Phys. 51, 1157 (1980)

S. Oda, J. Noda, M. Matsumura, MRS Symp. Proc. 118, 117 (1988)
H. Richter, Z. P. Wang, L. Ley, Sol. St. Commun. 39, 625 (1981)
M. Schubert, G. Bauer, Phil. Mag. B, 62, 59 (1990)
J. Y. W. Seto, J. Appl. Phys. 46, 5247 (1975)
H. Shanks, C.J. Fang, L. Ley, M. Cardona, F. J. Demond, S. Kalbitzer, Phys. Stat. Sol. B 100, 43 (1980)
R. Shuker, R. W. Gammon, Phys. Rev. Lett. 25, 222 (1970)
C. C. Tsai, in 'Amorphous Silicon and Related Materials', Ed. by H. Fritzsche, World Scientific Co. (1988), New Jersey, 123
R. Tsu, J. G. -Hemandez, S. S.Chao, S. C.Lee, K.Tanaka, Appl. Phys. Lett. 40,534 (1982)
Y. Uchida, T. Ichimura, A. Ueno, M. Ohsawa, J. de Phys. 42 - Suppl., C4-265 (1981)
S. Veprek, F.-A. Sarott, M. Rückschloß, Proc. of ICAS-14, Garmisch-Partenkirchen (1991)
G. Willeke, in ' Amorphous and Microcrystalline Semiconductor Devices: Materials and Device Physics', Ed. J. Kanicki, Artech House, Norwood (in Press) (1991)
N. Wyrsch, F. Finger, T. J. McMahon, M. Vanacek, Proc. of ICAS-14, Garmisch-Partenkirchen (1991)

4. *MICROCRYSTALLINE SILICON FORMATION PROCESS*

4.1 Introduction

Three important conditions have been claimed to be necessary for the formation of microcrystalline silicon (μc-Si:H) using PE-CVD processes. These are (1) high dilution of silane in hydrogen, (2) high discharge power and (3) a high substrate temperature. The first two enrich the plasma with atomic hydrogen and the interface between the plasma and the film growth surface approaches partial chemical equilibrium PCE [Ensslen; 1987; Veprek, 1988]. Under these conditions a balance is reached between the deposition of silicon atoms and radicals and erosion of weak and disordered bonds promoting microcrystalline growth. The atomic hydrogen is understood to play a predominant role in the preferential elimination of the weak and disordered bonds by a chemical etching mechanism [Tsai, 1987 and 1988a] opening the way for tetrahedral configuration. Along with the first two, the high substrate temperature provides the necessary energy to enhance the surface mobility of the oncoming reactive species and for the desorption of surplus hydrogen [Matsuda, 1989]. Atomic hydrogen is also claimed to perform 'chemical annealing' i.e. interact with the weak silicon bonds and dangling bonds under the growth zone to induce energetic relaxation and restructure the silicon network [Shimizu, 1989].

In this chapter, a detailed investigation of the formation of undoped and doped μc-Si:H films, having a thickness of about 0.5 μm, using the VHF-GD technique will be presented. The influence of two of the important parameters, namely, the dilution of silane in hydrogen and the discharge power has been studied. A detailed investigation of the influence of substrate temperature indicated that μc-Si:H films with highest conductivity and maximum crystallinity was obtained at the optimum substrate temperature in the range of 150 to 200 °C [Prasad, 1991a]. This is the temperature range used for the series presented here. First, the influence of the silane concentration and discharge power on the different film properties are presented and discussed. The critical values of the deposition parameters influencing the microcrystalline to amorphous transition are elucidated. Microcrystallinity is verified by different techniques and is discussed in relation to the process parameters. Finally, the favourable influence of the VHF-GD on the preparation of μc-Si:H is considered, based on certain measurements of electrical potentials within the plasma and at the sheaths neighbouring the electrodes.

4.2 Deposition parameters

Dilution of silane in hydrogen

Four series of samples were deposited to study the influence of hydrogen dilution of silane for the deposition of undoped ('U'), phosphorus doped and boron doped films. Table 4.1 gives the details of the deposition parameters. The silane concentration is varied over a range where the transition from microcrystalline to amorphous silicon was observed. The discharge power is rather low (23 mW/cm^2) in the case of undoped and the two n-type series (1,2_a, & 2_b). For the p-type series (3) it is higher (150 mW/cm^2). The gas phase doping levels are 0.6 and 2% in the n-type series and 0.9% for the p-type series .

Table 4.1 Deposition parameters for the 'dilution' series:

no.	type	[Doping gas]/[SiH_4] (%)	[SiH_4]/[total] (%)	T_s (°C)	Power (mW/cm^2)	Pressure (mbar)
1.	'U'	0	3 to 10	200	23	0.4
2_a.	n	0.6	3 to 10	200	23	0.4
2_b.	n	2.0	1 to 5	150	23	0.4
3	p	0.9	1.5 to 5.5	160	150	0.8

Discharge power

Table 4.2 gives the details of the deposition parameters for the three series in which the discharge power has been varied. The doping levels are 0.6% for the n-type and 0.9% for the p-type series. Silane concentration of about 3.3% is used in the first two series, and for the last p-type series it is 1.6%. The power range is selected so as to study the influence of both relatively low and high power levels. In the first two series the minimum power used is just above the threshold required for plasma stability.

Table 4.2 Deposition parameters for the 'power' series:

no.	type	[Doping gas]/[SiH_4] (%)	[SiH_4]/[total] (%)	T_s (°C)	Power (mW/cm^2)	Pressure (mbar)
4.	'U'	0	3.3	200	23 to 190	0.4
5.	n	0.6	3.3	200	23 to 190	0.4
6.	p	0.9	1.6	160	37 to 375	0.8

4.3 Results

First, the results of the influence of silane dilution will be presented followed by that of discharge power.

4.3a Dilution of silane in hydrogen

Deposition rate

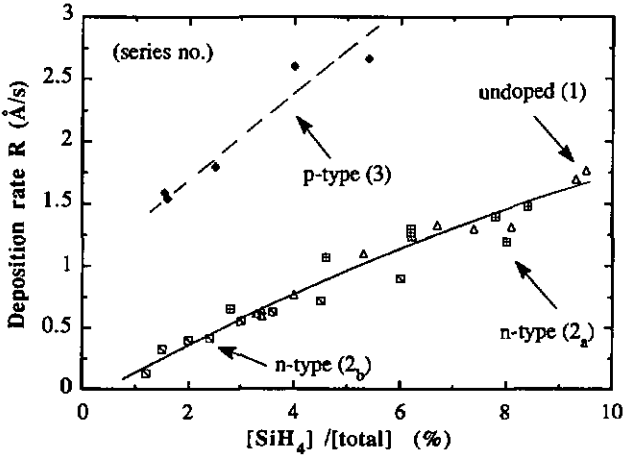

Figure 4.1 Deposition rate for the undoped, n-type and p-type series as a function of silane concentration.

Figure 4.1 illustrates the deposition rate as a function of the total silane concentration. For the first three series, an undoped and two n-type series which were deposited at the same low discharge power (23 mW/cm^2), the deposition rate is similar for a given silane concentration within the experimental scatter of 0.2 Å/s. It increases monotonously with increasing silane concentration. The deposition rate is significantly higher for the p-type series as it was deposited at higher power (150 mW/cm^2). It also increases more rapidly as the silane concentration increases from 1.6 % to 4%. In all the cases, one does not observe any discontinuous increase in the deposition rate from which one can expect any significant change in film morphology. In the p-type series, the increase of deposition rate from 1.5 Å/s to more than 2.5 Å/s could influence the film structure, since lower deposition rates are more favourable for microcrystallite nucleation while higher deposition rates lead to a-Si:H formation [Veprek, 1989].

Dark conductivity

The dark conductivities σ of these series are plotted in figure 4.2 respecting the same symbols. Here the sharp transitions of several orders of magnitude, indicating an amorphous to microcrystalline transition, is clearly observed as the silane concentration is increased.

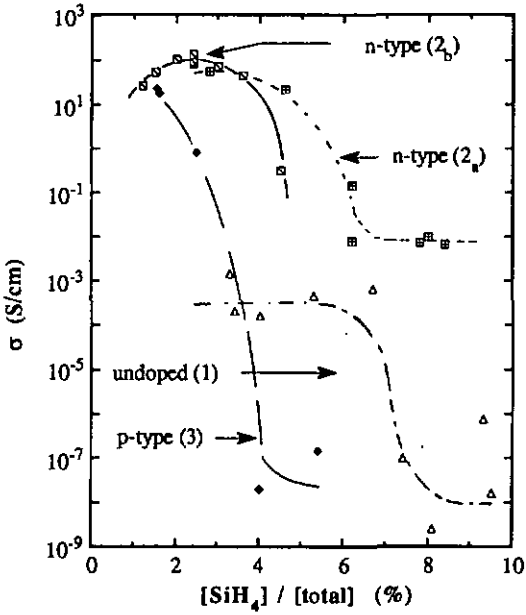

Figure 4.2 Influence of silane concentration on the dark conductivity.

First let us look at the undoped series (no.1). Below 6.5% of silane the dark conductivity σ is between 10^{-4} and 10^{-3} S/cm with an activation energy E_a in the range of 0.15 - 0.2 eV. Such a high conductivity is 4 to 6 orders of magnitude higher than those obtained for quality undoped a-Si:H, which has a dark conductivity typically in the 10^{-9} to 10^{-11} S/cm range. The wide scatter between 10^{-3} and 10^{-4} S/cm is possibly due to unintentional doping from the dopants outgassed from the walls since the specimens were produced in the same reactor where previously phosphorus doping was performed. Upon increasing the silane concentration beyond 7% the conductivity drops abruptly to 10^{-6} to 10^{-9} S/cm range and the activation energy rises to more than 0.6 eV. These values correspond to those found in undoped a-Si:H. From these results one can expect that these films are amorphous in structure though not fully optimised as compared to the solar-grade a-Si:H: i.e. having low defect density ($<10^{16}$ cm^{-3})

in the mid gap and viable for photovoltaic applications. Here too, the influence of stray doping could explain the wide scatter in conductivity observed in these films. In comparison the films obtained at lower silane concentrations and having much higher conductivities appear distinctly different and, upon further investigations described later in the chapter, are recognised as being microcrystalline in structure.

Let us now look at the two phosphorous doped series: no.2_a ($[PH_3]/[SiH_4]$=0.6% and Ts=200°C) and no.2_b ($[PH_3]/[SiH_4]$=2% and Ts=150°C). In both cases a transition from higher to lower conductivities by several orders of magnitude is observed upon increasing the silane concentration. In the case of series 2_a, which is deposited using the same temperature as the undoped series and a low doping level, the transition seems to occur at almost the same silane concentration. For the series 2_b which was deposited at a slightly lower temperature and a higher doping level the transition seems to occur in the vicinity of 4%. This difference in the transition threshold may be caused either due to the difference in temperature or the doping level. It could also result simply from a wide scatter in film properties in the transition region. A separate study of the influence of temperature indicates that this small temperature difference (from 200 °C to 150 °C) has little influence on the film conductivity [Prasad, 1991a]. On the other hand, from the results presented below, it is learnt that at higher doping levels the average crystallite grain size tends to decrease, suggesting that very high doping of phosphorous or boron may impede crystalline growth. Therefore, it is suspected that the possible shift in the microcrystalline to amorphous transition threshold to lower silane concentrations for series 2_b could be influenced by the higher doping level.

The highest conductivity of 130 S/cm with E_a of 12 meV is obtained for the specimen deposited at 2.3% of silane in series 2_b. Interestingly below this optimum concentration, the conductivity decreases, suggesting that the crystallinity of the film degrades. The maximum conductivity obtained at 2.8% silane in series 2_a is lower (53 S/cm) due to the lower doping level (0.6 %). The specimens having conductivities in the range of 1 to 130 S/cm are suspected to be microcrystalline. This is confirmed using other measurement techniques described later. In comparison, for silane concentrations higher than the transition threshold the conductivities obtained in series 2_a are close to 10^{-2} S/cm with E_a equal to 0.2 eV corresponding to that of phosphorus doped a-Si:H. Therefore, we can expect these samples to be amorphous. As observed in the figure, the transition is not complete in the case of series 2_b for the specimen deposited at 4% SiH_4. The conductivity is relatively high as compared to that of the previous series.

For the phosphorus doped series the range of silane concentration for which good quality microcrystalline film is produced is relatively large and comparable to the undoped series.

Finally, in the p-series (no 3) the highest conductivity of 22 S/cm with E_a of 15 meV is obtained only in the case of very low silane concentration (1.6%). This highly conductive material is also verified to be microcrystalline. The transition from the high to low conductivity is much steeper in this serie as σ drops by more than 9 orders of magnitude, to $2x10^{-8}$ S/cm with E_a= 0.6 eV, as the silane concentration increases to 4%. These values of σ and E_a do not correspond to those of p-type a-Si:H which has a conductivity typically in the range of 10^{-3} to 10^{-5} S/cm for comparable doping levels [Beyer,1984]. It appears that the specimen is undergoing a change from boron doped microcrystalline to poorly doped a-Si:H. The high discharge power (150 mW/cm^2) used for the deposition seems to produce a defect rich material which favours incorporation of all the dopant atoms in an inactive 3 fold coordination within the amorphous network [Street, 1985].

As the transition from microcrystalline to amorphous structure occurs at silane concentrations of about 2.5%, the range of silane concentration required for the formation of μc-Si:H seems to be rather small.

Structure

The X-ray spectra of three samples deposited at different silane concentrations and belonging to the undoped series (no.1) are plotted in figure 4.3 (bottom three curves). The sample deposited using 3.3 % silane exhibits sharp peaks corresponding to the <111>, <220> and <311> crystallographic planes parallel to the film surface. The ratios of the peak intensities correspond quite closely to those observed for polysilicon powder indicating that crystallite orientation within this material is random, i.e. without any specific preferential orientation, like in the polysilicon powder. For the sample belonging to the microcrystalline to amorphous transition threshold ([SiH_4] = 6.7%) the peaks are still weakly present with reduced intensity and broader full width at half maximum (FWHM). These indicate a decrease in the total number of coherently diffracting centres implying a reduction in the size of the crystallites. The last specimen, deposited using 8.1 % silane is identified as X-ray amorphous since it does not contribute any diffraction peak. Its amorphous structure is also confirmed by Raman scattering measurements presented later (figure 4.6). Thus the transition from the high conductivity to low conductivity correlates to the transition from a crystalline to a purely amorphous structure.

The X-ray measurements of phosphorus doped series also indicate similar modifications in the crystalline peaks. A noticeable difference is seen already for the most conductive specimens prepared at the lowest silane concentrations. In the case of series 2_a, the crystallite peaks are smaller in size (3rd curve from the top in figure 4.3) than for the undoped specimen prepared at comparable silane concentration. The peaks are reduced still further to the extent of

disappearing against the background noise in certain highly conductive specimens belonging to series 2_b - implying a structure that is amorphous to X-rays (2nd curve from the top). The sensitivity of the present system enables us to detect crystallites equal or larger than 100 Å only. The specimen defined as amorphous to X-ray is expected to be μc-Si:H as it has a conductivity of 70 S/cm. In fact its crystalline structure is verified by grazing angle X-ray diffraction described in the next paragraph. In p-type series, the <111> and <311> peaks are weak or absent while a strong <220> appears for the most conductive sample deposited at 1.6% of silane (top most curve). The peak situated near 39° is resulting from the diffraction on the aluminium contacts. The highly resistive samples are purely amorphous to the X-rays in all the cases. These results indicate that doping influences the film morphology. Boron doping causes a crystalline growth with preferential orientation of <220> planes parallel to the film surface, while high phosphorus doping seems to reduce the crystallite size.

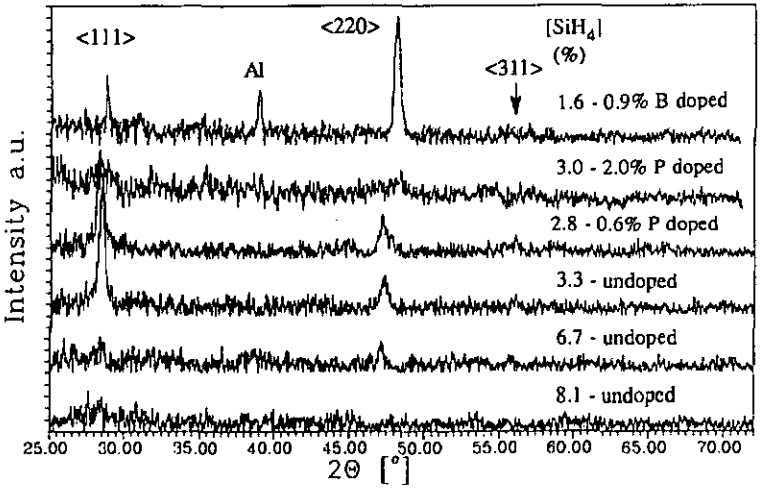

Figure 4.3. X-ray results for undoped series indicating the transition from microcrystalline to amorphous structure as the silane concentration is increased (bottom three curves). Top 3 curves indicate typical spectra of doped μc-Si:H showing the decrease and widening of <111> peak intensities upon doping as compared to the undoped specimen (3rd curve from bottom). The preferential orientation is observed in the <220> direction for the p-type specimen (top most curve).

A verification on the highly doped n-type specimen which appeared amorphous to the X-ray, was carried out using grazing angle X-ray measurement at CNRS-Grenoble. A grazing angle of 0.3° increases the volume of the probed specimen which reacts to the X-rays increasing the

sensitivity of the measurement [Brunel,1989]. The result is illustrated in figure 4.4. Clearly a vast difference is observed between this result and that presented earlier. Peaks corresponding to the <111>, <220> and <311> crystallite orientations are distinctly present and their evaluation corresponds to a grain size of about 60 Å. The resolution and sensitivity of the present set-up is clearly superior to that of the θ-2θ system used for most of our specimens.

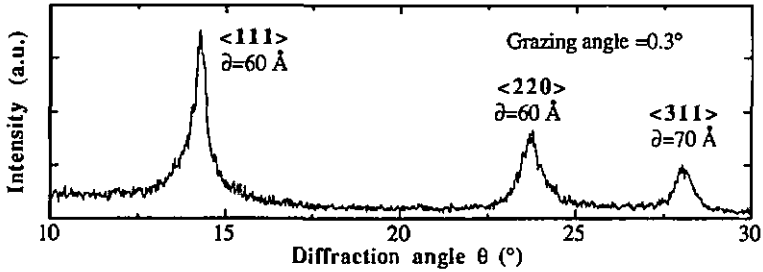

Figure 4.4 Grazing angle (0.3°) X-ray diffraction spectra of highly conductive n-type specimen which was identified as X-ray amorphous (2nd from the top) in figure 4.3.

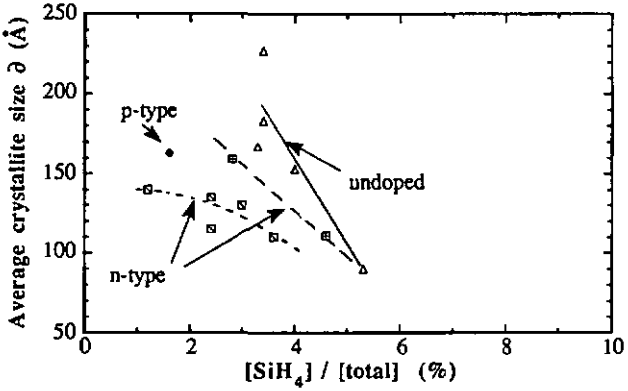

Figure 4.5 Average crystallite size ∂ determined using the FWHM and Scherrer's formula.

The average size ∂ of the crystallites have been determined by using Scherrer's formula and FWHM of the <111> peaks in the first three series and the FWHM of <220> of the p-type series. This is represented in figure 4.5. The figure indicates that the average grain sizes ∂ of the best undoped microcrystalline lies between 160 and 250 Å and reduces to less than 100 Å as the silane concentration increases to the microcrystalline to amorphous transition threshold.

For comparable low silane concentrations, ∂ is lower for phosphorus doped samples as compared to the undoped ones. This decrease is more pronounced in the case of more heavily doped 2_b series. For the p-type highly conductive sample ∂ is 160 Å. Thus one observes, in spite of the wide scatter in the evaluated values of ∂, a large difference in the average grain size of good quality μc-Si:H depending on whether they are doped or undoped. Segregation of dopants at the grain boundaries is suspected to reduce the crystallite sizes. The grain boundaries are low energy sites which allow dopant incorporation in 3 fold coordination as also observed in a-Si:H [Fripp, 1975; Street, 1985]. More on the influence of doping on ∂ will be presented in chapter 5. It can be concluded that the X-ray results, though indicative and with some limitations, provide evidence of the presence of crystallites in most of the highly conductive specimens. It also confirms the purely amorphous structure expected for the highly resistive samples.

The transition from microcrystalline to amorphous structure is also confirmed using Raman scattering experiments. Figure 4.6 illustrates the spectra for the films corresponding to the undoped series. An almost symmetric sharp peak, corresponding to the crystalline component, centred at 517 cm^{-1} wavenumber is observed for the most conductive film deposited at low silane concentrations. The shift of the peak of the crystalline component from 522 cm^{-1} obtained for c-Si is an effect of crystallite size and stress within the film [Richter, 1981; Fauchet, 1989]. The small asymmetry of the peak can be deconvoluted into another small contribution centred at a lower wavenumber which is attributed to the amorphous component. For the film belonging to the transition threshold concentration of 6.7%, a broad bump at lower wavenumbers is present along with the crystalline component. This is even more prominent in the specimen with 7.4% silane. This indicates a mixed phase morphology consisting of crystallites and disordered or amorphous network. The latter increases in proportion within the film with increasing silane concentrations. In the last spectrum ($[SiH_4]$ = 9.5%), the crystalline component has disappeared totally and the broad gaussian amorphous component confirms a purely amorphous or disordered structure. Similar results are also obtained for the doped series as well (series 2_a and 3). The data correlate nicely with the conductivity results and confirm the crystalline and amorphous structure of the specimens deposited at low and high silane concentrations, respectively.

The Raman spectrum of a microcrystalline structure consisting of uniform sized crystallites is best fitted with a Lorentzian line. For our specimens both the amorphous and crystalline components in the Raman spectra are best fitted by Gaussian lines. This implies that the crystallites within these specimens have a wide distribution in size which introduces a statistical broadening and enlarges the distribution of crystalline TO vibrational modes. The Gaussian distributions were used to determine the integrated intensities of both the peaks for the

evaluation of the crystalline volume fraction X_c. The FWHM of the amorphous component and its peak position were also determined to characterize the degree of disorder and the nature of the amorphous structure, respectively.

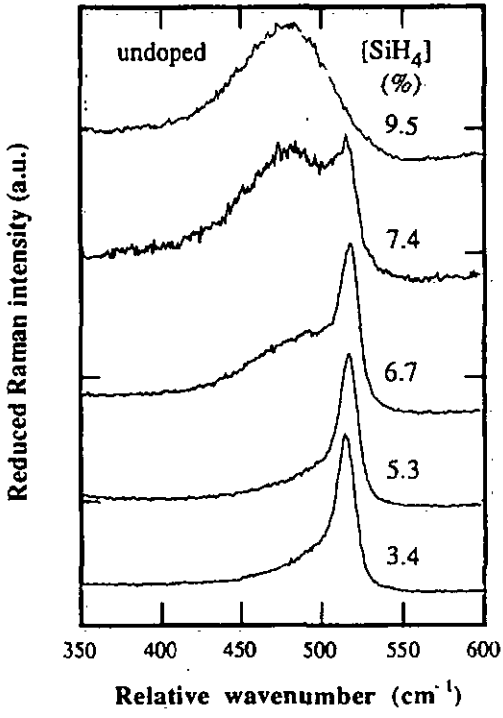

Figure 4.6 Raman spectra of undoped series indicating the transition from μc-Si:H to amorphous structure as the silane concentration is increased.

In figure 4.7 the crystalline volume fraction X_c has been plotted for series 1, 2_a and 3. The sharp transition behaviour is similar to that observed for the conductivity (figure 4.2) of these specimens. In all the three series, for the specimens having the highest conductivities, X_c is as high as 80 to 90% in the film. It drops down to 0 as the silane concentration is increased. The transition from crystalline to amorphous structure for the p-type series correlates rather nicely with the conductivity results. The transition is somewhat different for the n-type series(2_a) and the undoped series. For the n-type series it occurs at lower silane concentrations than for the undoped series, whereas in conductivity results (figure 4.2) this transition was weakly observed at similar silane concentration of 6-7% for both the series. A wide scatter in

the film property and measurement results in the transition zone is suspected to be at the origin of this descripancy. Besides, different influences of limited crystallite size on the Raman scattering cross section and the transport phenomena could be another possible reason. As mentioned in section 3.6 the drop in X_c can be expected to be more steep if one could introduce the effect of decreasing crystallite grain size on the Raman scattering cross sections [Bustarret, 1988].

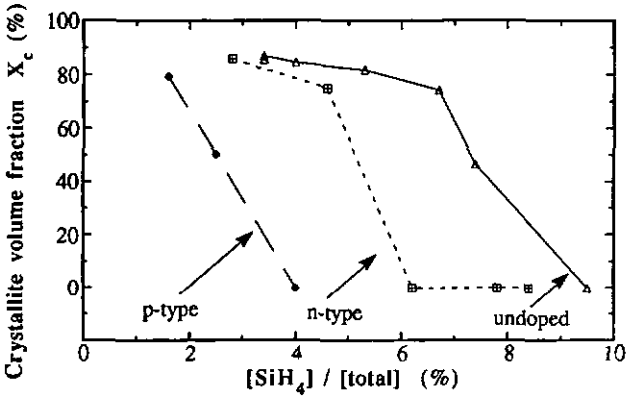

Figure 4.7 Crystalline volume fraction X_c as a function of silane concentration.

In figure 4.8a the FWHM of the amorphous component is represented for the three series: no.1, 2a and 3. A higher value of FWHM indicates a larger distribution of the bond angles and the presence of a greater degree of disorder in the material [Lannin, 1984]. One can see here that for increasing silane concentration the FWHM increases indicating an increasing disorder. The FWHM is minimum for the undoped microcrystalline specimen and has a value of less than 60 cm^{-1}. Such low values have not been observed in an amorphous network. Studies on structural modification in GD and LPCVD deposited specimen as a function of temperature indicate a discontinuous transition in the FWHM from values greater than 60 cm^{-1} in amorphous films to less than 50 cm^{-1} in crystallized ones [Bustarret, 1984]. Therefore, it seems that the disordered component existing in these μc-Si:H films, contributing to the amorphous peak, is different from what is commonly found in a-Si:H. The disordered or distorted silicon bonds at the surfaces of the crystallites forming the grain boundaries between two neighbouring crystallites contribute to this scattered broad 'amorphous-component'. The low values of a-FWHM implies that these specimens do not really contain any bulk amorphous tissue and the asymmetry observed at the low wavenumbers of the crystalline component in the Raman spectra is due to the phonon scattering at the grain boundaries. This is supported by the amorphous TO-peak position of these spectra (Figure 4.8b). The data resembles that of

figure 4.7 with the wave numbers in the y axis, ranging from 475 to 505 cm^{-1}. The TO-peak position of the amorphous component for normal a-Si:H specimens is generally situated around 481 cm^{-1}. This is well the case for all our amorphous specimens, undoped and doped, mentioned earlier. For the quality μc-Si:H specimens, having high values of X_c and low a-FWHM, the TO-peak is situated at 495 cm^{-1} or higher wavenumbers. Such a shift in the TO peak position is a signature of grain boundaries consisting of lattice mismatch in polycrystalline silicon and not due to the presence of any amorphous tissue [P. Fauchet, 1988 &1991]. Therefore, we seem to be dealing with a polycrystalline - like structure having crystallite size in nanometer range.

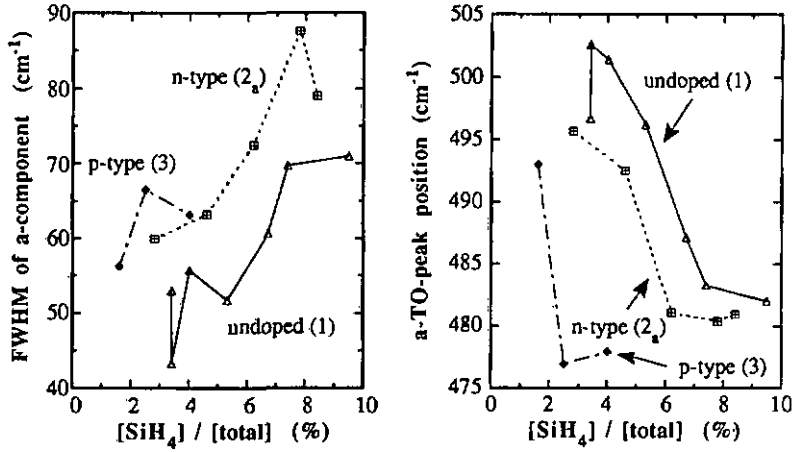

Figure 4.8a FWHM of the amorphous component for varying silane concentration.
Figure 4.8b TO peak position of the amorphous component for the same series.

The FWHM for the doped specimens is higher than for the undoped series (figure 4.8a). An increase in disorder as deduced from subgap absorption or ESR due to increasing defect states and dopant states is well known in doped a-Si:H [Street, 1985]. Recently, similar influence of doping on the a-FWHM has been reported for a-Si:H [Dusane, 1991]. Such an increase of disorder is observed in our doped amorphous films by the higher value of the FWHM of the a-component, as compared to that of the undoped specimens. From similar vertical shift also observed for the microcrystalline specimen, it is suspected that doping increases the disorder at the grain boundaries in μc-Si:H as well. Dopant segregation at the grain boundaries may be a possible source for such increase in the disorder. Additional proof for this is obtained from the higher value of absorption coefficient found in the high energy

range of the highly doped specimen. Such increase in the non-direct absorption is attributed to an increase in the grain boundary disorder and will be discussed in the chapter 5.

Figure 4.9 illustrates a high resolution TEM photograph of a highly conductive (σ=70 S/cm) n-type specimen, belonging to series 2_b, deposited on a c-Si substrate. The insert illustrates an electron diffraction image for the same specimen. Here, the regular diffraction points are obtained from the c-Si substrate while the concentric sharp rings formed by discrete spots indicate a random orientation of crystallites within the specimen. In the TEM photograph, on top one sees the c-Si substrate and the μc-Si:H/c-Si interface. It is interesting to observe that an orderless structure having a thickness of about 20 to 30 Å lies at this interface. This is thought to be the native Si-oxide, as it also has around the same thickness and as no in-situ cleaning process was performed on these substrates. A comparable experiment with an in-situ etching of the native oxyde should provide more evidence on this. Below this interface, the μc-Si:H structure can be seen. Crystallites ranging from 50 Å to more than 500 Å , oriented in all directions can be identified throughout the film thickness. Taking into account the magnification factor of 340000, one can identify lattice spacing of about 3 Å of the <111> orientation in many crystallites. The crystallites are indeed separated by lattice mismatch, as speculated earlier. Hardly any amorphous tissue can be identified between these crystallites (although this specimen was X-ray amorphous due to system limitations - 2nd curve from the top in figure 4.3). However, some amorphous layer can be identified at the air/film interface. This is attributed to a surface oxide which has a thickness of a few nm. This oxide layer is thicker and more non-uniform than the native oxide observed at the substrate/film interface. This is due to the defects introduced in the specimen during specimen preparation [Müller, 1991]. Note that, as one moves away into the film, from the air/film interface, the structural details are lost due to decreasing resolution.

TEM results of undoped specimen are found to be very similar to the n-type specimen. Besides, no difference was observed on the film structure for films prepared on glass or c-Si substrate. The crystalline structure is present from glass/film interface upto the top of the film. From the results of Raman scattering and TEM, we conclude that our undoped and n-type specimens resemble polysilicon material, usually prepared by thermal CVD process at higher than 500°C [Kamins, 1988], but with somewhat smaller grain size. In thermal CVD deposited poly-Si the grain size lies between 400 and 1000 Å.

The structural details are significantly different in a p-type specimen. Figure 4.10 illustrates a TEM photograph of a p-type highly conductive (σ=22 S/cm) specimen on glass. It was deposited using the process conditions of series 3, excepting for the gas phase doping level which was 0.4 % instead of 0.9%. In the insert, a typical electron diffraction image is also

included. Besides the sharp concentric rings as observed previously, it also illustrates some regularly spaced bright points resulting from some preferential crystalline orientation. However, it is not possible to identify the orientation due to the absence of any diffraction pattern from a known lattice orientation on the same image. These bright points may very likely be the diffraction from the <220> orientation since a preferential orientation in this direction is identified from the X-ray results (figure 4.3 and chapter 5).

The TEM photograph, indicates a strong columnar growth of crystallites and grain boundaries in form of needles extending more or less vertically throughout the specimen. A high power hydrogen plasma, as used in the present case, has a behaviour similar to a physical vapour deposition (PVD) [Tsai, 1987]. PVD is characterised by a line of sight deposition process which results in a strong columnar morphology. The high power plasma used for the preparation of the p-type specimen is suspected to behave more like a PVD process and is responsible for the resulting different structure. Compared to the n-type specimen which has a homogeneous crystalline structure, prominent fibrous structure is observed in the p-type specimen. Such a structure can be expected to have an anisotropic influence on the film properties. For example, the electrical charge carriers would encounter more grain boundaries while travelling perpendicular to the needles (coplanar mode) than vertically along the needles (transversal mode). This could produce a strong difference in the coplanar and transversal conductivity. Note that it is difficult to measure the latter, since the film growth on a conductive back contact may not be identical to that obtained on glass. A separate study needs to be undertaken to verify this.

A strange zone is observed at the film-glass interface. An amorphous layer having a thickness of about 330 Å forms a buffer layer between the glass substrate and the strong columnar morphology of the film. It is of importance to understand whether this is part of the glass substrate or the initial deposition of the film in the amorphous phase. A further investigation on a 250 Å thick p-type specimen, deposited under the same conditions also revealed such an interface, but was identified as belonging to the glass substrate as it was situated 250 Å below the film surface (details will be presented in chapter 6). Therefore, it is concluded that the buffer layer observed here forms part of the glass substrate which undergoes some reaction with the argon or hydrogen plasma. The precise reactions are still not clear. It is likely that this reaction occurs during the annealing process in which a 150 mW/cm^2 argon and hydrogen plasma is used to clean the substrate prior to the deposition. Similar interface for undoped or n-type specimens were unfortunately not photographed to verify if similar amorphous zone was also present on these specimens. Detailed investigation of glass surface by TEM after plasma annealing would be useful to understand the influence of such cleaning processes.

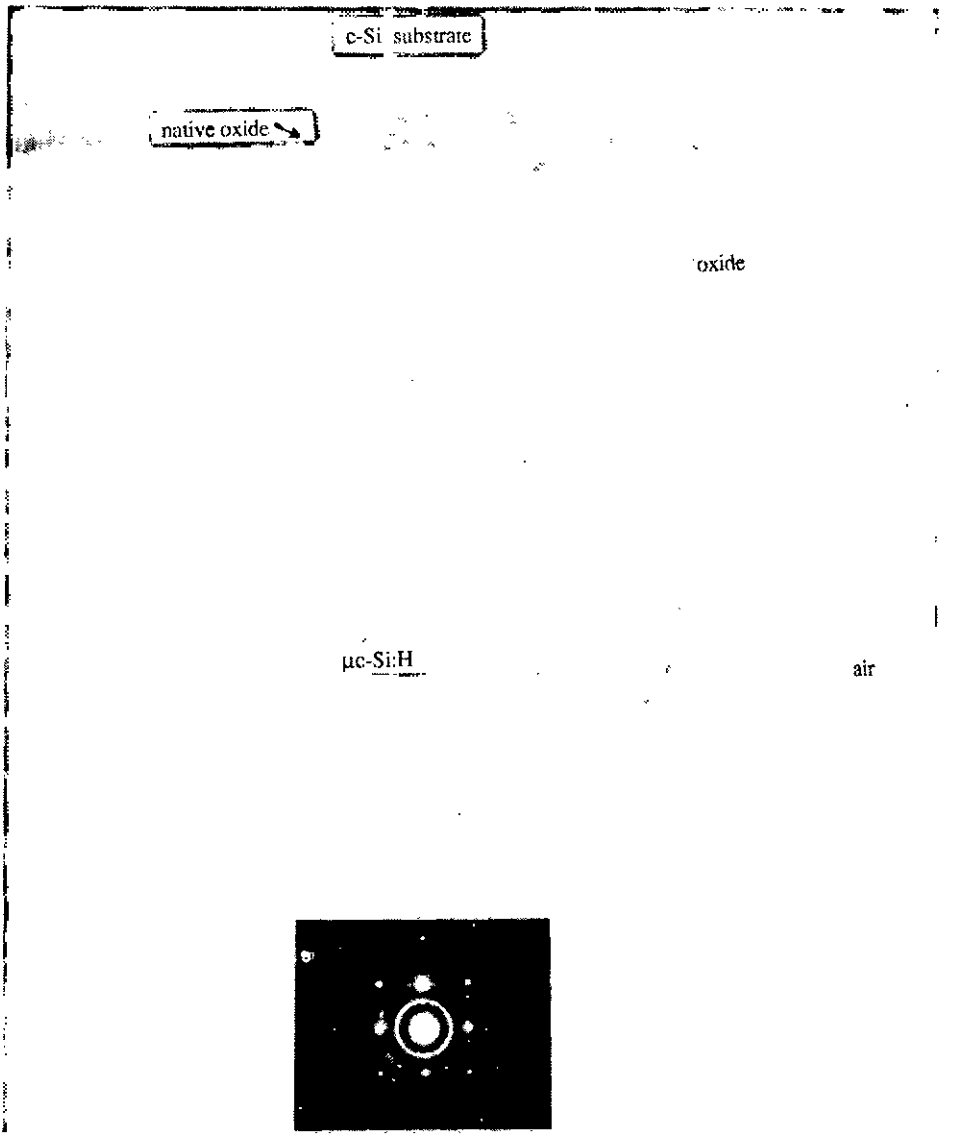

Figure 4.9 High resolution TEM photograph of a highly conductive n-type µc-Si:H (series 2_b, σ=70 S/cm) deposited on c-Si substrate (magnification factor: 340000).

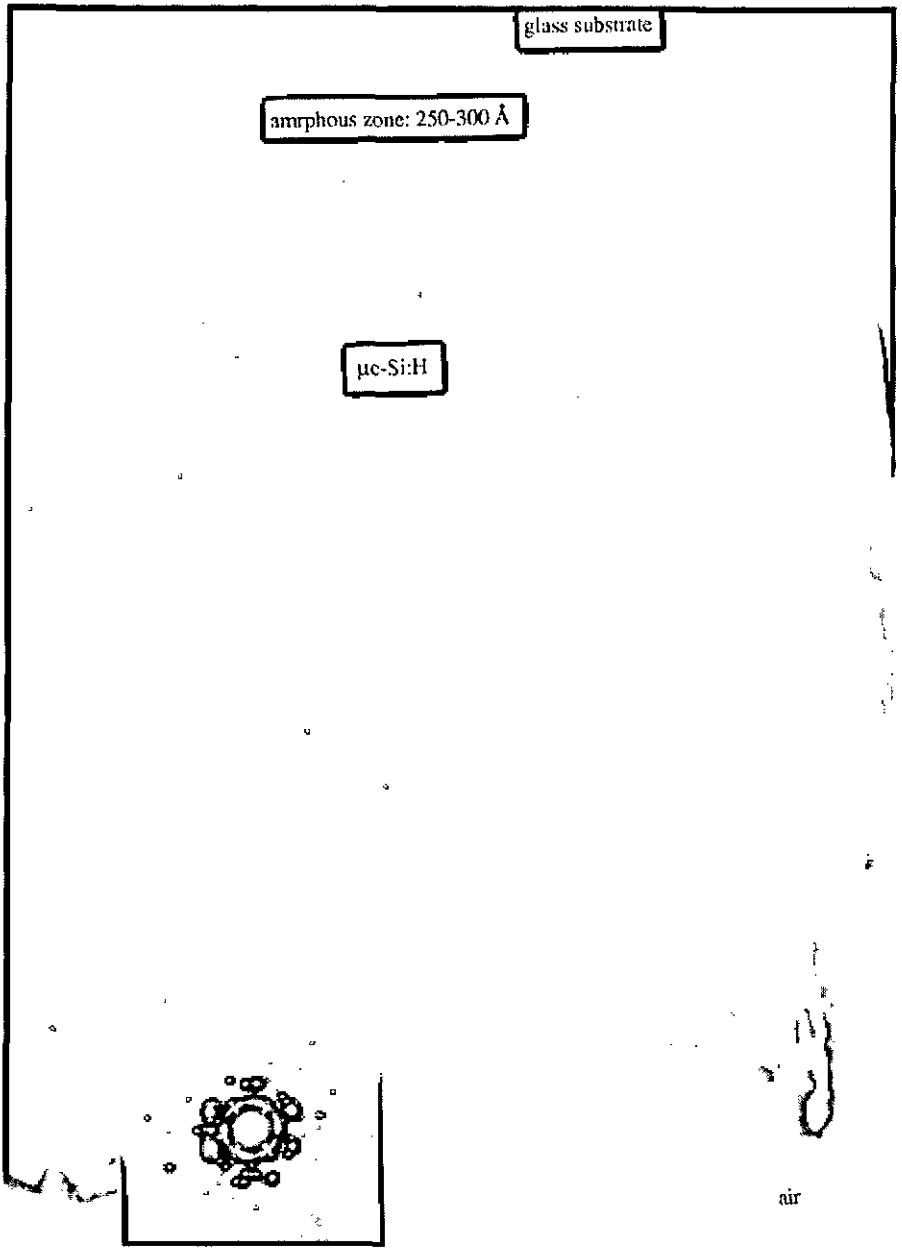

Figure 4.10 TEM photograph of p-type μc-Si:H (series 8, σ=22 S/cm) grown on glass substrate (magnification factor 110000).

Optical absorption

The modification in the film structure has important influence on the optical absorption property of these films as well. Figure 4.11a &b illustrates the absorption property of the undoped and phosphorus doped series, 1 and 2_a respectively. One can observe that, in both cases for films deposited at high silane concentrations and having an amorphous structure the optical absorption resembles that observed in a-Si:H. The absorption is very high for photon energies greater than 2 eV and below this energy level, it drops exponentially by several orders of magnitude. The Urbach energy E_0 in the case of the undoped film (figure a) is about 60 meV as determined from the experimental slope and 50 meV after subtracting the contribution of defects [Pierz, 1991]. The absorption $\alpha_{1.2}$ at 1.2 eV is 7 cm^{-1}. In usual high-quality undoped a-Si:H, having similar film thickness, the typical values of E_0 and $\alpha_{1.2}$ are less than 50 meV and 2 to 4 cm^{-1}, respectively. While the value of E_0 is comparable, the difference in $\alpha_{1.2}$ could be due to the the fact that our film has not been optimized in the amorphous structure. Influence from residual dopants which would increase the defect concentrations in the band gap could be another possible explanation.

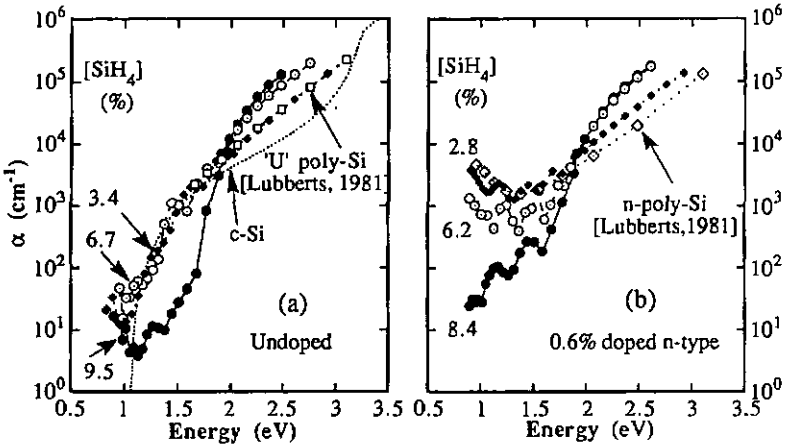

Figure 4.11 Optical absorption for (a) undoped series-1, and (b) for n-type series-2_a.

In comparison, for the n-type film deposited at 8.4% of silane the corrected E_0 is 68 meV and $\alpha_{1.2}$ is 80 cm^{-1}. Usually for n-type a-Si:H deposited using a comparable doping level, the corrected E_0 is reported to be less than 60 meV and $\alpha_{1.2}$ is about 200 cm^{-1} [Pierz, 1991]. This difference in E_0 is not clear. $\alpha_{1.2}$ is lower in our specimen suggesting that the total density of defects in the energy gap is lower for the same gas phase doping ratio. Similar results have been observed previously in n-type a-Si:H using the VHF-GD process where,

for similar gas phase doping ratios, the total defect densities and the solid phase incorporation of dopants were lower than those reported at 13.56 MHz. As the conductivities were also lower in this case [Prasad, 1988] it was concluded that the doping efficiency in a-Si:H is lower in the 70 MHz-GD than in 13.56 MHz. By doping efficiency we mean the ratio of the total active dopant concentration in the film over the total concentration of the dopant molecules in the gas phase during the preparation of the specimen.

As the film morphology changes from purely amorphous to microcrystalline with decreasing silane concentration, in both the series the absorption for energies greater than 2 eV is reduced, as compare to that of a-Si:H. This indicates a change in the electronic transitions and/or a decrease in contributions originating from the disordered grain boundary zones which undergo modifications. Interestingly, in this energy range the absorption coincides with that of undoped LPCVD poly-Si [Lubberts, 1981] and supports our previous assumption that the μc-Si:H resembles poly-Si. For energies lower than 2 eV the absorption increases indicating again a change in the nature of the electronic transitions. For undoped specimens, the increased absorption matches nicely with the absorption characteristic of c-Si (dotted curve) and is therefore attributed to the indirect transitions occuring within the crystallites. Based on this close resemblance one can also attribute the same energy gap of 1.1 eV of c-Si to the crystalline part of the μc-Si:H. Absorption data for poly-Si in this region was not available for comparison. The indirect transitions appear to mask out the subgap absorption resulting from defects in the gap of the disordered grain boundary regions. The latter would be comparable to values found in defect rich a-Si:H and would have a profile corresponding to that of the undoped specimen shifted upward by about an order of magnitude in the energy range between 1 and 1.5 eV. Considering the close resemblance of the absorption property of the undoped μc-Si:H with poly-Si in the high energy range, and with c-Si in the low energy range it would be of interest to study photoluminescence on μc-Si:H and poly-Si. This could probably be useful, in combination with Raman scattering measurements, to identify the proportion of photo-luminescent and non-photoluminescent amorphous tissues in both these materials.

The increase of absorption in the low energy range is much more pronounced in the case of doped films where, in fact, it tends to remain very high and even increases somewhat at very low energies. Such a pronounced increase has been explained by the collective excitation of free carriers originating from the doping effect, within the conduction or valence band [Mishima, 1980; Finger, 1991]. This increase is also accompanied by a decrease in the IR transmission for such doped films. This is observed in figure 4.12 and 4.13 where the optical absorption and the corresponding IR transmission curves are plotted for the highly doped n-type series (no. 2_b) and the p-type series (no.3), respectively.

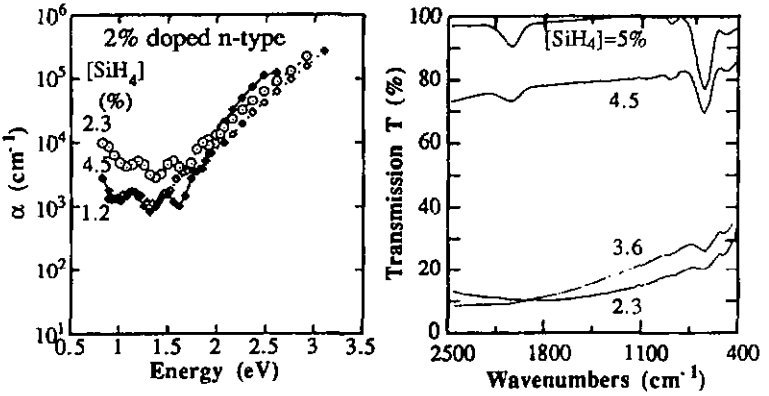

Figure 4.12 (a) Optical absorption and (b) IR transmission for n-type series-2_b.

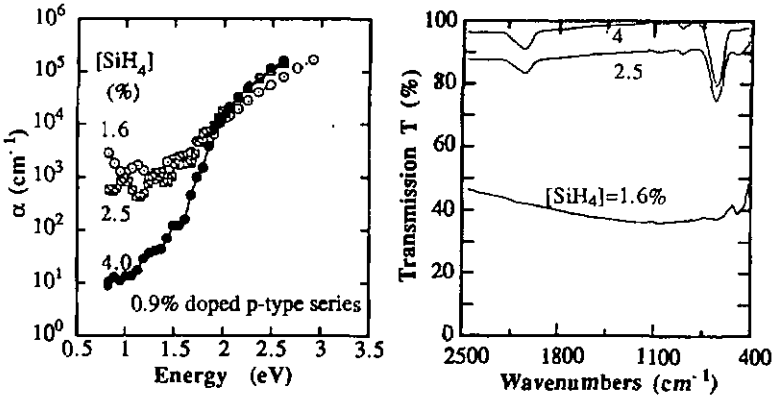

Figure 4.13 (a) Optical absorption and (b) IR transmission for p-type series-3.

The increase of absorption at low energy also correlates nicely with increase in conductivity which is expected to be due to an increase in the number of free carriers. Free carrier absorption is well known from doped crystalline semiconductors [Spitzer, 1957], and has also been used as an explanation of earlier studies of μc-Si:H [M. Stutzmann, 1989] and poly-Si [Mishima, 1980, Lubberts, 1981]. In those studies the Drude theory for free carriers was applied to the IR absorption or reflection spectra to determine the conductivity or mobility and free carrier density. This is done from a plot of $1/\alpha$ vs $1/\lambda^2$ using the absorption coefficient near the

plasma edge [Mishima, 1980]. This model has also been applied to some of the specimens presented in figure 4.12 [Finger, 1991]. Here we recapitulate the essential results very briefly. A quantitative evaluation of the specimen deposited using 2.4% of silane and having a coplanar electrical dark conductivity of 92 S/cm, yields unrealistic values of σ, μ and N. One obtains σ=360 S/cm, μ=76 cm^2/Vs and N =$3x10^{19}$ cm^{-3}. Carrier concentrations of about 10^{20} cm^{-3} have been reported from Hall measurements for highly conductive (σ=20 S/cm) μc-Si:H prepared at 40 MHz using comparable doping levels [Spear, 1983]. The maximum Hall mobility in such films, having an activation energy less than 40 meV, is reported to be close to 2 cm^2/Vs [Le Comber, 1983]. In comparison, in our results the values of σ and μ seem too high, whereas the value of the carrier concentration N appears too low. As seen from this wide discrepancy, a simple use of the Drude theory is therefore inadequate. Similar conclusions are also reached for poly-Si [Lubberts,1981]. It is surprising that below 1500 cm^{-1} the transmission also increases with an increase in the IR reflection coefficient, although one would expect it to decrease since the absorption is expected to increase. Besides, as the higher values of σ and μ obtained from the above analysis corresponds more closely to that observed in c-Si [Sze, 1981] it is likely that it reflects the values of these parameters within the crystallite itself, without the interaction of the charge carriers at the grain boundaries. We shall later try some estimation of the carrier concentration to estimate the effect of dopant segregation.

As mentioned before, in the case of a-Si:H the absorption coefficient drops steeply below a photon energy of about 2 eV. For evaluating the optical gap, in the case of a-Si:H, the energy at which the absorption coefficient has a value of 10^4 cm^{-1} (E_{04}) is often used. This value marks an energy threshold below which the optical absorption is reduced by several orders of magnitude due to a change in the nature of the transitions. In the case of doped μc-Si:H, however, below this energy level, because of the contribution from free carriers, the absorption barely reduces by an order of magnitude. Therefore, it is meaningless to evaluate E_{04} and use it as a parameter to compare 'optical gaps' which is commonly associated with transparency of the material. Attempts to determine an 'amorphous gap' using Taucs model $(\alpha E)^{1/2}$ vs E and a 'microcrystalline gap' using $\alpha^{1/2}$ vs E, for μc-Si:H, as suggested by Hachicha [Hachicha, 1988] also do not lead to any conclusive results. No suitable fit is obtained over large range as obtained for a-Si:H and therefore one cannot obtain an unambiguous extrapolated 'gap'. Recently some new results have emerged by fitting the results of photo emission spectroscopy (PES) which are interpreted in terms of composit band structure - one having a crystalline silicon like band and the other a wider gap resembling amorphous silicon [Willeke, 1991]. Further investigation in this direction may lead to a better understanding of the 'energy gap'.

IR Transmission

In figure 4.12b and 4.13b, besides the drop of the IR transmission changes in the features of the absorption peaks are also observed. In amorphous films deposited at high silane concentrations, the peak at 630 cm^{-1} is attributed to vibrational excitations of SiH, SiH_2 and SiH_3 bonds. The signatures situated at 850 cm^{-1} and 890 cm^{-1} are associated with dihydride ($=SiH_2$) and polyhydride ($(=SiH_2)_n$) vibrational modes. These bonds also produce a signature at 2100 cm^{-1}, as seen from the assymetry of the 2000 cm^{-1} peak, in these figures. Finally the peak centred at 2000 cm^{-1} is attributed to the stretching vibrations of monohydrides (Si-H). As the film grows microcrystalline, most of the signatures maintain their energetic positions whereas their amplitudes and symmetry are modified. The signature at 2000 cm^{-1} is asymmetric towards or completely shifted to 2100 cm^{-1}. This is attributed to SiH_3 and $(SiH_2)_n$ or Si-H vibrational modes [Tsai , 1988a &b]. These groups are mainly situated at the surfaces of the crystallites and in the disordered tissue forming the grain boundaries, as only very small amount of hydrogen can be expected within the crystallites [Johnson, 1991]. In the very highly conductive films, the 2100 cm^{-1} peak is almost imperceptible due to the shift of the base line. Note that the asymmetry of the 630 cm^{-1} peak is an artifact resulting from the slope of the background signal. Upon correction, the peak reappears symmetric. The hydrogen concentration measured by hydrogen evolution and elastic recoil detection analysis (ERDA) is typically about 5 to 7 at% in our μc-Si:H specimens [Finger, 1991]. Most of this hydrogen is expected to be situated at the grain boundaries, passivating defects or even dopants.

Dopant incorporation and carrier concentration

The dopant incorporation within the films is plotted in figure 4.14. In all cases, the dopant incorporation is lower in films deposited using lower silane concentration which resulted in μc-Si:H and higher in the a-Si:H prepared at higher silane concentration. This tendency is particularly pronounced in the p-type series where the boron concentration increases by almost a factor five as the film morphology changes from microcrystalline to amorphous. In spite of a higher dopant incorporation the conductivities are significantly lower in the latter case due to a completely different doping mechanism. It is known that in a-Si:H most dopants tend to remain unionised by three fold coordination, and not contribute any free carriers [Street, 1985]. Besides, a correlation exists with the density of defects in the gap and the shift of the Fermi level caused by the active dopants [Street, 1985]. This is seen by the higher value of $\alpha_{1.2}$ in the doped a-Si:H as compared to the undoped one [Pierz, 1991].

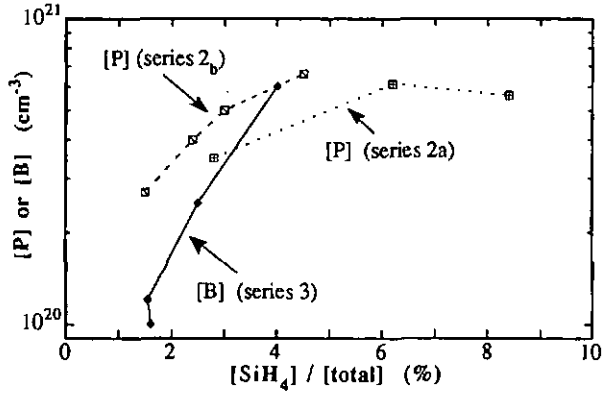

Figure 4.14 Incorporated dopant concentration as a function of silane concentration.

In μc-Si:H, a significant amount of dopants are expected to be incorporated in the 4-fold coordination within the crystallites, as found in c-Si. At this point, however, it is not clear whether all the dopants in the μc-Si:H are ionised. One needs to know additional parameters such as the mobility to determine the concentration of the active dopants which contribute free carriers. It cannot be excluded that even in μc-Si:H, a certain amount of dopants segregate into the disordered grain boundary zone and remain inactive. Such behaviour has been reported for p-type μc-Si:H [Hamasaki, 1983]. To obtain some information the carrier concentration has been evaluated for the n-type series 2_a and the p-type series 3. The values of mobilities have been selected as follows. For microcrystalline specimen, as the structure is found to be similar to that of polysilicon a mobility of 10 cm^2/Vs has been assumed. Drift mobilities ranging between 10 and 50 cm^2/Vs have been reported for n- and p-type polysilicon having grain sizes greater than 1000 Å and having high concentrations of dopants [Kamins, ch.5, 1988; Seto, 1975]. Considering that due to the smaller grains in our μc-Si:H carriers would encounter more grain boundaries, we have selected the minimum value of mobility of 10 for our μc-Si:H specimens. On the other hand, preliminary Hall measurements on the highly conductive n-type μc-Si:H belonging to the doping series (no. 7) presented in the next chapter gives a Hall mobility between 1 and 3 cm^2/Vs [Dubois, 1991]. So a mobility of 1 cm^2/Vs has also been used in our estimations.

For a-Si:H, free electron and hole mobility μ of 10 and 1 cm^2/Vs, respectively, have been reported recently [Kocka, 1991]. The drift mobility μ_D in a-Si:H is related to the free mobility by the relation [Tiedje, 1984],

$$\mu_D = \mu x n_{free}/(n_{free} + n_{trap}) \qquad (4.1)$$

Considering that most of the carriers generated from the active dopants are trapped in the band tails or deep defects, and only 10 % of the generated carriers at most are free, the value of 1 and 0.1 cm^2/Vs have been considered for the drift mobilities of electron and hole, respectively, for our doped a-Si:H films.

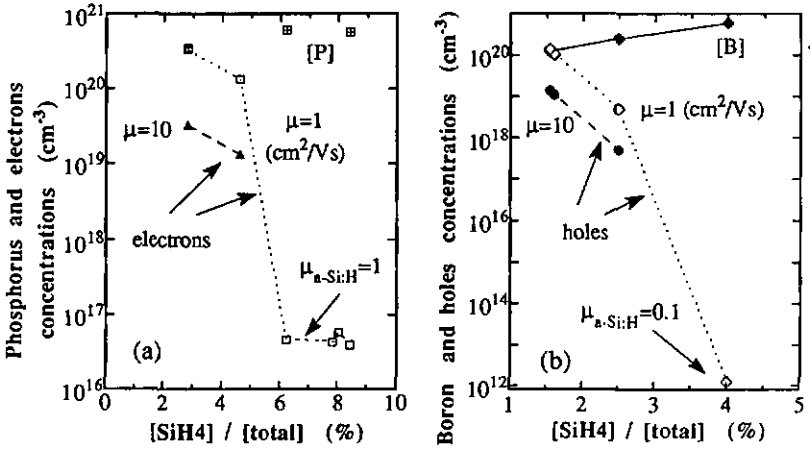

Figure 4.15 Variation of dopant and total carrier concentration in the films as a function of silane concentration in (a) n-type series no. 2_a, and (b) p-type series 3.

The concentration of the electron and holes for these films have been determined by substituting the corresponding values of mobility and conductivity in the equation $\sigma=Ne\mu$. The results are plotted in figure 4.15a and b for the n- and p-type series, respectively. For $\mu=1$ cm^2/Vs the free carrier concentration coincides with the dopant concentration in good quality μc-Si:H obtained at the lowest silane concentrations. In less crystalline specimen obtained at higher silane concentration the carrier concentration is much lower than the dopant concentration. This indicates that some of the dopants are not contributing any free carriers. Two explanations are possible: 1) dopant segregation at the grain boundaries as the incorporation of the dopants in the grain boundaries is energetically favourable [Fripp, 1975]. Dopant segregation and their inactivity within grain boundaries has been observed in polycrystalline [Polyse '90, 1991]. Moreover, as in μc-Si:H the ratio of surface to volume of the crystallites is increased due to the smaller crystallites, one can expect a more pronounced effect of segregation than found in poly-Si. And 2) carrier loss due to trapping in states situated at the grain boundaries, as found in poly-Si [Mandurah, 1980]. If one assumes $\mu=10$ cm^2/Vs, the difference in the carrier and dopant concentration is more pronounced than before and present even in the best μc-Si:H films. The grain boundaries, which are influenced by the

structural properties of the specimen, control the carrier trapping and dopant segregation. These in turn define the transport properties such as the conductivity and mobility. At this point it is not possible to obtain any conclusive information on the mobility or carrier concentration in our specimens: both of them being inter related. Detailed studies of Hall measurements are necessary for this.

In a-Si:H specimens, the free carrier concentration lies several orders of magnitude below the total dopant concentration. It is four orders of magnitude lower than the phosphorus concentration for the n-type series resulting from the poor doping efficiency observed in a-Si:H due to the three-fold inactive incorporation of dopants. As can be expected from the poor conductivity results, for the p-type a-Si:H specimen, the concentration of holes is extremely low indicating the poor doping effect in these films.

4.3b Influence of discharge power

Let us now look at the influence of discharge power for the three series described in table 4.2.

Deposition rate

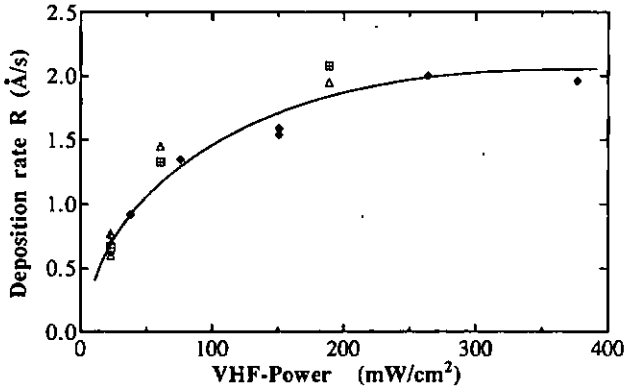

Figure 4.16 Deposition rate as a function of discharge Power.

The deposition rates for the undoped (series no. 4), n-type (no.5) and p-type (no.6) series are plotted in figure 4.16. In all the series they are comparable for a fixed discharge power. For the p-type series, which is prepared using the largest power range and 1.6 % of silane, the deposition rate increases monotonously and reaches a saturation around 2 Å/s. This is possibly

due to silane depletion within the plasma. A rough estimation considering a silane flow of 1.6 sccm yields a deposition rate of 4.5 Å/s under the assumption that all the silane molecules are consumed and contribute to the deposition on all the surfaces around the plasma zone. The value of 2 Å/s compares well with the above estimate, if one takes into account that due to the accompanying high flux of hydrogen, all the silane molecules may not enter the plasma zone, or may not have sufficient time to decompose. Thus, the prominent influence of the discharge power is to influence the deposition rate until depletion of the source gas occurs.

Dark conductivity

The dark conductivities of the three power series are represented in figure 4.17. The increase of the discharge power does not seem to influence the undoped films. It maintains an almost constant conductivity corresponding to μc-Si:H.

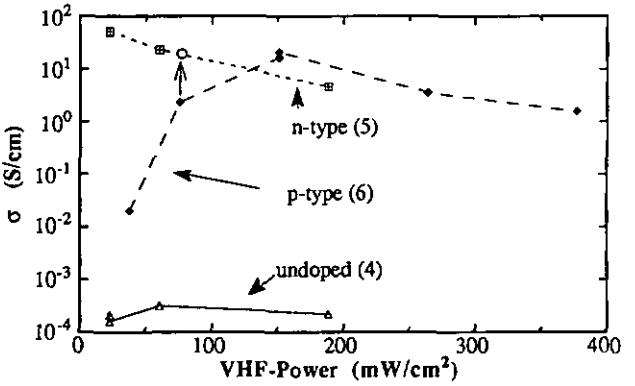

Figure 4.17 Dark conductivity as a function of discharge power.

In the phosphorus doped series (no.5) the highest conductivity is obtained for the lowest discharge power. Upon increasing the power from 23 to 188 mW/cm^2 the conductivity drops by almost an order of magnitude suggesting a deterioration of the film property. Changes in either the crystalline structure or the doping effect could influence such a change in conductivity. An increase of the disorder in the grain boundaries would increase the potential barrier E_b which the charge carriers have to overcome while crossing over the grain boundaries and would therefore decrease their mobility. Alternatively, such an increase of disorder could enhance dopant segregation, thus decreasing the total number of active dopants that contribute free carrier. Both these effects would result in a lower conductivity.

The strongest influence of power on conductivity is found for p-type films (series 6). Initially for the lowest discharge power it is very resistive comparable to doped a-Si:H. The conductivity increases with power and reaches the highest conductivity of 22 S/cm at 150 mW/cm^2. Once again, for still higher powers, like in the n-type series, the conductivity deteriorates. The initial strong increase suggests a transition from an amorphous to microcrystalline structure, which is confirmed by structural measurements presented later. As compared to phosphorus doping, boron doping critically influences the microcrystalline formation. A minimum power threshold needs to be reached before microcrystalline formation can take place. In spite of the lower silane concentration this threshold is relatively high as compared to the n-type series. This threshold also seems to be dependent on the doping level since upon reducing the doping level to 0.4%, conductivity of 30 S/cm is obtained using half the discharge power (75 mW/cm^2) (see point o in figure 4.17).

Film Structure

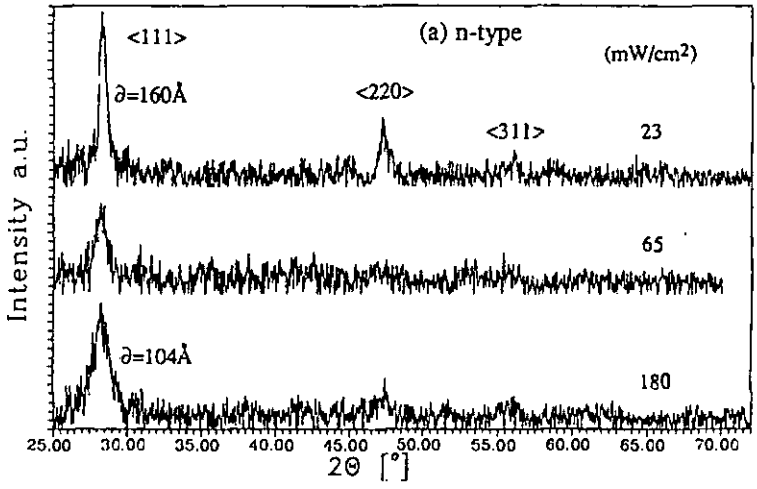

Figure 4.18 Influence of discharge power on the X-ray spectra of n-type series (no.5).

The deterioration of the film conductivity, at higher discharge powers, is also accompanied by a structural modification as expected in the n-type series. Figure 4.18 shows how the crystallite peaks are reduced and enlarged for increasing discharge power for the series 5 confirming the deterioration in the film structure. The average crystallite size ∂ evaluated from the FWHM of the <111> peak decreases from 160 to 104 Å as the discharge power is increased from 23 to 188 mW/cm^2. This decrease results in an increase in the total grain boundary zone which

surrounds the crystallites. From this we can expect the crystalline volume fraction X_c also to decrease.

In figure 4.19 the spectra for the p-type series are plotted. First the transition from amorphous to microcrystalline structure by the appearance of the <220> peak indicating the preferential orientation of the crystallites can be noted. At still higher powers the deterioration of the crystalline structure is clearly observed again by the reduction in the peak intensity, in agreement with the conductivity results. A maximum crystallite size ∂ of 160 Å is evaluated from the <220> peak of the most conductive specimen prepared at 150 mW/cm^2. It decreases at higher discharge powers and cannot be evaluated at lower discharge powers.

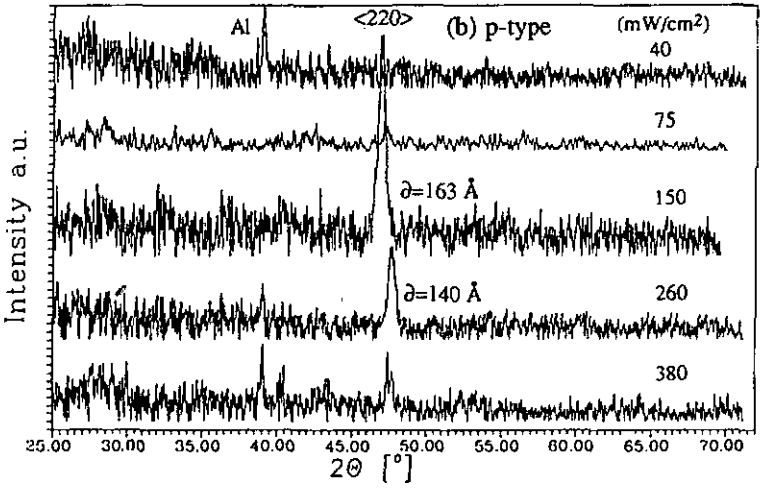

Figure 4.19 Influence of discharge power on the X-ray spectra of p-type series (no.6).

This structural modification is also confirmed by Raman scattering. Figure 4.20a and b illustrates the Raman results for the *n* and *p-type series, respectively. For the n-type series* (figure a), the increase of the asymmetry of the crystalline peak from the increasing contribution in the low wavenumbers is seen in the specimen deposited at higher discharge power. This reflects an increase in the grain boundary disorder which contributes to the amorphous-like component . The crystalline volume fraction X_c decreases slightly from 86 %, in the low power specimen, to 80 % in the high power one. The increase in the ratio of the surface to volume of the crystallites due to the decrease in the crystallite size, mentioned before, can explain this small increase in the grain boundary disorder.

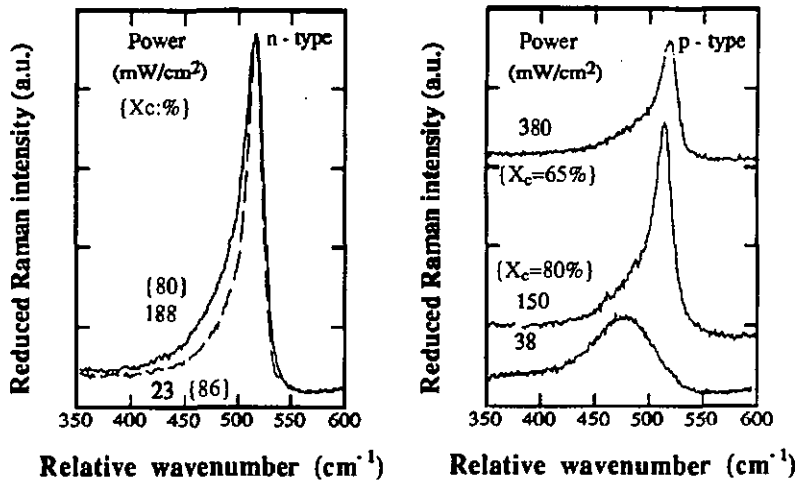

Figure 4.20 Raman spectra of (a) n-type series-5 and (b) p-type series-6, showing the influence of discharge power on the structure of the specimens.

In the p-type series (figure b), the amorphous structure suspected at low power is confirmed by the presence of a broad amorphous component centred at 480 cm^{-1} and the absence of any crystalline signature. For the most conductive specimen deposited at 150 mW/cm^2, a large crystalline peak is obtained, though with some small contribution in the low wavenumbers. The reduced peak intensity of the crystalline component and the increase in its asymmetry for the film deposited at the highest power indicates a deterioration in the crystalline structure of this film and supports the X-ray and conductivity results. The crystalline volume fraction X_c decreases from 80 % to 65 % in the high power specimen. The deterioration of the film crystallinity at high powers is therefore confirmed. It is suspected that this structural deterioration can be induced by the high energy ions impinging onto the film growth surface. These could for example introduce local dislocations during the film growth, thereby cumulating more defects and grain boundaries in the material. Such structural modification is also observed in the undoped specimens. However, as the conductivity remains unaffected in this series, the decrease of conductivity in doped specimens cannot be explained merely from an increase in the potential at the grain boundaries. As mentioned earlier, the decrease of conductivity in doped specimens deposited using high discharge powers, could be related with the doping mechanism. The increased disorder could enhance the dopant segregation at the grain boundaries, thereby reducing the total number of free carriers participating in electrical transport.

Optical absorption

The optical absorption for the n and p-type series are represented in figure 4.21. For the n-type specimens (figure a) the absorption at high energies (E>2 eV) corresponds to that observed previously for the μc-Si:H. It is not influenced by the discharge power, since the structure does not undergo any transition from microcrystalline to amorphous phase. However, in the low energy range, a decrease in the free carrier absorption is observed at higher discharge power. A similar downward shift is also observed in the p-type series (figure b) as one goes from the 150 to 380 mW/cm^2 specimens. The decrease of the free carrier absorption at higher discharge powers provides an independent qualitative confirmation of the decrease in the total number of active dopants within the crystallites. A correlation with the total density of dopants incorporated in the material could provide some information on whether the decrease of free carriers is due to an enhanced segregation of dopants to the grain boundaries or if the dopant incorporation itself is influenced at high discharge powers.

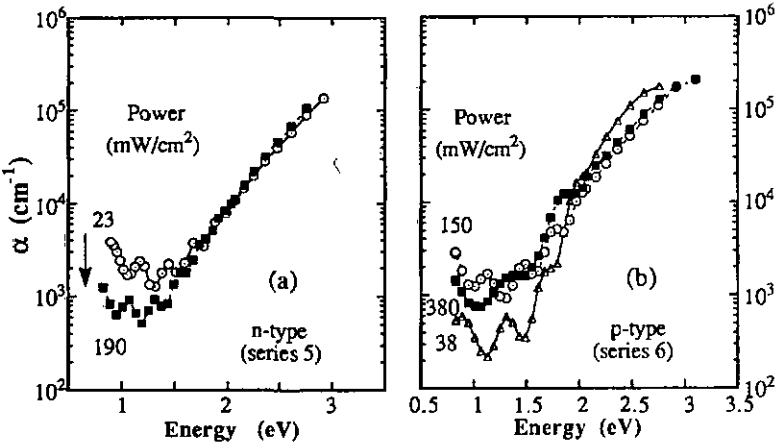

Figure 4.21 Optical absorption for (a) n-type series and (b) p-type series.

The absorption characteristics of the specimen obtained at 38 mW/cm^2 corresponds to that of a doped amorphous silicon film, and confirms its amorphous structure. Its conductivity of $2x10^{-2}$ S/cm suggests a better doping effect in this specimen, as compared to the conductivity of 10^{-8} S/cm obtained in a poorly doped amorphous specimen deposited at 4% of silane concentration discussed in section 4.3a. The influence of this higher doping effect is also observed in the higher value of $\alpha_{1.2}$ (350 cm^{-1}). This reflects the increase of the subgap defect density due to the shift of the Fermi level by doping [Street, 1985; Pierz, 1991].

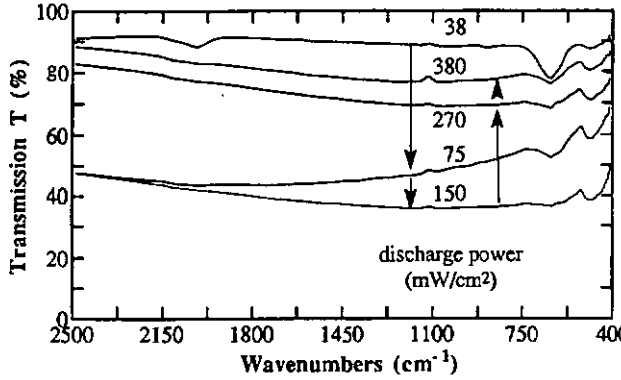

Figure 4.22 IR transmission results of p-type series (no.6) showing the rise of the of the total transmission with increasing disorder in the structural properties.

The shift in the low energy range is also observed in the IR transmission for the p-type series (figure 4.22). Similar features as discussed in the previous IR results can also be noticed here. The vertical shift downward of the transmission can be observed as the film structure changes from amorphous to microcrystalline and the contribution of the free carriers become significant. Beyond the optimum discharge power of 150 mW/cm^2, the transmission rises, as expected from the suspected decrease in the free carrier contribution, which explains their lower conductivities as well. It should be noted that although the transmission of the 380 mW/cm^2 sample is very close to that of the amorphous one prepared at 38 mW/cm^2, the absorption features are different. The 38 mW/cm^2 specimen exhibits a more pronounced peaks at 630 and 2000 wavenumbers corresponding to that of a-Si:H. The peak intensities in the microcrystalline specimen is smaller suggesting a lower hydrogen content. Besides, the contribution at 2100 cm^{-1} is more pronounced as compared to at 2000 cm^{-1}. In the absence of any absorption peak around 850 and 900 cm^{-1}, as observed in our case, it is attributed to the presence of Si-H bonds on the crystallite surfaces [Beyer, 1985].

Dopant incorporation and carrier concentration

To verify how the higher discharge power influences the dopant and carrier concentrations in these specimens, the dopant concentrations have been analysed by SIMS and the carrier concentration is determined assuming a mobility of 1 cm^2/Vs in all μc-Si:H specimens and 0.1 cm^2/Vs in p-type a-Si:H. The results are plotted in figure 4.23. The concentration of phosphorus and electrons coincide in the most conductive specimen obtained at the lowest

discharge power. This is also observed in the most conductive p-type specimen obtained at 150 mW/cm^2. While the phosphorus concentration decreases a little at higher discharge powers, the evaluated concentration of electrons decreases much more rapidly. This tendency is even more pronounced in the p-type series. While the boron concentration remains almost constant over the entire range of the discharge power, the concentration of holes decreases rapidly in the high power range where the structural deterioration is observed. These results show that in the n-type series, the dopant incorporation decreases at higher powers by a factor two whereas the conductivity decreases by almost one order of magnitude. In the p-type series, the dopant incorporation seems to be unaffected by the discharge power within experimental scatter while the concentration of holes decreases by more than a factor 10. Two explanations are possible for the strong decrease of the estimated free carriers, observed in both the series, which lead to a lower conductivity and a decrease in the low energy absorption. Either, as speculated previously, the increased structural damage produced at high discharge powers leads to an enhanced dopant segregation at the grain boundaries and reduces the number of active dopants. Or, due to the structural defects the mobility is reduced strongly and the mobility values used here for the high power specimens lead to a wrong evaluation. We suspect that both play some role.

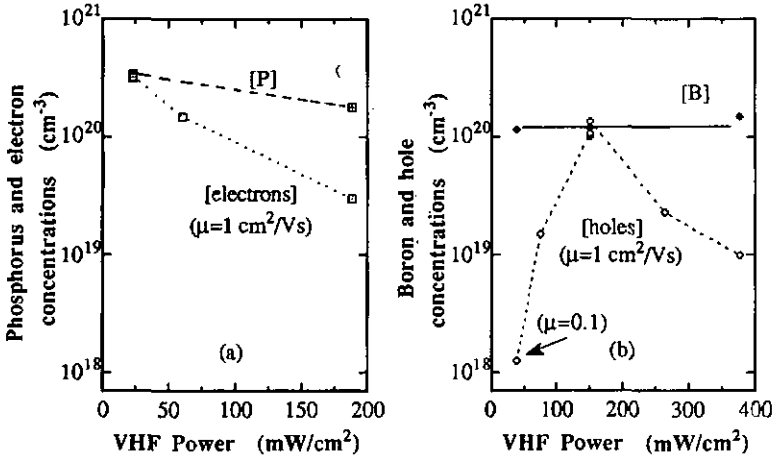

Figure 4.23 Influence of power on the dopant and carrier concentration for (a) n-type and (b) p-type series.

It is even surprising that the incorporation of dopant in the low power p-type amorphous specimen is similar to that obtained in μc-Si:H specimen prepared at higher powers. In the previous section we had observed a much higher concentration of boron (6×10^{20} cm^{-3}) in the amorphous specimen prepare at 4% of silane and 150 mW/cm^2. However, the doping effect

seems to be higher in the present specimen as its conductivity is much higher ($2x10^{-2}$ S/cm) than of the poorly doped a-Si:H ($\sigma=10^{-8}$ S/cm)mentioned before. Boron incorporation in inactive configuration appears to be favourised at high discharge power. However, it has not been possible to correlate this with any increase in the structural disorder. The Raman spectra does not indicate a higher bond angle distortions and the Urbach energy is about 80 meV, comparable to that of moderately doped n-type a-Si:H specimen having a conductivity of $6x10^{-3}$ S/cm.

4.4 Discussion

The necessity of hydrogen, especially in atomic form for the growth of microcrystalline silicon has been emphasized earlier [Ensslen, 1987; Tsai, 1987]. The kinetics of the formation of μc-Si:H has been explained there as a combination of, on one hand, the deposition of silicon atoms and Si-H radicals and on the other hand a selective erosion of unfavourable bonds such as hydrogen or weakly bonded silicon atoms from the film growth surface. The erosion is performed by chemical reactions between the growth surface and the atomic hydrogen within the plasma. The total reaction is expressed by the following equation:

$$SiH_{n\,(plasma)} \text{ <----------> } Si_{(solid)} + nH_{(plasma)} \qquad (4.1)$$

The forward reaction, here, describes the deposition process and the reverse reaction the etching mechanism. The equilibrium condition satisfying the sufficiency of hydrogen by which a balance is achieved between the deposition and etching mechanism is refered to as the partial chemical equilibrium (PCE) [Ensslen, 1987]. This can be achieved by decreasing the silane concentration in hydrogen, or increasing the discharge power so as to increase the atomic hydrogen by enhancing the dissociations of the reaction gases. The drawback of the first method lies in the rather low deposition rates, typically less than 0.2 Å/s reported for discharge powers greater than 150 mW/cm^2 using 13.56 MHz [Matsuda, 1987 and references therein]. Some improvement on the deposition rate can be achieved by increasing further the discharge power but at the detriment of the film quality. Alternatively, a higher silane concentration has been used in combination with a higher discharge power to obtain higher deposition rates [Matsuda, 1987]. In all these cases the substrate temperature is higher than 250 °C.

The role of a higher substrate temperature is explained by the thermally activated diffusion of the oncoming species on the film growth surface. In this process, the silicon radicals are able to migrate over the hydrogen covered film surface and locate the existing free silicon bond to form a covalent bond which continues the crystalline network [Matsuda,1989]. This thermally

activated process is also accompanied by the effusion of surplus hydrogen from the growth surface. The fact that, at 70 MHz quality μc-Si:H is obtained at substrate temperatures as low as 150°C is quite attractive. In fact, using similar process parameters (especially such low discharge powers) we have obtained μc-Si:H films at substrate temperature of 60 °C [Prasad, 1991a and b]. The temperature has even been lowered down to room temperature by decreasing the silane concentration further. Therefore, it is reasonable to say that, in VHF-GD, the high dilution of hydrogen is sufficient to induce microcrystallinity and that additional migration of the radicals due to a high substrate temperature does not seem necessary. In general, one can expect both to individually influence the film structure in the same manner. It is possible that the energy released by the reactions occuring at the film growth surface may raise locally the temperature of a few atomic layers at the growing surface, as claimed by Perrin [Perrin, 1991] and favour structural relaxation defined as 'chemical annealing' [Shimizu, 1989]. The precise mechanisms of the μc-Si:H film formation remains still an unsettled issue in this respect.

The deposition rates obtained at very low silane concentrations and low discharge powers, as for example for the undoped and phosphorus doped series, is still relatively high compared with those reported at 13.56 MHz. A different plasma chemistry and the surface reactions occuring at the higher discharge frequency (70 MHz) in our process could play an important role in this. One way to explain would be that at 70 MHz, crystallite formation is enhanced as compared to at 13.56 MHz and that the amount of disordered material needed to be etched away is much smaller. Alternatively, as the film growth process is a balance of deposition and etching, for obtaining quality μc-Si:H, one can expect that both the deposition and the etching process should be relatively high so as to increase the growth rate while producing the quality μc-Si:H material at these high growth rates. This means that along with the higher flux of silicon radicals, we should be having a high flux of atomic hydrogen which performs the etching process at the film growth surface. Previous results of high deposition rate using pure silane [Curtins, 1987] is now explained by the higher dissociation rates of silane obtained in a pure silane plasma at 70 MHz. Recent studies of OES of pure silane plasma at 70 MHz and 13.56 MHz, using constant discharge power within the plasma, has provided clear evidence for this [Hollenstein, 1991]. Based on the former results and on the high growth rates obtained for μc-Si:H, it is reasonable to expect that, as compared to 13.56 MHz-GD, a higher dissociation of the silane and hydrogen is also achieved in the diluted silane plasma at 70 MHz. By dissociation we mean the decomposition of the source gas molecules into neutral and ionised radicals and atoms by the plasma. However, no direct evidence is as yet available for the diluted silane plasma to confirm this. Recently, a higher dissociations in diluted silane plasma have been claimed for 144 MHz discharges [Oda, 1988] based on OES studies of silane and hydrogen mixed plasmas. In our preliminary OES measurements of diluted silane plasmas, we fail to find any correlation between the ratio of atomic hydrogen H* and SiH as

claimed by Oda et al. A comparative study of diluted silane plasmas by OES at 13.56 MHz and 70 MHz under the same conditions should provide more information on this subject.

A comparative study about the electrical power transfer efficiency, plasma potential and self bias has been performed for the two frequencies in a similar reactor for varying silane concentrations and discharge powers [J.-L. Dorrier, 1990; K. Prasad, 1991a]. The results obtained using 2% silane concentration in hydrogen are plotted in figures 24, 25 and 26 as a function of input power density as measured on the power meter. Similar results are also obtained at other low concentrations of silane used in the present work.

These results indicate that:

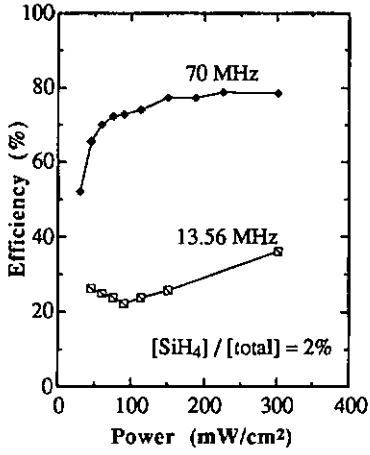

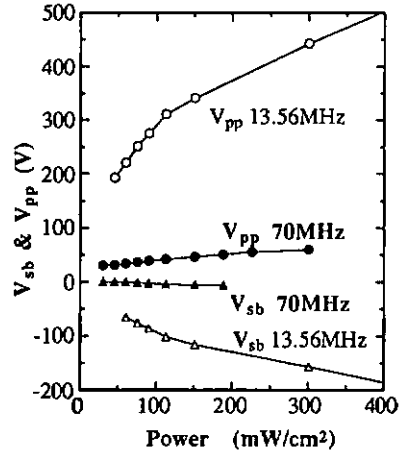

Figure 24 Power transfer efficiency into the reactor at 13.56 MHz and 70 MHz.
Figure 25 Self bias V_{sb} and peak to peak potential V_{pp} in 13.56 and 70 MHz-GD.

(1) At 70 MHz, the RF power transfer efficiency is higher than at 13.56 MHz by a factor two for such low silane concentrations (figure 4.24) even at power densities as low as 30 mW/cm^2. The ratio is even greater at higher power levels. In 13.56 MHz the transfer efficiency improves somewhat only at very high power levels, though it still remains about a factor two lower than at 70 MHz.

(2) For a given input power, the self bias voltage is lower by almost a factor ten in 70 MHz-GD (figure 4.25). The peak to peak potential is also much lower than in 13.56 MHz. The increase of input power causes a strong increase in the potentials in 13.56 MHz, whereas

at 70 MHz its influence is small in comparison. As the mean plasma potential <Vp> can be expressed as $1/2(V_{pp}/2 + V_{sb})$ [Perrin, 1988], in 70 MHz the plasma potential is much lower than in 13.56 MHz.

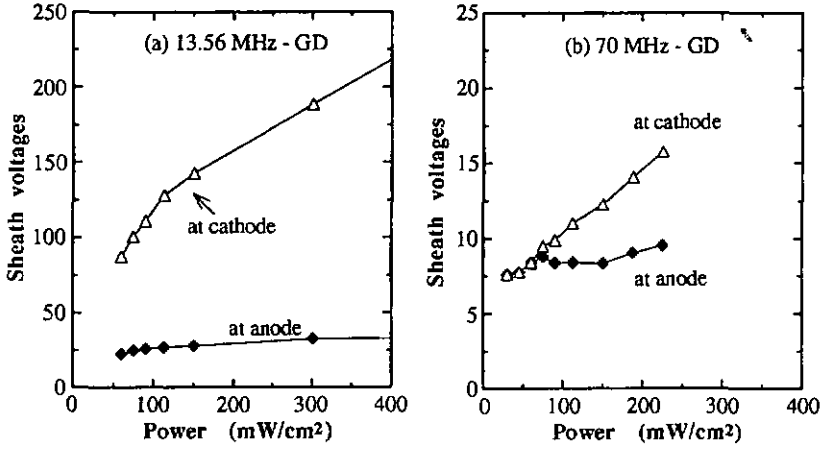

Figure 26 Comparison of the sheath voltages developed at the cathode and anode in (a) 13.56 MHz-GD and (b) 70 MHz-GD

(3) Finally, the difference of plasma and electrode potentials define the sheath potentials that develop at the anode (grounded electrode) and the cathode (powered electrode). In 70 MHz plasma,even for higher input powers, the anode sheath potential does not exceed 10 V and consequently the energy gained by the ions in crossing the sheath is low (figure 4.26b). In comparison, at 13.56 MHz, the anode sheath potential is higher by a factor three for comparable input powers (figure 4.26a). This would result in a high energetic ion bombardment at the film growth surface which will introduce structural damage. Note that the increase of the sheath potential, neighbouring the cathode, is even more pronounced than the anode sheath potential. This is also higher by almost a factor 10 in 13.56 MHz-GD as compared to in 70 MHz-GD.

At 70 MHz, even at low discharge powers the suspected high dissociation of the reaction gases could be achieved as a consequence of the higher power transfer efficiency. It could also be an outcome from changes in the plasma itself, such as the electron energy distribution function (EEDF). As the sheath potentials are low the film growth proceeds under a moderate ion bombardment. This enhances the etching process without introducing morphological damage and favours crystallite nucleations. However, it is not clear how such a film formation occurs at such low powers (23 mW/cm^2). It appears that, in 70 MHz-GD, even at

such low discharge power levels, the plasma seems to generate the required amount of atomic hydrogen so as to produce the partial chemical equilibrium in the vicinity of the film growth surface. A different profile of the EEDF having a wider tail extending in the high energy range can be one explanation. Investigations to determine the radical flux density at the substrate and the electron energy distribution function (EEDF) are required to elucidate this issue. Nevertheless, these results indicate the technological advantage of VHF-GD over the standard 13.56 MHz for the formation of μc-Si:H.

The resulting films are very similar to LPCVD polysilicon in structure, having smaller crystallite sizes and intergrain mismatch forming the grain boundaries. No clear evidence of the presence of any amorphous tissue is obtained in this high quality μc-Si:H. The degradation of the film properties at higher powers can be explained by the morphological damage introduced by radiation damage from higher energy ions as the substrate/sheath potential increases upon increasing the input power. The decrease of the crystallite size for increasing ion bombardment by varying the substrate potential has been reported earlier [Matsuda 1983]. Although at higher discharge powers the sheath potentials do not indicate a strong increase, a significant deterioration in structural and electrical properties is observed in our specimen. Combination of both a higher ion flux density, assuming a high dissociation rate of hydrogen, and the higher sheath potential could influence the structural roorphology. The poor electrical properties are estimated to be due to enhanced segregation of dopants at the grain boundaries, where they remain inactive and carrier trapping. The latter will also decrease carrier mobility due to an increase of potential at these grain boundaries [Le Comber, 1983].

Higher hydrogen dilution and discharge power are required for the formation of microcrystalline structure in boron doped series. Boron atoms seem to impede the formation of μc-Si:H by forming amorphous structures. Therefore, a stronger etching process is required for their elimination. The higher hydrogen dilution and discharge powers presumably generate an increasing concentration of atomic hydrogen within the plasma which enhance the etching process and favour crystallite nucleation. The threshold of power required for the microcrystalline formation can be lowered by reducing the doping concentration, as the hampering behaviour of boron atoms for the formation of μc-Si:H is then reduced.

The influence of high power used for the formation of boron doped μc-Si:H is seen in the TEM photograph. It provides evidence of strong columnar growth with long needle like crystalline structures, which is not present in the phosphorus doped specimen. Such growth is observed to result from a process resembling more a physical vapour deposition (PVD) instead of a chemical vapour deposition (CVD) [Tsai,1987 and 1988a]. The former is characterised by a line of sight process with poor step coverage, whereas the latter results in

a conformal step coverage with soft deposition. In comparison, the low power μc-Si:H formation of the undoped and phosphorus doped specimen appears to resemble CVD type, in spite of the moderate etching process involved.

Transport in μc-Si:H is understood to occur by percolation of free carriers between the crystallites [Komuro, 1984]. Since very little of any amorphous tissue is observed, one can expect that the potential fluctuation introduced by the grain boundary is very similar to that observed in a polysilicon where conductivities of 200 S/cm for n-type material are obtained on specimens deposited by thermal CVD at 600°C [Adams 1983]. Conductivities of 166 S/cm is also reported for p-type material prepared at 515 °C and containing around 10^{20} cm^{-3} of boron [Haji, 1989]. In the p-type material, besides the expected lower hole mobility due to the higher effective mass of holes, the lateral conductivity could be poorer because of the increasing surface regions of the grain boundaries around the cigar like crystallites. The transversal conductivity can be expected to be different due to the structural anisotropy.

Conductivities as high as 130 S/cm and 30 S/cm are obtained in the n- and p-type samples respectively at low silane concentration. The highest conductivities reported, upto now, for μc-Si:H, using simple capacitive or inductive GD, are 10 S/cm for the n-type [Usui, 1979] and 20 for the p-type specimen [Simon 1982]. The latter has been obtained using power densities of 400 mW/cm^2 and substrate temperature higher than 300 °C. Films prepared at discharge powers comparable to our's result in amorphous morphology and poor conductivities. Conductivity of 20 S/cm has been reported in 40 MHz-GD for the n-type films [Spear, 1981]. These results have been obtained at higher substrate temperatures and discharge powers, and have deposition rates less than 0.2 Å/s. Due to the latter limitation very often the thickness of the specimen is less 2000 Å, which may partly explain for the lower conductivities. However, even for such thin films, conductivities in our specimen is higher. More details on the influence of film thickness will be reported in chapter 6. High conductivities have been reported in μc-Si:H deposited using magnetically confined plasmas but still they lie below those obtained in the present work [Kausche,1989; Ray, 1989]. Comparison with these results suggest the favourable influence of high plasma excitation frequency for the formation of μc-Si:H. Some favourable influence of a higher excitation frequency can be seen at 40 MHz where improved properties are obtained as compared to the 13.56 MHz [Spear, 1981]. Similarly, at 70 MHz one obtains even better conductivity results without any additional complications of magnetic confinements. The preliminary results of mobility suggest that this is due to a higher carrier concentration.

From the above results one can draw a qualitative curve for the deposition parameter space which favours microcrystalline formation at 70 MHz. This is illustrated in Figure 4.27. First,

deposition of undoped and phosphorus doped films at a minimum power which guarantees plasma stability at low silane concentration results in microcrystalline structure. To obtain boron doped μc-Si:H specimen the power threshold is shifted to higher powers. This shift depends on the doping level, and would be higher for higher doping levels. While the range of silane concentration which yields a microcrystalline structure is relatively large for the undoped and phosphorus doped samples, it is narrowed down for the boron doping. This range is also expected to depend on the doping level, and should enlarge for lower doping levels. Basing ourselves on the information obtained from our results, on our present understanding of the microcrystalline process and on that reported by others, we extend the parameter space qualitatively. It can be expected that at higher silane concentrations, higher discharge power would be required to compensate for the higher deposition rate by a higher etching rate to still obtain μc-Si:H. On the other hand, beyond a certain critical silane concentration even at very high discharge powers one would fail to reach a sufficiently hydrogen rich plasma to produce the required etching effect. Instead, due to the resulting high substrate/sheath potentials significant structural damage by the ion bombardment will be caused within the film. This would result in a damaged low quality a-Si:H. One may also reach amorphisation of a film, which initially is microcrystalline at low powers, by increasing the discharge power to very high levels.

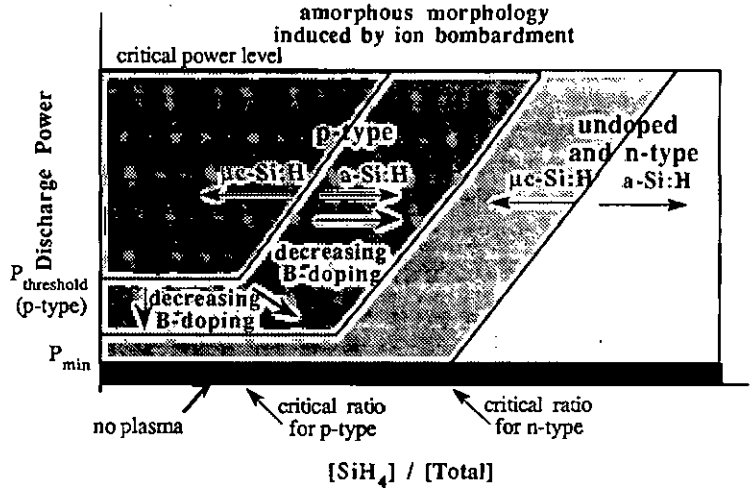

Figure 4.27 Sketch of parametric space required for the formation of μc-Si:H and a-Si:H.

4.5 Conclusions

The technological advantage of the VHF-GD using 70 MHz as the plasma excitation frequency over the standard 13.56 MHz has been demonstrated by the preparation and properties of μc-Si:H. Due to the resulting lower plasma and sheath potentials the high plasma excitation frequency proves to be favourable for μc-Si:H formation.

Best quality μc-Si:H films are produced at silane concentrations of less than 4%. The p-type films require a minimum power threshold for microcrystalline formation. Higher power introduces structural defects and degrades film properties. Substrate temperatures of 150 to 200°C are sufficient for obtaining highly conductive material. High substrate temperatures (>250°C) or power levels (>200 mW/cm^2) are not necessary conditions in our VHF-GD.

Boron doping impedes the crystalline formation and requires a higher flux of hydrogen, and higher power levels to accentuate the etching process that will eliminate the hampering boron atoms. The resulting films present strong columnar growth in form of needles with preferential crystallite orientations in <220> direction. The structure of undoped and n-type specimens resembles closely small grained polysilicon.

These highly conductive films can find applications as conductive layers in devices based on a-Si:H, such as solar cells or detectors, or as contact layers in microelectronics. The possibility to deposit them at a reasonably high rate at such low temperatures can be of interest in microelectronics, where otherwise most of these processes are performed at temperatures higher than 700°C. Such a possibility would reduce the problems incurring from diffusion of dopants when the devices are annealed at high temperatures. It would be useful to have higher conductivities and mobilities to make these layers more attractive for such applications.

References

A. C. Adams, Ch.3 in ' VLSI Technology' Ed.S. M. Sze, McGraq Hill (1983)

W. Beyer, J. Non-Cryst. Sol. 66, 1 (1984)

W. Beyer, pp.129 in 'Tetrahedrally Bonded Amorphous Semiconductors', Ed. D. Adler and H. Fritzsche, Plenum Press-New York (1985)

M. Brunel, Analusis 17, 125 (1989)

E. Bustarret, A. Deneuville, R. Grosleau, L. C. Brunel, M. Brunel, J. Elec. Mat. 13, 673 (1984)

E. Bustarret, M. A. Hachicha, M. Brunel, Appl. Phys. Lett. 52, 1675 (1988)

H. Curtins, N. Wyrsch, A. Shah, Elec. Lett. 23, 228 (1987)

J.-L. Dorier, Diploma thesis, EPFL (1991)

J. M. Dubois, Diploma work, IMT, (1991)

R. O. Dusane, S. R. Dusane, V. G. Bhide, ICAS-14, Garmisch-Patenkirchen (1991)

K. Ensslen, S. Veprek, Plasma Chem. and Plasma Process. 7, 139 (1987)

P. M. Fauchet, I. H. Campbell, Sol. State. and Mat. Science 14, S79 (1988)

P. M. Fauchet, I. H. Cambell, MRS Symp. Proc. 164, 259 (1989)

P. Faucher, Private communication at ICAS-14 (1991)

F. Finger, K. Prasad, S. Dubail, A. Shah, X. M. Tang, J. Weber, W. Beyer, MRS Symp. Proc.219, 383 (1991)

A. L. Fripp, J. Appl. Phys 46, 1240 (1975)

M. A. Hachicha, Ph.D. thesis, Université Joseph Fourier, Grenoble (1988)

L. Haji, L. Hamedi, A. Rupert, B. Loisel, P. Joubertin, Polycrystalline Semiconductors, Ed. H.J.Möller, H.P.Strunke,J.H.Werner, Springer Proc. in Physics 35, 387 (1989)

T. Hamasaki, M. Ueda, Y. Osaka, M. Hirose, J. Non-Cryst. Sol. 59&60, 811 (1983)

Ch. Hollenstein, J.-L. Dorier, A. Howling, U. Kroll, F. Finger, Amer. Vac. Soc. (1991)

N.M. Johnson, Proc. of ICAS-14, Garmisch-Partenkirchen (1991)

T. Kamins, 'Polycrystalline Silicon for Integrated Circuit Application', Kluwer Academic Publishers, Boston (1988)

H. Kausche, K. Prasad, R. Plättner, Proc. of 9th EC.PVSEC, 595, Freiburg (1989)

J. Kocka, Phil. Mag. B 63, 235 (1991)

S. Komuro, Y. Aoyagi, Y. Segawa, S. Namba, J. Appl. Phys. 56, 1658 (1984)

J. S. Lannin, Ch.6 in Semiconductors and Semimetals, Vol. 21 'Hydrogenated Amorphous Silicon' Part B, Ed. J. I. Pankov, Academic Press, New York (1984)

P. G. Le Comber, G. Willeke, W. E. Spear, J. Non-Cryst. Sol. 59&60, 795 (1983)

G. Lubberts, B. C. Burkey, F. Moser, E. A. Trabka, J. Appl. Phys. 52, 6870 (1981)

M.M. Mandurah, K.C. Saraswat, C.R. Heims, T.I. Kamins, J. Appl. Phys. 51, 5755 (1980)

A. Matsuda, J. Non-Cryst. Sol. 59&60, 767 (1983)

A. Matsuda, Ch. 3.4 in 'Amorphous Semiconductor Technologies and Devices', JARECT Vol. 22, Ed. Y. Hamakawa, OHMSHA LTD (1987)

A. Matsuda, T. Goto, MRS Symp. Proc. 164, 3 (1989)

Y. Mishima, M. Hirose, Y. Osaka, J. Appl. Phys. 51, 1157 (1980)

E. Müller, private communication, (1991)

S. Oda, J. Noda, M. Matsumura, MRS Symp. Proc. 118, 117 (1988)

J. Perrin, Jap. J. Appl. Phys. 27, 2041 (1988)

J. Perrin, Proc. of ICAS-14, Garmisch-Partenkirchen (1991)

K.Pierz, W. Fuhs, H. Mell, Phil. Mag. B 61, 123 (1991)

K. Prasad, Internal report on doping of a-Si:H by VHF-GD, Inst. of Microtechnology (1988)

K. Prasad, U. Kroll, F. Finger, A. Shah, J-L. Dorier, A. Howling, J. Baumann, M. Schubert, MRS Symp. Proc. 219, 469 (1991a)

K. Prasad, F. Finger, S. Dubail, A. Shah, M. Schubert, Proc. of ICAS-14, Garmisch-Partenkirchen (1991b)

Polyse '90, Proc. of the Satellite conference of the 20th Int. Conf. on the Physics of Semiconductors, Ed. H. Strunk, J. Werner, Springer Verlag (1990)

S. Ray, Review summery 6.25 , p248 in 'Properties of Amorphous Silicon', 2nd Edition, EMIS Datareview Series no.1, INSPEC, London (1989)

H. Richter, Z. P. Wang, L. Ley, Sol. St. Commun. 39, 625 (1981)

J. Y. W. Seto, J. Appl. Phys. 46, 5247 (1975)

I. Shimizu, J. Non-Cryst. Sol. 114, 145 (1989)

H. Simon, G. Winterling, G. Müller, Proc. of European PV-SEC p.542, Stresa (1982)

W. E. Spear, G. Willeke, P. G. Le Comber, A. G. Fitzgerald, J. de Phys. 42, C4-257 (1981)

W. Spitzer, H. Y. Fan, Phys. Rev. 108, 268 (1957)

R. A. Street, D. K. Beigelsen, W. B. Jackson, N. M. Johnson, M. Stutzmann, Phil. Mag. B. 52, 235 (1985)

M. Stutzman, C. P. Herrero, M. Ingels, A. Breitschwerdt, MRS Symp. Proc. 164,189 (1989)

S. M. Sze, 'Physics of Semiconductor Device', John Wiley and Sons, New York (1981)

T. Tiedje, Ch.6 in Topics in Applied Physics, Vol 56, 'The Physics of Hydrogenated Silicon II', Ed. J. Joannopoulos, G. Lucovsky, Springer-Verlag, Berlin (1984)

C. C. Tsai, J. G. Shaw, B. Wacker, J. C. Knights, MRS Symp. Proc. 95, 219 (1987)

C. C. Tsai, pp. 43 in Proc. of the Int. Workshop on Amorphous Semiconductors, Ed. H. Fritzsche, D. Han, C. C. Tsai, World Scinetific Publ. Co. (1987)

C. C. Tsai, pp 123 in 'Amorphous Silicon and Related Materials' Ed. H. Fritzsche, World Scientific Publ. Co, (1988a)

C. C. Tsai, R. Thompson, C. Doland, F. A. Ponce, G. B. Anderson, B. Wacker, MRS Symp. Proc. 118, 49 (1988b)

S. Usui, M. Kikuchi, J. Non-Cryst. Sol. 34, 1 (1979)

S. Veprek, M. Heintze, S. A. Sarott, M. Jurcik-Rajman, P. Willmot,
MRS Symp. Proc. 118, 3 (1988)
S. Veprek, M. Heintze, R. Bayer, M. Jurcik-Rajman, MRS Symp. Proc. 149, 3 (1989)
G. Willeke, K. Prasad, R. Fischer, A. Shah, E. Bucher,
10th European PV-SEC, Lisbon (1991)

5. PHOSPHORUS AND BORON DOPING OF μc-Si:H

5.1 Introduction

The optimum parameters required for the formation of good quality undoped and doped μc-Si:H were identified in the previous chapter. There, in the case of doped series the gas phase doping was maintained as constant. At high doping levels (0.1-1%) the electrical conductivity is reported to be increasing with increasing doping [Spear, 1981]. At still higher doping levels (> a few percent), however, one may produce alloying with the dopant atoms which can influence the structural morphology such as amorphisation and alter the film properties. With the interest of obtaining the most conductive films, and studying how the doping with phosphorus and boron, using VHF-GD, influences film properties, a detailed investigation of doping was carried out. The results are presented and discussed in this chapter. The difference between the two types of doping is elucidated. Optimum doping level necessary to obtain the highest conductivity and the critical doping levels above which film properties degrade, presumably due to alloying, are identified.

This study was performed on film having thicknesses around 0.5 μm. For application in devices such as solar cells, one would require films having thicknesses between 100 and 500 Å. This will be presented in the next chapter.

5.2 Deposition parameters

The deposition parameters which produced good quality μc-Si:H described in chapter 4, were selected as starting point for the present study. Phosphine (PH_3) and diborane (B_2H_6) diluted to 500 ppm or 1000 ppm in hydrogen was used as the source gas for the n- and p-type doping, respectively. The ratio of the amount of pure doping gas over silane was varied in the range between 10^{-4} to $3x10^{-2}$ (0.01 to 3%). This range was selected based on the limitations imposed by the gas concentration, flow meter ranges and the pumping system. Table 5.1. gives the details of the deposition parameters.

Table 5.1 Deposition parameters for 'doping' series:

no.	type	[Doping gas]/[SiH_4] (%)	[SiH_4]/[total] (%)	T_s (°C)	Power (mW/cm^2)	Pressure (mbar)
7.	n	0.03 to 1.4	3.0	200	23	0.4
8.	p	0.1 to 3.1	1.6	160	150	0.8

5.3 Results

Deposition rate

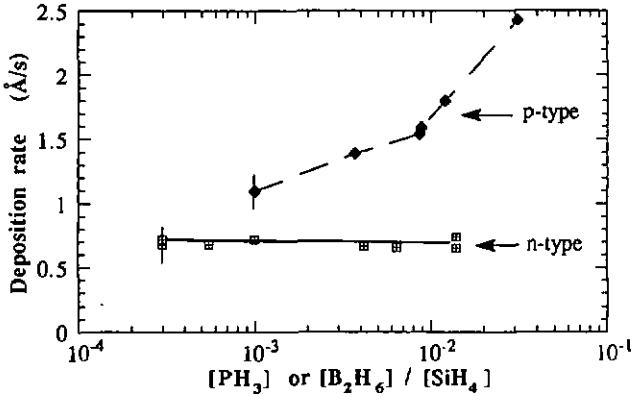

Figure 5.1 Deposition rate as a function of gas phase doping.

The deposition rate as a function of the gas phase doping ratio is plotted in figure 5.1. The deposition rate remains constant at 0.6-0.7 Å/s for the n-type series, and is not influenced by doping in the entire doping range. On the other hand, the deposition rate increases with p-type doping. This increase is accentuated for doping levels higher than 1%. Such increase in the deposition rate of μc-Si:H has been explained by the cataliytic effect of diborane which scavenges hydrogen from the film growth surface [Perrin, 1989; Matsuda, 1991]. Reactions between the oncoming BH_3 radicals and the surface hydrogen is claimed to produce unstable BH_5. Consequently, the molecule breaks off liberating H_2 and leaves behind two vacant sites at the film growth surface. This vacancy increases the surface sticking coefficient and causes an increase in the deposition rate. In contrast, both PH_3 and PH_5 are claimed to be stable molecules and therefore no increase in the deposition rate is expected upon phosphorus doping. An increase in the deposition rate by a factor 2.5, with increase in doping in a comparable doping range has also been reported for poly-Si prepared by LPCVD at 680 °C [Rai-Chudhuri, 1981]. This is explained by the catalytic role played by boron in the decomposition of the oncoming silicon radicals.

As good quality μc-Si:H is understood to be obtained at lower deposition rates [Veprek, 1989] the increase of the deposition rate, in the p-type series, may influence the film structure. At lower deposition rates, the oncoming radicals have more time to locate a suitable vacant site to continue crystallite growth. Up to now, in our results, the highest deposition rate yielding μc-Si:H, at high powers, was 2 Å/s. For the 3.1 % doping the deposition rate is 2.5 Å/s. On

the other hand no change is expected in the film structure from the constant deposition rate observed for the n-type series.

Dark conductivity

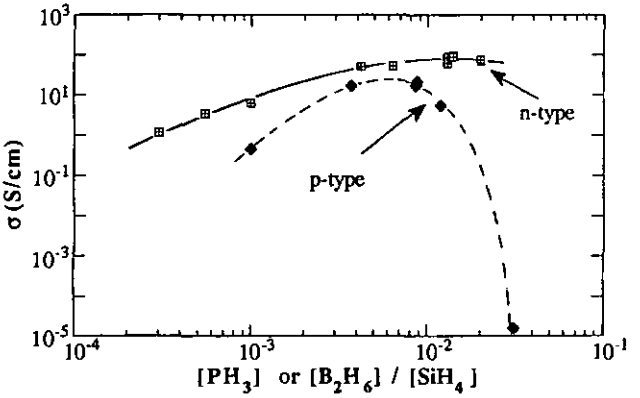

Figure 5.2 Dark conductivity as a function of gas phase doping.

The dark conductivity as a function of the doping level is plotted in figure 5.2. Let us first consider the n-type series. The dark conductivity increases monotonously by two orders of magnitude: from 1 S/cm to 100 S/cm, with activation energy decreasing from 50 to 15 meV, respectively, when the gas phase doping ratio is also increased by about two orders of magnitude: from $3x10^{-4}$ to 1.4 %. It appears to reach an asymptote at 100 S/cm. Conductivities upto 130 S/cm have also been reached at 2% of doping level using a lower silane concentration of 2.3 %. This is the highest conductivity as yet reported for n-type μc-Si:H [Ray, 1989; Willeke, 1991]. The highest values of conductivity are obtained for doping ratios between 1 and 2 %. The increase in conductivity suggests that it is directly related to the doping level, either with the dopant concentration or dopant activation.

Figure 5.3 illustrates the concentration of phosphorus as measured by SIMS and the estimated concentration of electrons. The latter is estimated assuming a mobility of 1 cm^2/Vs measured on our highly conductive n-type specimen [Dubois, 1991]. The evaluated values are plotted using open circles in figure 5.3. Hall mobilities ranging from 0.2 to 0.8 cm^2/Vs have been previously reported for μc-Si:H having crystallite sizes of 40-60 Å [Spear, 1981], and 2 cm^2/Vs for specimens having an activation energy of about 40 meV [Le Comber, 1983]. The mobility is expected to approach the value of 10 cm^2/Vs as the barrier height E_b decreases [Le Comber, 1983]. Although the value of 1 cm^2/Vs compares well with the reported results, we

would have expected it to lie between 1 and 10 cm^2/Vs considering the high volume fraction of crystallites in this material, its low activation energy and its quasi poly-Si like structure, as deduced in chapter 4. As an exercise of comparison we also plot the carrier concentration evaluated using a mobility of 10 cm^2/Vs (dotted curve without data points in figure 5.3). In our estimation of the free carriers we assume, based on the high conductivities, that all the films are microcrystalline. This is confirmed from the Raman scattering discussed later. We also assume that the influence of film structure on the mobility may be neglected as all these specimens have almost a constant volume fraction of crystallites. At higher doping levels, while the mobility within the crystallites would decrease due to impurity scattering, the mobility at the grain boundary would increase due to a decrease in the barrier height [Le Comber, 1983]. It is, therefore, assumed that the two effects compensate each other and the measured mobility remains constant.

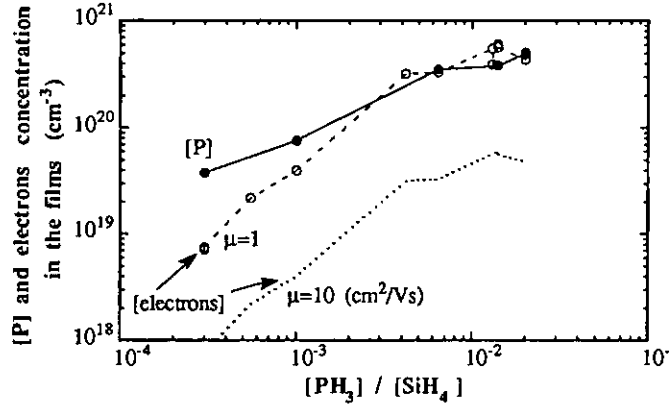

Figure 5.3 Phosphorus and electron concentration in the films as a function of the gas phase doping ratio.

The SIMS results (full circles) show that in the lower doping range one obtains an almost one to one relation between the dopant concentration in the film and the doping ratio. Phosphorus incorporation increases from $3.9x10^{19}$ to $3.6x10^{20}$ cm^{-3} as the doping ratio increases from $3x10^{-4}$ to $6x10^{-3}$. Beyond this doping level, the phosphorus concentration seems to saturate around 4 to $5x10^{20}$ cm^{-3}. A similar concentration is also measured in μc-Si:H films doped at 2% of gas phase doping ratio using 2.3 % of silane concentration, yielding a conductivity of 115 to 130 S/cm. Thus, this concentration appears to be the upper limit for the phosphorus concentration within such highly conductive μc-Si:H. Similar phosphorus concentration is also reported by Kaya for 2 % doping levels [Kaya, 1984], although no saturation level is observed in his results. Due to the systems limitations it was not possible to push the doping

level still higher to see whether this would induce alloying and increase the phosphorus concentration. The latter is observed to be higher by a factor 2 to 3 in amorphous specimen (see section 4.3). Concentrations as high as $3x10^{21}$ cm^{-3} is reported in a-Si:H [Kaya, 1984].

In comparison, the estimated free electron concentration (open circles) is almost an order of magnitude below the dopant concentration at the lowest doping level. It increases by almost two orders of magnitude, reflecting the conductivity results, while the phosphorus concentration increases from $3.9x10^{19}$ to $3.6x10^{20}$ cm^{-3}. The increase is relatively small at a doping level higher than $6x10^{-3}$ and equals the phosphorus concentration which remains almost constant. The absence of one to one relation between the conductivity or free charge carrier density and the dopant concentration over a wide doping range has been previously observed in doped poly-Si. Influence of both carrier trapping and dopant segregation at the grain boundaries are held responsible for this behaviour [Mandurah, 1980]. As the structure of our μc-Si:H appears to resemble closely that of small grained poly-Si, it is reasonable to expect similar trapping and segregation behaviour. In our case, one may even expect a higher degree of segregation to occur in the μc-Si:H, as the segregation is proportional to the volume density of the grain boundary segregation sites. The latter is inversely proportional to the crystallite size [Mandurah, 1980]. Besides, passivation of dopants by hydrogen would also contribute to render them inactive [Johnson, 1991; Stutzmann, 1989; Pankov, 1985]. Comparing the free electron concentration estimated using μ=1 cm^2/Vs and the dopant concentration, some effect of carrier trapping or dopant segregation seems to predominate, in our results, at lower doping levels. The effect appears to be even more pronounced if one assumes a higher value of mobility as seen from the dotted curve plotted using μ=10. However, at lower doping levels the barrier height could increase due to a stronger charge depletion within the crystallites and lead to a decrease in the mobility. This decrease in mobility would of course increase the estimated free carrier concentration. It is not possible to separate the two microscopic effects, of dopant segregation and carrier trapping, that result in the decrease of the free carrier concentration, as they have identical macroscopic effect on the electrical transport.

The results of the boron doping studies are significantly different. The conductivity (figure 5.2) first increases, like in the n-type series and reaches a maximum of 20 S/cm for 0.4 and 0.9 % doping. Then, as the doping level increases further, it decreases rapidly. For the highest doping level of 3.1 % in the gas phase, a conductivity of $1.1x10^{-5}$ S/cm, corresponding to that of doped amorphous specimens, is reached. The amorphous structure of this specimen was also confirmed by structural measurements and is discussed later. The optimum doping level resulting in the highest conductivity, for the p-type specimen, is lower as compared to the n-type specimen, and lies between 0.4 and 0.9 %.

The SIMS results (Figure 5.4) indicate that the boron incorporation is in the range of $5x10^{19}$ to 10^{20} cm^{-3} in the low doping range. For doping levels higher than 1% it increases beyond 10^{21} cm^{-3}. Note that due to the charging effects in the 3.1 % doped resistive film, the measurement of boron is underestimated. It could be higher by a factor 3 to 5[A. Eicke, 1991]. The high deposition rate resulting at the high doping level is thought to be associated with structural modifications such as an increase in the degree of disorder and even amorphisation of the film structure. Such an increase in the structural disorder would allow a higher boron incorporation beyond the solubility limit, as also observed in our amorphous films. The quasi-constant concentration of boron obtained at doping levels lower than 1 % differs from that reported by Kaya [Kaya, 1984]. There, a monotonous increase in the boron concentration, upon doping, is reported using 13.56 MHz-GD.

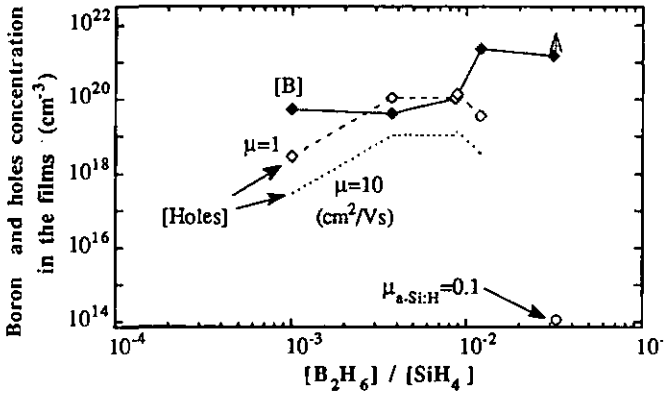

Figure 5.4 Boron and holes concentration as a function of the gas phase doping ratio.

The hole concentration estimated using mobility μ of 1 and 10 cm^2/Vs for μc-Si:H and a μ of 0.1 for the a-Si:H specimen obtained at 3.1% of doping level is also plotted in figure 5.4. Looking at the curve obtained using μ=1 (open diamonds) the low hole concentration found at the lowest doping level can again be attributed to the carrier trapping and /or dopant segregation at the grain boundaries as the specimen is confirmed to have good microcrystalline structure. Influence of hydrogen passivation of dopants may also be present. At the optimum doping levels the hole concentrations correspond to that of the incorporated boron. The small difference observed at 0.4 % doping level is possibly due to a scatter. Alternatively, if the mobility is assumed to be higher (10 cm^2/Vs) the estimated hole concentration would be lower (see dotted curve). This would imply that the effects of carrier trapping and/or dopant segregation at the grain boundaries are present even at the optimum doping level and they are

even more pronounced at other doping levels. Some evidence of possible higher mobilities will be presented in the discussion.

Beyond a 1% doping level, the hole concentration drops rapidly by several orders of magnitude below the boron concentration. This sharp decrease can be explained by the inactive three fold incorporation of boron within the amorphous structure of these specimens. The low doping efficiency in a-Si:H is imposed by the compensation effect of the defect creation with doping which pins the Fermi level away from the band edge, limiting the number of free carriers [Street, 1985].

The highest conductivity of 20 S/cm obtained at 0.4 and 0.9 % of doping in the present experiment is comparable to the highest as yet reported for the boron doped μc-Si:H deposited by glow-discharge [Simon, 1982]. Higher conductivities of upto 35 S/cm have been reached using sophisticated magnetic confinements in a GD [Mori, 1981].

Structure

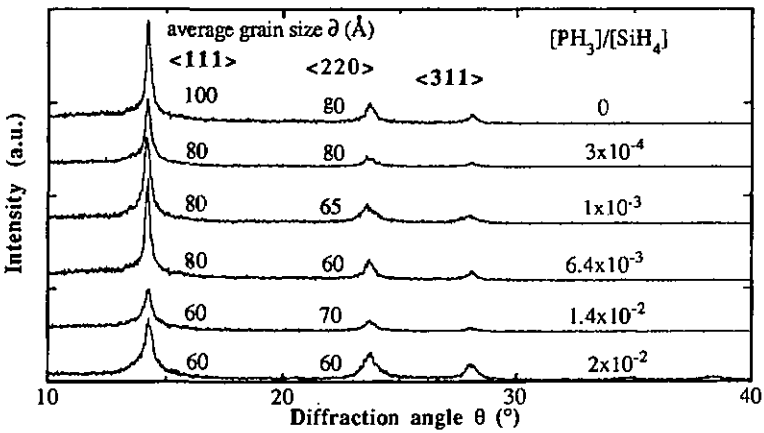

Figure 5.5 Grazing angle X-ray spectra for the n-type series showing the change in the crystallites peaks as a function of doping.

The grazing angle X-ray spectra for the phosphorus doped series are plotted in figure 5.5. The influence of doping on the structure is seen from the tendency of broadening of all the crystalline peaks and the decrease of the peak intensity. This indicates a reduction in the crystallite size. The average crystallite size ∂, evaluated from the FWHM of the <111> and <220> peaks, decreases slightly upon doping as compared to the undoped specimen (top most

curve). A further decrease in ∂ occurs at high doping levels of 1.4 to 2 %. Considering that a maximum error on the evaluation is about ±10 Å, a tendency in the decrease the crystallite size upon increasing doping is observed. The tendency of decrease in ∂ was seen in figure 4.5 when comparing the doped series with the undoped ones. Note that while the average grain sizes ∂ evaluated from the θ–2θ diffraction results are bigger, the error on the evaluation is rather large due to the poor resolution of the system and the background noise. The present results are more reliable due to the higher sensitivity of the grazing angle diffraction technique.

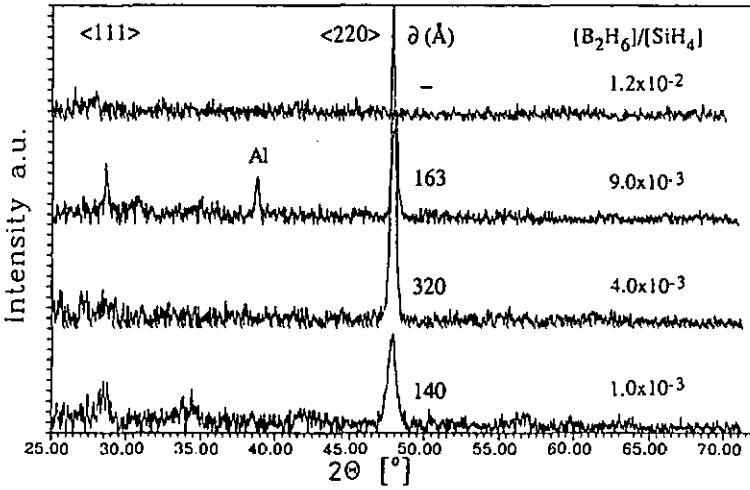

Figure 5.6 X-Ray spectra for the boron doped series.

The preferential crystallite orientation resulting from the boron doping is reconfirmed from the θ–2θ X-ray diffraction spectra of the p-type series (figure 5.6). The change in the crystalline structure is observed from the change in (220) peak. The (220) peak reaches a maximum intensity for the doping level of 0.4 %, which represents a rather large crystallite size of 320 Å. At higher or lower doping levels of 0.1 % and 0.9 %, the peak decreases, implying a decrease in the crystallite size ∂. All the peaks disappear totally for the specimen doped at 1.2 % for which we had a high deposition rate, a high dopant incorporation and lower conductivity. This suggest that the structure is less crystalline due to the increasing boron incorporation which possibly inhibits the crystallite formation. Due to high resistivity and the decreasing crystalline trend we assume that the specimen doped at 3.1% is amorphous which was confirmed by Raman scattering.

The high resolution TEM photograph (figure 4.10) of the specimen doped at 0.4% shows strong evidence of columnar growth with crystallites in the form of long needles extending vertically from the substrate upto the top of the film. This geometry suggests that the structure is inhomogeneous and one may expect anisotropic properties in the material.This is in contrast to the n-type material doped at 2 % which exhibits a more homogeneous crystalline structure within the film. It is likely that X-ray evaluation tends to give an average value of ∂. As mentioned before, the anisotropic structural property could result in an anisotropy in its electrical property. For example, the conductivities may be different and possibly higher perpendicular to the film surface than parallel to it. The curious amorphous zone seen at the substrate/film interface was identified as part of the substrate and was discussed in detail in the previous chapter.

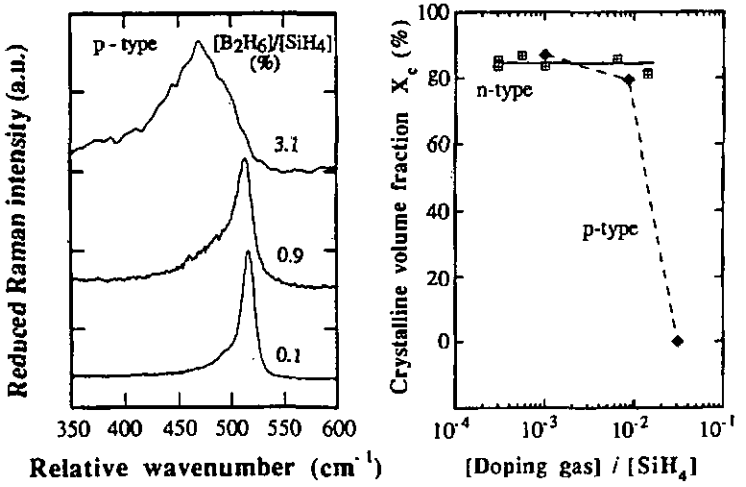

Figure 5.7 (a) Raman spectra of boron doped specimens and
(b) Crystalline volume fraction X_c as a function of doping level.

The change in structure in the p-type series is also clearly observed in the Raman scattering results (figure 5.7a). As the doping level is increased, first the increase of the degree of disorder is seen from the broadening of the crystalline peak and an increase in the amorphous component. For the last specimen, doped at 3.1%, the purely amorphous structure is confirmed as was expected from its conductivity and the trend of the X-ray results. The evaluated crystallite volume fraction X_c is plotted in figure 5.7b. The highest X_c is obtained for the least doped specimen and it decreases at doping level. Finally the highest doping level seems to induce a microcrystalline to amorphous transition. Therefore, boron doping is suspected to have a strong influence on the structural morphology of the film to the extent of

inducing microcrystalline to amorphous transition at very high doping levels [Makino, 1981]. In comparison, phosphorus doping seems to have only small influences on the crystallite size ∂ and none on the crystalline volume fraction X_c of the film. The results of n-type doping show no change in the Raman spectra and X_c is more or less constant over the entire doping range (figure 5.7b).

Optical absorption

Figure 5.8 illustrates the optical absorption characteristics for the phosphorus doped films. Absorption data of an undoped c-Si, μc-Si:H, and doped and undoped poly-Si [Lubberts,1980] is also given for comparison. For the doped μc-Si:H films the absorption coefficient for photon energies higher than 2 eV does not seem to be influenced by the increasing doping level up to 1%. It is a little higher for doping levels higher than 1% which produce specimens with conductivities around 100 S/cm. Although one would expect this to be due to some experimental scatter, it has been observed on all the highly conductive n and p-type specimens. Such a vertical shift is also observed on specimens which increase in conductivity upon annealing upto 300 °C. Upon annealing the hydrogen content decreases although no modification is observed in the structural properties. This can be explained by depassivation of previously passivated dopants by annealing which lead to an enhancement of the free carrier concentration. The hydrogen effusion may also leave behind a higher disordered structure in the grain boundary which is too small to be detected in structural measurements. It is however noticed in the optical absorption as it enhances the non-direct transitions, for photon energies greater than 2 eV. In spite of the fact that these defects would also trap some carriers, the results indicate a net increase, after compensating the traps, in the carrier concentration as observed from the rise in the subgap absorption.

The contribution from the non-direct transitions occuring at the grain boundaries can be deduced by comparing the absorption of LPCVD poly-Si and crystalline silicon. The absorption for photon energies greater than 1.6 eV is higher in poly-Si. This increase can be associated with grain boundaries effects. The still higher absorption observed in the μc-Si:H is therefore attributed to the presence of a higher degree of disorder at the grain boundaries and/or an increased proportion of the disordered tissue. Based on these assumptions, the still higher absorption observed in the highly doped specimens appears to be the effect of high doping. In section 4.3a (figure 4.8a) we had deduced an increase in the grain boundary disorder in doped μc-Si:H films as compared to undoped ones. In the present absorption results, high doping seems to deteriorate grain boundary structure, although the amount is small enough to be detected by Raman scattering. Decrease in the grain boundary passivation due to annealing

effects possibly leads to similar structural changes, which would, in fact, increase the concentration of the trapped carriers.

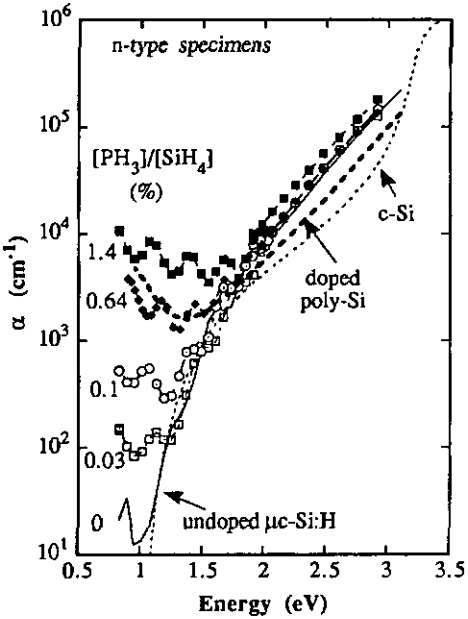

Figure 5.8 Absorption characteristics for n-doped specimens as a function of doping.

In the low energy range (E<2 eV), the absorption increases with increasing doping (and conductivity). In the previous chapter such an increase was attributed to free carrier absorption. Similar increase of free carrier absorption in the low energy range is also observed in phosphorus doped poly-Si [Lubberts, 1980; Mishima, 1980]. Note that doping in poly-Si, reported by Lubberts, was performed by ion implantation at a rate of 10^{16} cm^{-2}, and the carrier concentration is estimated to be about 3×10^{20} cm^{-3}. This compares quite well with the carrier concentration estimated in the μc-Si:H specimen prepared at a 0.64 to 1.4 % doping level. In comparison, the increase of absorption in the low energy range in doped a-Si:H originates from defect creation in the band gap [Street, 1985]. There, a correlation exists between the Fermi level shift and defect creation such that, even for the most conductive specimen ($\sigma=10^{-2}$ S/cm) having a minimum activation energy of 0.2 eV, the absorption does not rise higher than 100 cm^{-1} [Pierz, 1991]. For a qualitative estimation of microcrystallinity we shall later present a plot relating the absorption coefficient $\alpha_{1.2}$ at 1.2 eV and the film conductivity. Let us first look at the absorption in the p-type series.

For the p-type series, the optical absorption is plotted in figure 5.9. The data is separated into two plots to make it easier to read. In figure a, as in the case of n-type specimens and comparing to the absorption characteristics of an undoped μc-Si:H, one can see a strong increase of the absorption coefficient for the low energy photons as the doping level is increased from 0.1 to 0.9 %. We remind the reader that the microcrystalline structure of these films was confirmed by X-ray and Raman scattering measurements. For photons having energy greater than 2 eV, the absorption does not change and resembles that of undoped μc-Si:H, except for a slight upward shift observed in the most conductive specimen. This behaviour is similar to that observed in the highly conductive n-type films which is attributed to increased non-direct transitions occuring in the grain boundaries, and was discussed earlier.

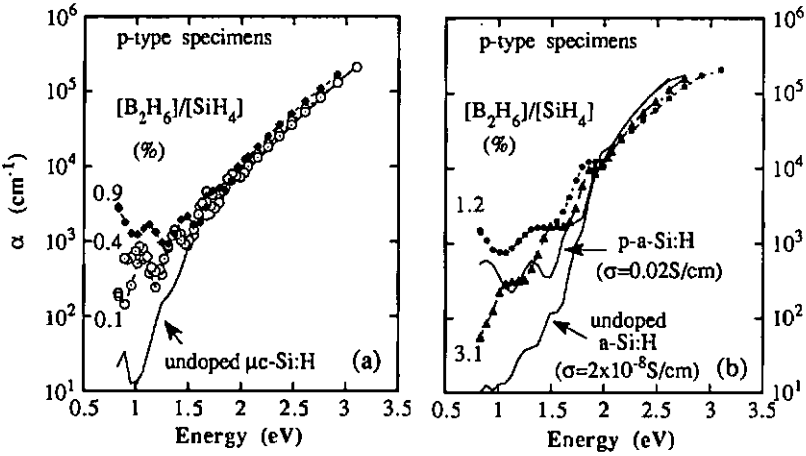

Figure 5.9 Absorption characteristics of boron doped specimens as a function of doping.

In figure b, the absorption behaviour for the highly doped specimens is plotted along with that of doped and undoped a-Si:H for comparison. As compared to the 0.9 % doped specimen, the absorption of the specimen doped with 1.2 % of diborane is slightly higher for E>2 eV and lower for E<2 eV. The former indicates an increase in the amorphous tissue and the latter suggests a decrease in the free carrier concentration. On the other hand, the highly doped specimen (at 3.1%), which has a very low conductivity ($1.5x10^{-5}$ S/cm) and pure amorphous structure, has a behaviour corresponding to that of a doped a-Si:H. However, the Urbach slope is wider than that of the doped a-Si:H plotted for comparison. This increase could possibly result from the influence of high powers used for the preparation of this specimen. Structural damage induced by the ion bombardment could enhance the morphological

distortion in the film structure leading to wider band tails as compared to what is found in optimised doped a-Si:H.

In figure 5.10 the absorption coefficient $\alpha_{1.2}$ of the smoothed curve at an energy level of 1.2 eV is represented in relation to the dark conductivities for the two series. For the n-type series, $\alpha_{1.2}$ appears to have an almost one to one dependence on the conductivity. Results from Raman scattering experiment confirmed a high and almost constant crystallite volume fraction in the entire doping range. The one to one relation between $\alpha_{1.2}$ and conductivity does not seem to apply so well to the p-type series. The observed wide scatter may be due to the influence of increasing disorder in the film structure which was seen in the Raman and X-ray results. A similar scatter is also observed for other n-type and p-type series presented in chapter 4, which have a strong variation in the structural properties.

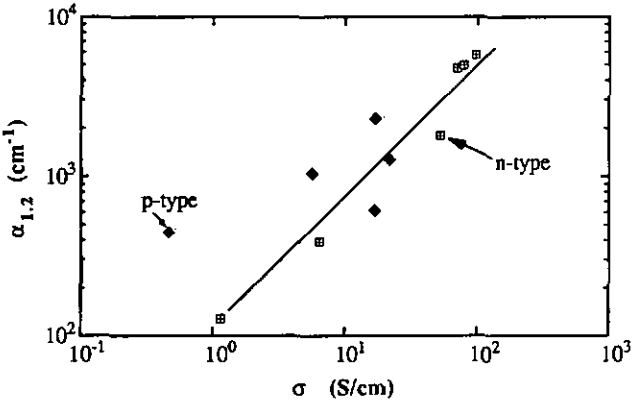

Figure 5.10 Absorption $\alpha_{1.2}$ Vs σ in μc-Si:H indicating a linear relation between $\alpha_{1.2}$ and the conductivity for the n-type series. A wide scatter is observed for the p-type series.

The IR transmission correlates nicely with the absorption data with the transmission decreasing for specimens having an increase in the low energy absorption. No additional new information is further obtained from these plots.

Verification of free carrier absorption

To ensure that the increase in the absorption at low energy is in fact due to free carriers and not due to any other effects such as light scattering from the inhomogeneous nature of the μc-Si:H material a series of compensated samples, prepared using a discharge power of 75

mW/cm^2, have been investigated. Starting with the best p-type specimen doped at 0.4% and having a conductivity of 30 S/cm, the ratio $[PH_3]/[B_2H_6]$ has been increased from 0 to 8. Figure 5.11 shows the optical absorption spectra of three of these specimens: a pure p-type (PH_3/B_2H_6=0), a fully compensated (PH_3/B_2H_6=1.2) and an over-compensated (PH_3/B_2H_6=8) n-type specimen. The corresponding conductivities are indicated in brackets. The microcrystalline structure of all these films is confirmed from Raman scattering and indicates a crystalline volume fraction of about 80 %. This is not surprising since no structural modification was observed by increasing the phosphorus concentration in the n-type doping series.

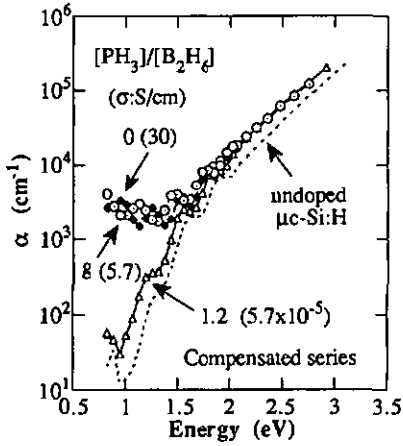

Figure 5.11 Optical absorption characteristics of p-type (•), fully compensated (Δ) and over compensated n-type (○) specimens.

Due to the absence of any significant modification in the film structure the absorption for energies greater than 2 eV undergoes little change for the three specimens. In the low energy range, the absorption is high for the p-type and over-compensated n-type specimens, both of which have a high conductivity. Whereas, in the fully compensated resistive film the absorption is much lower and resembles that of an undoped μc-Si:H. The correlation between the conductivity resulting from the free carriers resulting from the net doping effect and the upward shift in the low energy absorption is clearly seen. For the fully compensated specimen the net free carrier concentration is significantly reduced, resulting in low value of absorption in the low energy range.

The transmission in the IR also drops to low levels for the high conductive specimens and exhibits a plasma edge in the reflection measurements [Finger, 1991]. Whereas, it is close to

100 % for the fully compensated specimen [Finger, 1991]. These vertical shifts show that we are essentially dealing with free carriers that are influencing the absorption in the low energy range and influences of light scattering are not the dominant effects. Some contribution in absorption resulting from the effect of the shift of the Fermi level cannot be excluded.

5.4 Discussion and conclusions

The results obtained in the present investigation indicate that in order to obtain high quality μc-Si:H having high conductivity and high crystalline volume fraction, the doping level needs to be optimised. This is less critical for phosphorus doping than it is for boron doping.

Very little change in the structure is observed for n-type doping, for the gas phase doping range extending from 0.03% to 0.6 %, whereas conductivity and dopant incorporation increase monotonously. Raman results hardly show any change in the crystalline volume fraction of the material over this broad doping range. Some increase in the grain boundary disorder is suggested from the decrease in the crystallite size and the increase in the optical absorption in the high energy range. A highest conductivity of 130 S/cm is obtained at optimum doping levels between 1% and 2%.

Boron doping has a strong influence on the film properties. Two distinct doping regions are identified. Below 1% of doping, the specimen are microcrystalline with a preferential <220> orientation. For increasing doping from 0.1 % upto 1%, the increase in the deposition rate is small, the dopant concentration is low and almost constant, and the conductivity increases. In this region, atomic hydrogen seems to perform satisfactorily the necessary etching role for the formation of μc-Si:H. In the process, it also eliminates most of the excess boron atoms that would impede the crystallite growth. This results in low boron concentration and lower rise in the deposition rate. However, one would expect a monotonous increase in the boron concentration with the doping level. In fact, it is almost constant and is not controlled by doping.

For doping levels higher than 1%, a rapid increase in the deposition rate takes place. This is accompanied by a degradation in the structural properties and suppression of crystallinity. This also leads to an increase of the incorporated dopants and deterioration of the transport properties. In this regime, the excess boron appears to resist hydrogen etching. This leads to suppression of the microcrystalline nucleation and transition to amorphous structure. This is also accompanied by a strong increase in the deposition rate and boron incorporation. Based on the catalytic role of boron [Perrin, 1989,; Matsuda, 1991], one can argue that at higher

doping levels, the silane dissociation is enhanced in the plasma. This causes the growth process to move away from the equilibrium of deposition and etching, due to a stronger deposition rate and results in an amorphous morphology. It also enhances the concentration of boron which can incorporate in 3-fold inactive configuration within the network [Street, 1985].

The p-type specimen has number of effects similar to those reported in p-type LPCVD poly-silicon, namely: the increase in the deposition rate, the preferential orientation of the crystallites and the prominent columnar structure [Rai-Choudhury, 1973]. Amorphisation of the film structure has been reported in poly-Si for boron concentration exceeding the solubility limit [Makino, 1981]. High conductivities of 20 to 30 S/cm have been reached at optimum doping levels of 0.4 % and 0.9 %; the lower doping level is more favourable from structural point of view.

The fact that every molecule of diborane (B_2H_6) in the plasma supplies two atoms of boron as compared to one atom of phosphorus supplied by phosphine (PH_3) is tempting to use as an argument to explain why the optimum doping level is almost twice as high in the n-type doping than in the case of p-type doping. The higher discharge powers used for the p-type series would also increase the dissociation rate of diborane and increase the concentration of boron in the plasma. Systematic study to investigate the gas phase reactions within the plasma and at the film growth surface needs to be carried out to have a clearer idea on this issue. In such a study one needs to consider the influence of discharge power as well. Based on the microcrystalline to amorphous transition observed at high boron doping, it is suspected that if comparably high doping levels are used for n-type doping , i.e. 6 % as compared to 3 % in the p-type case, then one may also degrade the film properties or induce amorphisation of the film. Some results in this direction are observed in the study of very thin films and will be presented in the next chapter.

The increase of absorption in the low energy seems to correlate quite nicely with the increase in film conductivity, for the n-type series, where the structural properties are not strongly influenced by doping. In p-type specimens the structural properties are influenced strongly by increasing the doping level and have a complex influence on the dopant activation and carrier transport. Similar influence is also observed in both type of specimens upon increasing discharge power or silane concentration. It appears that the relation between $\alpha_{1.2}$ and σ hold true only so long as the structure is not modified significantly. Further investigation on the influence of structural modification on the dopant activation and mobility may contribute to a better understanding of the interaction between the optical absorption, conductivity and the active dopant concentration. Techniques used to elucidate the microscopic behaviour in grain

boundary of large grain polycrystalline silicon, as for example Electron Beam Induced Current technique (EBIC) cannot be used on the microcrystalline material as it is impossible to identify an individual grain boundary and scan across it. Other methods such as temperature dependence of conductivity and Hall mobility are therefore needed in the low temperature range (70 to 400 K) to improve our understanding of the grain boundary behaviour in these μc-Si:H material.

Both, carrier trapping and dopant segregation at the grain boundaries, as also observed in poly-Si, are suspected to be at the origin of the absence of one to one relation between the dopant incorporation and estimated free carrier concentration determined using the preliminary result of $\mu=1$. Hydrogen passivation of dopants is an additional effect that is present in these glow-discharge deposited samples. Annealing studies to temperatures upto 320 °C has provided evidence of effusion of hydrogen accompanied by an increase in the film conductivity and subgap absorption. These effects are explained based on depassivation of previously passivated dopants [Finger, 1991; Prasad, 1991]. Similar effects are also observed in crystalline silicon [Pankove,1985; Stutzmann, 1991]. A similar preliminary study of annealing to 250 °C of the 0.4 % doped p-type specimen indicates that its conductivity increases from 20 S/cm to 95 S/cm (by a factor 5) while its hydrogen content decreases from 6 at% to less than 1 at%. However, no alteration is observed in its structure (TEM and X-ray). Considering that all of its dopants ($4x10^{19}$ cm^{-3}) are then activated provides a mobility of 13 cm^2/Vs. Hall mobility larger than 5 cm^2/Vs has been deduced on this specimen from Hall measurements [Dubois, 1991]. Therefore, a mobility higher than 1 can be expected in this material. Detailed studies on transport characteristics and annealing behaviour should provide more information in this direction.

Conductivities as high as 130 S/cm and 30 S/cm have been reached for n- and p-type specimens, respectively at process temperatures as low as 160°C. In comparison, the conductivities of the in-situ doped LPCVD poly-silicon are 130 S/cm for n-type and 370 S/cm for p-type material prepared around 600 °C [Adams, 1983]. Though our results are comparable for the n-type, clearly they are rather unsatisfactory for the p-type. Besides, for applications in microelectronics the poly-Si layers are heat treated at temperatures beyond 1000 °C. This leads to an increased activation of dopants, an increase in the crystallite size and consequently an increase in its conductivity and mobility. The present VHF-GD μc-Si:H films could find some potential if low temperature processing becomes necessary for macroelectronics on large surfaces, such as glass, that do not tolerate high temperatures. However, to make them competitive for device applications more work is required to increase its conductivity and especially its mobility comparable to that found in poly-Si.

References

A. C. Adams, Ch. 3. in 'VLSI Technilogy', Ed. S. M. Sze, McGraw-Hill Book Company (1983)

J. M. Dubois, Diploma work, IMT, (1991)

A. Eicke, Private communication, (1991)

F. Finger, K. Prasad, S. Dubail, A. Shah, X. M. Tang, J. Weber, W. Beyer, MRS Symp. Proc.219, 383 (1991)

N. M. Johnson, 'Hydrogen in Semiconductors', Semiconductors and Semimetals Vol 34, Ed. J. I. Pankove, N. M. Johnson, Academic Publ., San Diego (1991)

H. Kausche, K. Prasad, R. Plättner, Proc. of 9th EC.PVSEC, 595, Freiburg (1989)

H. Kaya, T. Imura, T. Kusao, A. Hiroka, O. Nakamura, Y. Okayasu, M. Matsumura, Jap. J. Appl. Phys. 23, L549 (1984)

P. G. Le Comber, G. Willeke, W. E. Spear, J. Non-Cryst. Sol. 59&60, 795 (1983)

G. Lubberts, B. C. Burkey, F. Moser, E. A. Trabka, J. Appl. Phys. 52, 6870 (1981)

T. Makino, H. Nakamura, Sol. st. Elec. 24, 49 (1981)

M.M. Mandurah, K.C. Saraswat, C.R. Heims, T.I. Kamins, J. Appl. Phys. 51, 5755 (1980)

A. Matsuda, Private communication (1991)

K. Mori, M. Kitawaga, T. Hirao, S. Ishihara, M. Ohno, Jap. J. Appl. Phys. 20, 2431 (1981)

J. I. Pankov, Cryst. Latt. Def. and Amorph. Mat. 11, 203 (1985)

J. Perrin, Y. Takeda, N. Hirano, Y. Takeuchi, A. Matsuda, Surf. Sci. 210, 114 (1989)

K.Pierz, W. Fuhs, H. Mell, Phil. Mag. B 61, 123 (1991)

K. Prasad, F. Finger, S. Dubail, A. Shah, M. Schubert, Proc. of ICAS-14, Garmisch-Partenkirchen (1991)

P. Rai-Choudhury, P. L. Hower, J. Electrochem. Soc. 1761 (dec. 1973)

S. Ray, Review summery 6.25 , p248 in 'Properties of Amorphous Silicon', 2nd Edition, EMIS Datareview Series no.1, INSPEC, London (1989)

H. Simon, G. winterling, G. Müller, Proc. of European PV-SEC p.542, Stresa (1982)

W. E. Spear, G. Willeke, P. G. Le Comber, A. G. Fitzgerald, J. de Phys. 42, C4-257 (1981)

R. A. Street, J. Non-Cryst. Sol. 77&78, 1 (1985)

M. Stutzman, C. P. Herrero, M. Ingels, A. Breitschwerdt, MRS Symp. Proc. 164,189 (1989)

M. Stutzman, Physica B 170, 240 (1991)

S. Veprek, M. Heintze, R. Bayer, M. Jurcik-Rajman, P. Willmot, MRS Symp. Proc. 149, 3 (1989)

G. Willeke, in ' Amorphous and Microcrystalline Semiconductor Devices: Materials and Device Physics', Ed. J. Kanicki, Artech House, Norwood (in Press) (1991)

6. ULTRATHIN MICROCRYSTALLINE SILICON LAYERS FOR DEVICE APPLICATIONS

6.1 Introduction

Up to now, we have discussed the properties of μc-Si:H films having a thickness of around 5000 Å. We have seen that the VHF-GD is a promising technology to produce highly conductive μc-Si:H at rather low discharge powers and low substrate temperatures. This is particularly interesting for applications in device processes since it eliminates two of the critical limitations imposed by the empirical conditions required during the deposition of μc-Si:H using 13.56 MHz, namely: (1) high discharge powers and (2) high substrate temperatures. Both of these can contribute to damage the underlying layers by ion bombardment or thermally activated reactions. The favourable conditions of the VHF-GD process can be put to profit to integrate the highly conductive films as contact layers in microelectronics or as source and drain regions in thin film transistors for large scale display drivers. They can also be used to replace the doped a-Si:H layers which have conductivities lower by 3 to 4 orders of magnitude [Willeke, 1991]. One application of special interest would be the simple p-i-n structured amorphous silicon solar cell. On replacing the less conductive n and p layers by the corresponding μc-Si:H layers one would, on one hand, reduce the series resistance and on the other hand, due to a more pronounced shift of the Fermi level in these doped films, increase the V_{oc}. Thus, one can expect to improve the total cell performance. Some applications of n^+-μc-Si:H in solar cells have led to encouraging results [Uchida, 1981; Fischer, 1991]. Another interesting application would be the tandem solar cell where the n-p tunnel junction of the pin-pin structure could be made more conductive. This too should lead to an improved performance of the cell. However, as the absorption in μc-Si:H is much higher than in a-Si:H for lower energies (E<2 eV) it needs to be considered even though ultra thin layers having thicknesses in the 100 to 250 Å range are required in these applications.

The general problem encountered in such applications of μc-Si:H layers arises from their rather limited thickness, less than 300 Å, required for making n- and p-type layers. Such thin layers are observed to remain amorphous and highly resistive even though thicker films grow microcrystalline and are highly conductive [Nakabeppu,1989]. This is also the case using fluorinated gases which are more reactive and enhance the microcrystalline nucleation due to the strong etching process from the flourine atoms [Ray, 1989]. It is also claimed, from high resolution TEM micrographs of sputtered and 13.56 MHz glow discharge samples that a minimum thickness of 300 Å of disordered structure is necessary for the nucleation of crystallites to begin [Imura, 1984]. Therefore, it is of interest to see in how far the favourable conditions of the VHF-GD process can be explored to produce ultra thin μc-Si:H. In this

chapter we report our study on the influence of film thickness on the electrical properties of doped μc-Si:H layers. Simultaneously, the influence of both phosphorus and boron doping on the conductivity of ultra thin (250 Å) films is also studied.

The evaluation of ultra thin films is connected with several limitations. Basically, due to the roughness of the surface of the glass substrate which can be in the range of 50 to 100 Å, measurements of films having thicknesses in the same range, are difficult. Besides the determination of absorption at low energy range is not possible due to the low absorption value. Absorption can be determined only for photons having energies greater than 2.5 eV for which the absorption coefficient is high. X-ray and Raman technique also fail to produce reliable results for film thicknesses less than 500 Å due to the strong contribution coming from the glass substrate, masking the weak signal of the film. The penetration depth for the X-rays in μc-Si:H is about 20 μm and therefore the contribution of the substrate is always present in the results from θ–2θ diffractometer [J. Baumann, 1991]. Grazing angle X-ray would be a better tool for this purpose. In Raman scattering the laser probes a depth of 1000 Å and in case of thin films, the contribution of surface oxide and substrate predominate, making quantitative evaluation very difficult [M. Schubert, 1991]. Besides, if the film is purely amorphous it is not possible to distinguish the contribution of the amorphous network from that of the glass. Therefore, conductivity is one of the few possible methods still valid for the evaluation of these films. This could also, in fact, be influenced by surface effects such as contamination or band bending. The film thickness is determined as before, i.e. by etching a step and making a stylus profile across the step as described in section 3.1.

6.2 Deposition parameters

Table 6.1 Deposition parameters for the n-type thickness series:

no.	$[PH_3]/[SiH_4]$ (%)	$[SiH_4]/[total]$ (%)	T_S (°C)	Power (mW/cm^2)	Pressure (mbar)
n-1	2.0	2.3	160	30	0.4
n-2	1.4	3.2	160	23	0.4
n-3	0.4-5.0	2.3	160	30	0.4

Five different series have been deposited to study the influence of film thickness on the electrical properties of doped μc-Si:H. Table 6.1 and 6.2 give the deposition parameters of n- and p-type series, respectively. The silane concentrations, discharge powers and substrate temperatures are those found optimal from the previous results. The film thickness, in most cases, has been varied between 100 and 5000 Å for n-type and between 250 and 5000 Å for

p-type films. Series n-3 was deposited to study the influence of phosphorous doping on 250 Å thick layers.

Table 6.2 Deposition parameters for the p-type thickness series:

no.	$[B_2H_6]/[SiH_4]$ (%)	$[SiH_4]/[total]$ (%)	T_S (°C)	Power (mW/cm^2)	Pressure (mbar)
p-1	0.4	1.6	160	75	0.8
p-2	0.9	1.6	160	150	0.8
p-3	1.2	1.6	160	150	0.8

6.3 Results and discussions

Conductivity of n-type films

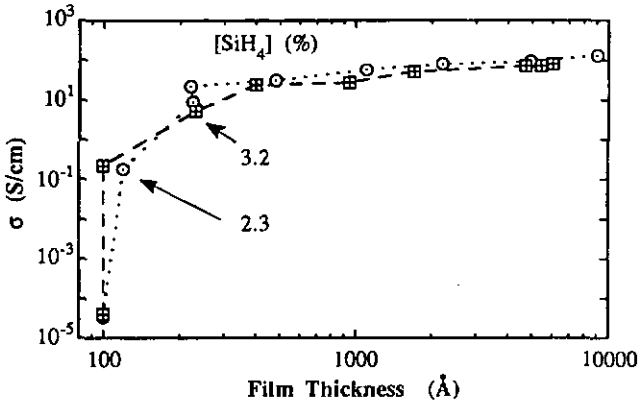

Figure 6.1. Influence of film thickness on the electrical conductivity of n-type μc-Si:H.

Let us first look at the n-type films. Two series of n-type films have been deposited using a silane concentration of 2.3 and 3.2% in hydrogen and a gas phase doping ratio $[PH_3]/[SiH_4]$ of 2% and 1.4%, respectively. Figure 6.1 illustrates their conductivity as a function of film thickness. The results indicate that the small changes in silane concentration at such high doping levels have very little influence on the film conductivity. The films deposited using a lower silane concentration are not more conductive considering the measurement scatter. In both cases, while the bulk conductivity is around 90 to 130 S/cm, the conductivity decreases down to 5-20 S/cm for a thickness of 250 Å and further down to 0.2 S/cm for an approximate thickness of 100 Å. The latter is still well above the range typically found for doped a-Si:H.

For similar thicknesses of 100 Å we have also obtained conductivities less than 10^{-4} S/cm, characteristic of doped a-Si:H. As mentioned earlier, one of the reasons for this large difference can be attributed to the problems associated with the measurement of the film thickness. Post deposition surface or bulk contamination by impurities such as oxygen could be another problem here. The films could also be amorphous in the beginning.

To invesögate the influence of phosphorus doping on very thin films, a set of samples having a thickness of 250 ± 20 Å as a function of doping was deposited (Table 1, series n-3). The gas doping ratio was varied from 0.4 % to 5 %. The variation of conductivity with doping is plotted in figure 6.2. For comparison the results of conductivity as a function of doping for thick films reported in the chapter 5 is also plotted. The conductivity of the thin films increases with doping and reaches a maximum of 22 S/cm for a doping ratio of 1.7%. For still higher doping level the conductivity appears to decrease rapidly. The increasing trend is very similar to that observed in the case of 0.5 μm thick films and in both cases the highest conductivities are obtained for doping levels between 1 and 2%. The strong decrease of conductivity for the 5% doped specimen suggests some important modification in the film structure or doping mechanism at such high doping levels. Although the conductivity is still well above the amorphous threshold, its strong decrease supports the suspicion deduced from the results of chapter 5 that at very high phosphorus doping levels the films may degrade and possibly even amorphise as previously observed in the p-type specimens.

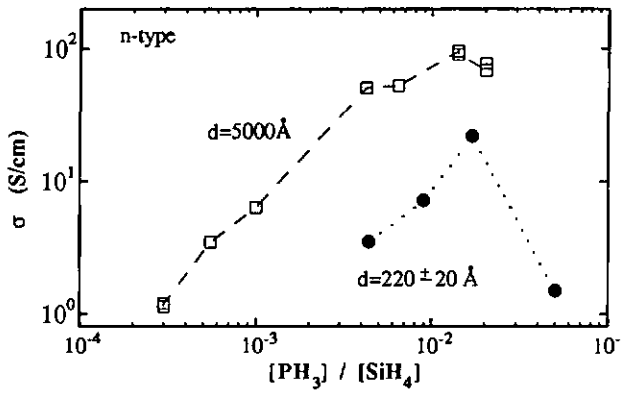

Figure 6.2 Conductivity as a function of doping for two film thicknesses. The data of films with 5000 Å is taken from figure 5.2.

Best results are obtained in both cases for a doping ratio around 1.5%. This amounts to a solid phase phosphorus incorporation of less than 1% as measured by SIMS in thick films. As compared to the properties of thick films, the reduction of the film thickness to 250 Å leads to the decrease of the conductivity by an order of magnitude. Possible explanations for this can be: (1) surface effects such as oxidation or band bendings whose contribution is usually negligible while studying thicker films or (2) presence of some amorphous phase, or incomplete coalescence of the crystallites in the first few tens of Å which leads to an effective lower conductivity within that zone. For a better understanding one would have to study the film-substrate interface using TEM on very thin samples.

Conductivity of p-type films

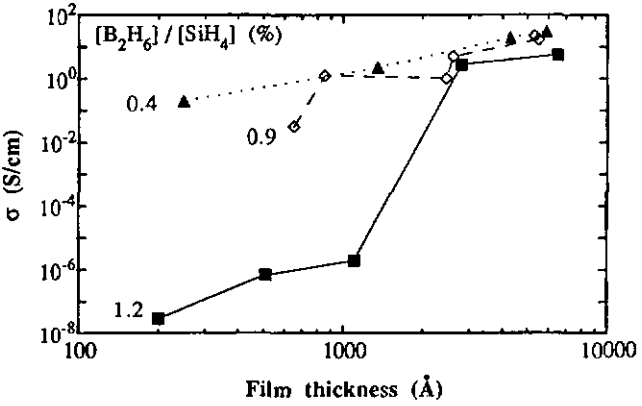

Figure 6.3 Influence of film thickness on the conductivity of p-type films.

Three series of p-type μc-Si:H were deposited for varying gas phase ratio and discharge power (Table 2). The first (no. p-1) was deposited using a doping ratio of 0.4 % and a discharge power of 75 mW/cm^2. Series p-2 and p-3 were deposited using doping ratio of 0.9 and 1.2 % respectively, and a higher discharge power of 150 mW/cm^2. The conductivity results of the three series are illustrated in figure 6.3. In all the three series, for thick films having thicknesses greater than 2000 Å, the conductivities lie in the range of 1 to 30 S/cm and the films are microcrystalline in structure. In particular, the conductivities are identical for the thickest films belonging to the first two series, although both the doping level and discharge are reduced by a factor two in series p-1. With the decrease of the film thickness, the conductivity decreases in all the cases. This decrease is most accentuated in the 1.2% doped series, where the conductivity drops by several orders of magnitude for films having a thickness less than or equal to 1000 Å. In fact, such low conductivities resemble that of a poorly doped a-Si:H and

suggest a possible change in the film structure. A similar trend in the decrease of conductivity is also observed for the specimens belonging to the 0.9 % doped series. Here, the conductivity begins to drop more significantly for a film thickness of 600 Å, for which the conductivity is just at the threshold of what is observed in doped a-Si:H. As data points are missing for thinner films, it is difficult to know whether it would drop still further or it would saturate at this level. In the series doped at 0.4%, the decrease in conductivity is monotonous down to 250 Å and no drastic drop suggesting structural change is observed. In this case, still relatively high conductivity of 0.2 S/cm is obtained for the 250 Å thick film.

These results indicate that, an increase of doping ratio needs to be accompanied by an increase of discharge power to obtain similar conductivity in thicker films. The results of thinner films indicate that a higher doping level has a strong influence on the initial nucleation. For a constant film thickness of 200 to 250 Å, the conductivity drops from 0.2 in specimen doped at 0.4 % to less than 10^{-7} S/cm in the specimen doped at 1.2 %. The latter corresponds to a poorly doped a-Si:H. In comparison, in films having a thickness of 5000 Å (Figure 5.2) the conductivity dropped just by about an order of magnitude when the doping was increased in the same range. Besides comparing the 0.9% doped and 1.2% doped series, it appears that the critical thickness below which the material is still resistive is higher at higher doping levels. This supports the previous conclusion that the high concentration of boron in the gas plasma enhances amorphous structure formation. This is particularly evident from series doped at 1.2%. The transition behaviour from amorphous to microcrystalline structure with increasing film thickness, observed in this series can be understood as follows: Based on the impeding behaviour of boron in crystallite formation, it is possible that in highly doped specimen, the initial nucleation is mostly amorphous in structure. This results in the poor conductivity observed in the thin films. With increasing film thickness, some crystallite nuclei formed initially increase in size and volume. This would increase the crystalline volume fraction and above the critical film thickness form a proper percolation path, as some crystallites touch each other, resulting in the higher conductivities obtained in thicker films.

Lowest doping level and discharge powers, used in our investigations, are most favourable to obtain p-type ultra thin μc-Si:H. Lower doping level is therefore more favourable to maintain microcrystalline nature possibly from the initial nucleation as observed from the TEM photograph. Doping levels lower than 0.4 % should be investigated to obtain highly conductive films with thicknesses less than 250 Å. A further reduction in the doping level, possibly accompanied with a lower discharge power could be more favourable to obtain more conductive ultra thin films. Such deposition conditions would result in a decrease of deposition rate due to the decreased influence of boron doping and lower silane dissociation rate. A lower deposition rate would favourise a better crystallite nucleation as is observed in the deposition of

our highly conductive n-type films, which have deposition rates of about 0.5 to 0.7 Å/s (see next section and section 5.3).

In previously presented highly conductive film, prepared using 0.4 % of doping and 150 mW/cm^2, the columnar structure is favourised from the very beginning as observed from high resolution TEM micrograph presented in the previous chapter: the crystallites extend vertically from the substrate surface to the top of the film surface. In the low power 250 Å thick specimen of series p-1 (figure 6.5) the columnar structure is less obvious. Rather, a more homogeneous crystallite structure is observed as also reported for undoped and n-type specimen (figure 4.10). The lower power used in this case appears to be more favourable in producing a softer CVD like deposition [Tsai, 1988]. More on this TEM result will be discussed in the next section.

Incubation time for the initial film deposition

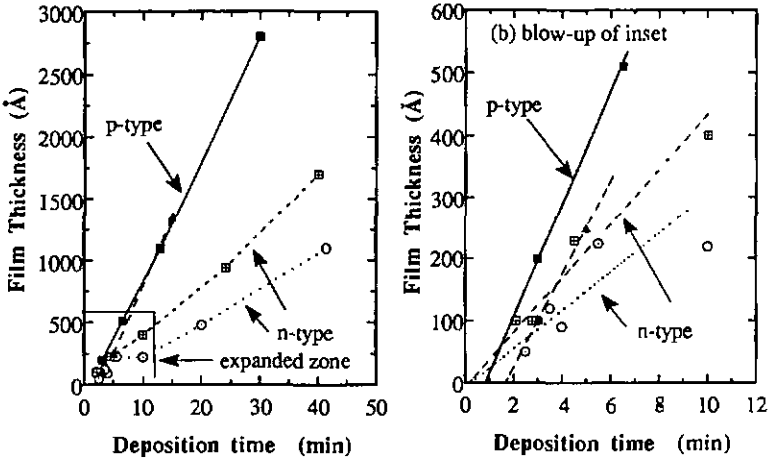

Figure 6.4. Film thickness as a function of deposition time for the series of table 6.1 and 6.2: (⊙)n-1, (⊞)n-2, (▲)p-1, (■)p-3. Figure b shows a blow up of the area close to the origin indicating a small incubation time.

The film thickness for series n-1, n-2, p-1 and p-3, as a function of deposition time is plotted in figure 6.4. Figure b shows a blow-up of the region close to the origin to have a better idea of the intercepts. The n-type series prepared at 2.4 and 3 % of silane intercept almost at the origin indicating a negligible incubation time. The intercepts of the p-type series prepared at

1.6 % of silane lies between 1 and 2 minutes. In comparison, Tsai et al. [Tsai, 1990] have reported on an increase of the incubation time from 3 minutes for 3% silane concentration in hydrogen to 15 minutes for a silane concentration of 1%. The incubation time observed in our results is much shorter. This difference may be due to higher growth rate obtained with VHF-GD [Prasad, 1989]. The effect of the higher discharge frequency is to increase the deposition rate while still producing good quality μc-Si:H. As discussed in chapter 4, the μc-Si:H film growth is, the balance between high deposition rate and a high 'etching rate' obtained in the hydrogen diluted silane plasma. The higher dissociation of hydrogen which is suspected from the high deposition rate of VHF-GD which has been observed in high frequency plasma [Oda, 1988] as compared to 13.56 MHz plasma can enhance the elimination of disordered and strained network which also forms along with the crystallites. Thus the initial disordered material is instantly etched away opening the way for a more stable nuclei to grow at the substrate. The predeposition hydrogen plasma could also possibly play a role in preparing the surface of the substrate for the film growth.

In situ ellipsometric studies performed during the initial growth of μc-Si:H layers deposited using 13.56 MHz indicate that the initial growth of μc-Si:H consists of spatially separated crystallite nucleation followed by the growth of inhomogeneous three phase material consisting of amorphous, microcrystals and voids [Drevillon, 1987]. The poor electrical properties of ultrathin films deposited at this frequency may be the result of an incomplete coalescence of the crystallites situated too far apart (>100 Å) and the presence of a higher degree of disordered or amorphous tissue forming the grain boundaries due to a less efficient etching effect. Both of these would fail to form a lateral percolation path for the charged carriers and lead to poor conductivity.

Based on the linear correlation of the deposition time with the film thickness, observed from film thickness as low as 100 Å onward we conclude that in VHF-GD the deposition process remains unchanged during the entire deposition process and that the initial growth itself is microcrystalline. The high conductivity obtained for the n-type ultra thin films, supports our hypothesis and suggests that the initial nucleation is formed of a dense accumulation of microcrystallites, with low degree of disorder in the grain boundaries, which even in ultra thin films are able to produce the percolation path for the charged carriers.

The TEM results showing the c-Si substrate-film interface of the n-type film (figure 4.9) gives little indication of the presence of amorphous tissues beyond the native oxyde of the c-Si. It confirms random oriented and variable sized crystallite growth throughout the film thickness. In the p-type specimen, the interface at the glass substrate showed presence of a strange amorphous zone having a thickness of about 250 Å, as observed on thick p-type specimen

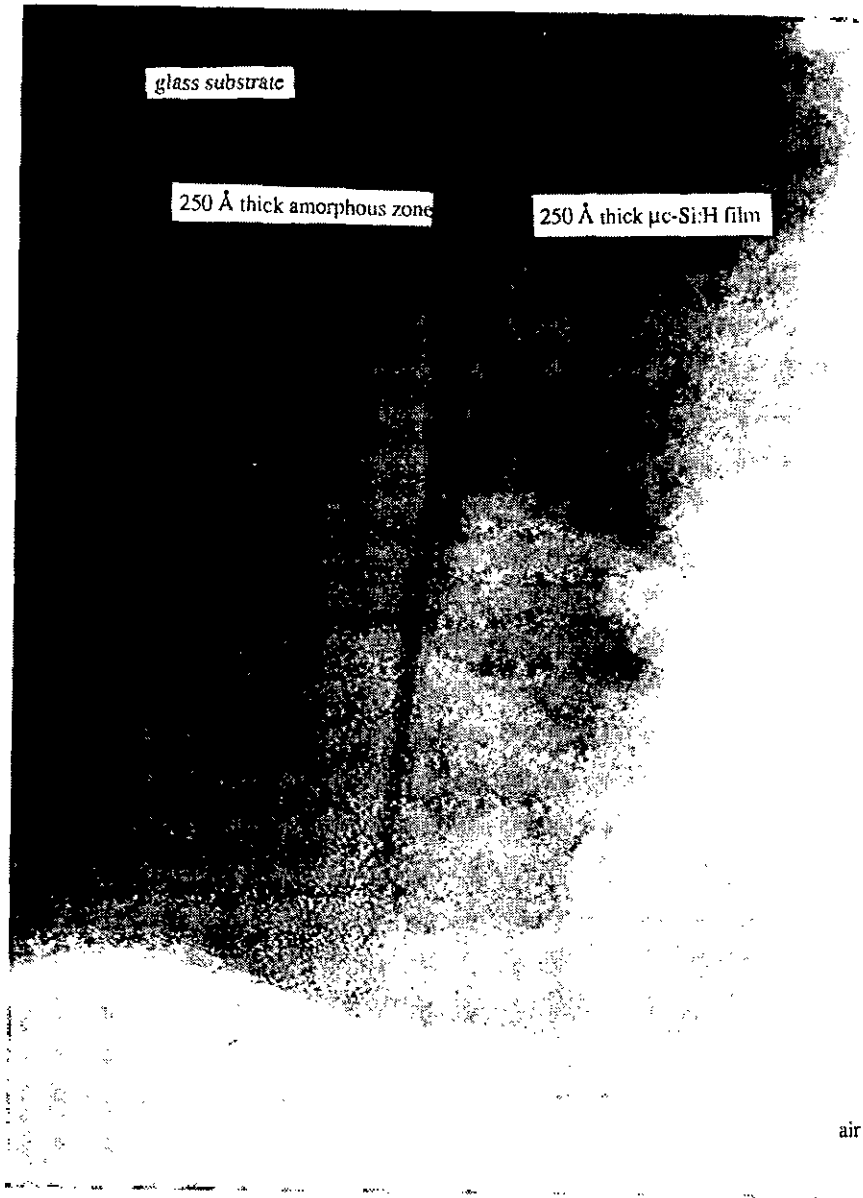

Figure 6.5 HRTEM micrograph (x340000) of a 250 Å thick p-type μc-Si:H on glass. The amorphous zone at the interface is 250 Å below the film surface.

presented in figure 4.10. In ultra thin film having a thickness of 250 Å, a similar strange amorphous structure is again observed at the interface (figure 6.5). However, as above this zone the 250 Å of polycrystalline film structure is clearly observed, it is concluded that the strange amorphous structure at the interface belongs to the glass substrate. Therefore, the strange amorphous zone identified at the glass/film interface in figure 4.10 is also attributed to the substrate. This strange transformation at the glass surface is suspected to originate from some chemical reactions occuring during the high power (150 mW/cm^2) hydrogen or argon plasma used during the annealing process. Due to absence of data, it has not been possible to observe glass-film interface in a n-type specimen. More detailed investigation on the influence of different plasmas on glass surface would be useful to improve our present understanding on this issue. In both, n- and p-type specimens the crystalline structure growth is confirmed from the very beginning of the nucleation process and extends uniformly till the top of the film. Besides, a more homogeneous structure is obtained in the p-type specimen prepared at low power.

Infra-red absorption

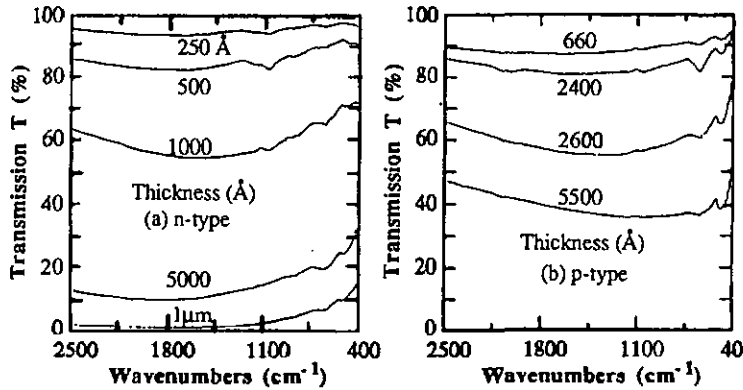

Figure 6.6 IR transmission of thickness series (no. n-1 and p-2).

Figure 6.6 illustrates the IR transmission data for n- and p-type films for increasing film thickness. The basic trend is the decrease in the total transmission with increasing film thickness (d) since the total transmission is proportional to exponential (-αd). The interesting feature though, of these transmission data, is the broad absorption peak observed, in the 1000 to 1300 cm-1 range of wave numbers, for the n-type samples (fig.6.6a) with thicknesses less or equal to 500 Å. This indicates the presence of oxygen in the form of Si-O which is understood to be situated within the voids and at the grain boundaries [Curtins,

1986]. Interestingly, for thicker films, this broad peak due to the Si-O stretching vibration is reduced or absent. A possible explanation can be the collapse of the initially formed voids and/or a decrease in the voids formation due to the building of internal stress within the film with increasing film thickness. The resulting compact film is less vulnerable to post deposition oxygen incorporation.

In contrast to the n-type films, no oxygen incorporation has been observed even in the very thin, conductive or resistive p-type μc-Si:H films. However, this effect is not understood since a highly columnar structure, as observed for the p-type specimen, is expected to be more porous as compared to the homogeneous structure observed for the n-type specimen.

It appears that under the deposition conditions favourising good quality μc-Si:H, initially the structure appears to be porous in n-type specimens due to the moderate ion bombardment resulting from the low substrate-plasma sheath potential. High discharge power results in a stronger ion bombardment due to an increase in the plasma-substrate sheath potential and seem to yield a dense structure. The lower conductivities observed in such p-type films could be due to the morphological damage introduced in the crystallite lattice by the high ion bombardment, as reported in section 4.3b or simply the effect of a higher effective mass of the holes.

6.4 Conclusions

Investigations of doping on film thickness reveal that boron doping plays an important role in the formation of thin μc-Si:H. High concentration of boron enhances the growth of disordered tissue that hinders crystalline growth, especially during the initial nucleation process. The optimal doping level is 0.4 % at low discharge power. In contrast, Phosphorus doping is less critical and best results are obtained at 1 to 2%. This difference could be due to the suspected higher boron concentration in the plasma resulting from the higher discharge powers used to crack diborane and that each diborane molecule contributes two atoms of boron. The tendency of inactive boron to incorporate as B-B bonds is another reason suspected of reducing crystallisation at higher doping levels. Conductivities of 22 and 0.2 S/cm are obtained for n and p-type μc-Si:H films having a thickness of 250 Å.

The short incubation time suggests a similarity between the initial nucleation and the rest of the film growth. The higher dissociation of gas suspected from the high deposition rates in the VHF-GD is thought to be responsible for this.

Low discharge powers used in the deposition of n-type μc-Si:H yields porous material, which is vulnerable to oxygen intake. More compact material is obtained at high discharge powers due to the increase in ion bombardment. It would be recommendable to increase slightly the discharge power in the case of n-type specimen to make it more compact. To obtain better p-type ultra thin films it is necessary to lower the doping level and discharge power so as to reduce structural deformations and anisotropy.

The ability to obtain ultra thin n- and p-type high conductive μc-Si:H films, using substrate temperatures as low as 150°C and low discharge powers offers the possibility to integrate such layers as tunnel junction in a tandem solar cell, or as contact layers in device fabrication with reduced risk of introducing morphological damage in the under layers.

References

J. Baumann, Private communication (1991)

H. Curtins and S. Veprek, Solid State Comm. 57, 215 (1986)

B. Drevillon, C. Godet, S. Kumar, Appl. Phys. Lett. 50 1651 (1987).

D. Fischer, Private communication (1991)

T. Imura, H. Kaya, H. Terauchi, H. Kiyono, A. Hiraki, M. Ichihara, Jap. J. Appl. Phys. 23, 179 (1984)

F. Nakabeppu, T. Ishimura, K. Kumagai, K. Fukui, MRS Symp. Proc. 164, 389 (1989)

S. Oda, J. Noda, M. Matsumura, Mat. Res. Soc. Symp. Proc. 118, 117 (1988)

K. Prasad, F. Finger, H. Curtins, A. Shah and J. Baumann, Mat. Res. Soc. Symp. Proc. 164, 27 (1989)

S. Ray, S.C. De, G. Ganguly, A. K. Barua, J. Appl. Phys. 65, 4024 (1989)

M. Schubert, Private communication, (19991)

C. C. Tsai, Amorphous Silicon and related Materials, Ed. H. Fritzche, World Scient. Publ. Co. 123, (1988)

C. C. Tsai, G. B. Anderson, R. Thompson, MRS Symp. Proc. 192, 475 (1990)

Y. Uchida, T. Ichimura, M. Ueno, H. Haraki, Jap. J. Appl. Phys. 21, L586 (1982).

7. GENERAL CONCLUSIONS

Using the VHF-GD at 70 MHz, good quality undoped and doped microcrystalline silicon is obtained under very favourable conditions of deposition i.e. low substrate temperature (150-200 °C) and low discharge power (25 to 75 mW/cm^2). Even at the low silane concentrations (<4%) used in our case the deposition rates are higher by a factor 3 to 5 than those reported for 13.56 MHz-GD. The conductivities are also higher than those reported earlier for the doped specimens.

The very high frequency plasma is understood to be responsible for these results. A hydrogen rich plasma is suspected to be produced from the high power transfer efficiency and the high dissociation rate deduced from the high deposition rates. In combination with the low plasma and substrate sheath potentials, a high flux of hydrogen atom or ions with moderate energy is developped at the film/plasma interface. These establish the required equilibrium, between deposition and etching, which result in the formation of quality μc-Si:H.

Conductivities of 130 S/cm and 30 S/cm have been obtained for Phosphorus and Boron doped films, respectively, having a thickness of 0.5 μm. The optimum doping is found to be 1-2% in the case of n-type and around 0.4-0.9% for the p-type specimens. Little changes in the structural properties are observed on increasing the gas phase doping ratio from 0.03 to 2% for the n-type, whereas with increasing boron doping the degree of crystallinity is reduced to the extent of inducing amorphisation at high doping levels of 5 %. Possibly this is related to the fact that each molecule of diborane supplies two boron atoms to the plasma as compared to phosphine which supplies only one, and the influence of higher discharge power used for the p-type series. It is possible that at comparable high doping levels which induced amorphisation in the p-type specimens (6% of phosphine for the n-type case), the n-type specimens would also become amorphous. Degradation of conductivity on doping at 5% was observed in films having a thickness of 220 Å.

Boron doping tends to inhibit crystalline formation and requires a higher flux of hydrogen than required for the undoped and n-type material to compensate this effect. This is obtained by decreasing the silane concentration and raising the discharge power. The outcome is a more columnar structure with preferential crystallite orientation in the <220> direction. TEM results of the optimised film indicates that the crystallites extend vertically in the form of needles almost from the substrate to film interface up to the top of the film. Some transformation of the glass surface is observed at the film glass interface which is suspected to originate from some reactions between the glass and the discharge plasma. Further investigation is necessary to understand the influence of the plasmas on the glass surface. This is an important issue since

the quality of the glass surface would influence the adhesion and the initial nucleation of the film.

Phosphorus doped specimens have crystallites in random orientation as found in poly-Si powder. TEM results of the highly conductive film show the crystallites' size extending from 50 to more than 500 Å and practically touching each other. The grain boundaries are identified as consisting of crystallographic mismatch rather than containing any bulk disordered tissue. Hardly 20 Å thick amorphous tissue is observed at the c-Si substrate-film interface which can be accounted for the native oxide of the c-Si. Similar film structure is observed between films deposited on glass substrate and c-Si substrates and also between undoped and n-type specimens. These structures resemble poly-silicon material having smaller crystallite sizes (50 to 500 Å) instead of the classical picture of crystallites imbedded in an amorphous matrix.

The rise in the absorption for low energy photons, attributed to the free carrier absorption correlates nicely with conductivity as long as the structural properties remain comparable. Structural disorder appears to influence the dopant segregation and carrier trapping at the grain boundaries, as observed in poly-Si, and control the transport properties.

Conductivities as high as 20 S/cm for the n-type and 0.2 S/cm for the p-type have been obtained in ultra thin films having thickness of 250 Å. From these high conductivities and the negligible incubation time, the film growth is deduced to be microcrystalline from the very beginning. Such conductive layers, deposited at 150°C could be potential candidates for device applications mentioned in chapter 1 [Kanicki, 1991]. For such applications the p-type layers need to be further optimised. Lowering of the doping and discharge power levels are expected to reduce the degree of disorder and strong columnar structure induced by doping and high ion bombardment, respectively.

The present study indicates the technological advantage of the VHF-GD by producing more conductive μc-Si:H films at higher deposition rates and under very favourable conditions. The potentiality of the VHF-GD can be extended to grow epitaxial silicon as has been recently carried out at 13.56 MHz [Tsai, 1991].

References

J. Kanicki, Ch. 1 in ' Amorphous and Microcrystalline Semiconductor Devices: Optoelectronic Devices', Ed. J. Kanicki, Artech House, London (1991)

C. C. Tsai, G. B. Anderson, R. Thompson, Proc. of ICAS-14, Garmisch-Partenkirchen (1991)

ANNEXE A

Cleaning proceedure for glass substrates

Phase 1: Manual cleaning

Solution: Dilute Vizir and water
Brushing: Each substrate using a paint brush- to follow only one direction of movement
Rinsing: Each substrate individually with hot and then cold tap water
Rinsing: The whole lot in deionised water

Phase 2: Cleaning using ultrasonic baths

* Bath 1: Solution of 0.5% DECONEX in deionised water
(60 ml of DECONEX in 12 l of water)
Temperature: 70°C
Duration: 3 minutes with ultrasound

* Bath 2: Ordinary water
Temperature: room temperature
Duration: 10 minutes without ultrasound

* Bath 3: Deionised water
Temperature: room temperature
simply rinsing without ultrasound

* Bath 4: Solution of 0.5% TRULIT SmW in deionised water
Temperature: 60°C
Duration 3 minutes with ultrasound

* Bath 5: Deionised water
Temperature: room temperature
Duration 10 minutes without ultrasound

Phase 3 : drying

To take each substrate one by one, while leaving the others under deionised water flow,
Spray very pure Isopropyl Alcool and immediately dry it with nitrogen flow.

ANNEXE B

Cleaning procedure for Crystalline Silicon substrates

Phase 1: Cleaning using ultrasonic baths

* Bath 1: solution of 10% DECONEX in deionised water
Temperature: 60°C
Duration: 10 minutes with ultrasound

* Bath 2: Ordinary water
Temperature: room temperature
Duration: 10 minutes without ultrasound

* Bath 3: Deionised water
Temperature: room temperature
Duration: 10 minutes without ultrasound

* Bath 4: Deionised water
Temperature: 40°C
Duration: 10 minutes without ultrasound

Phase 2 : drying
To take each substrate one by one, while leaving the others under deionised water flow, Spray very pure Isopropyl Alcool and immediately dry it with nitrogen flow.

ANNEXE C

Cleaning procedure for Stainless steel parts: substrate holder and RF electrode plate

* Remove the silicon powder using paper tissues

* Dip the pieces and screws for a few seconds in CP6 acid
(CP6= HNO_3(50%) + HF (25%) + CH_3COOH (25%)
-should not be stored in polyethylene bottles)

* Rinse them ordinary water for 10 to 15 minutes while frequently renewing the water

* Rinse in deionised water

* Heat the pieces in hot deionised water

* Dry the pieces using nitrogen (without prior rinsing with Isopropyl Alcool)

ACKNOWLEDGEMENTS

I would like to acknowledge the financial support from the Swiss Federal Energy department for the amorphous silicon solar cell project, in which the present work was integrated. It has been a privilege for me to be accepted by Professor Shah in his dynamic research group. I have appreciated the pleasant working atmosphere created by the whole staff of the institute. Especially the affectionate interaction of the secretaries has contributed significantly to making my stay at the institute a happy souvenir. I do hope this continues in the future for other foreign students. I thank all of them for their valuable contribution.

I hold in esteem my friend and guide Friedhelm Finger for his fruitful interactions. The time he devoted on scientific level and his encouragements against the odds have been of invaluable help to me.

It was also a great pleasure for me to work with my colleagues:
Ulrich Kroll whose advice on fundamental physics was most useful to me,
Sebastien Dubail for his unending enthusiasm to help and learn,
and the other colleagues of the group who all contributed on scientific or personal level.
I thank them all for their precious contributions.

My sincere feelings of gratitude to the followings people, without whose valuable contribution this work would have been incomplete:
Jurgen Baumann for the X-ray diffraction measurements at Konstanz,
Markus Schubert for the Raman scattering measurements at Stuttgart
Elizabeth Müller for the TEM photographs at Zurich ,
Laurant von Allmen for sparing his Macintosh without which this thesis would not have taken the present shape,
Dr. Gerhard Willeke whose interest in my work has been a source of encouragement to me,
Dr. Etienne Bustarret for his instructive suggestions.

My one year visit to the photovoltaic R&D group of Siemens AG. has been very beneficial on the level of technology. I thank Dr. R. Plættner for offering me this opportunity and Mr. H. Kausche for his encouraging collaboration. Thanks are also due to all those who contributed in making our stay in Germany so memorable that it has been one of the best in these past years.

I will always remember the efforts of Vijayalakshmi, Chamanlal Gupta, Marco Olgiati, and Professor Shah who originally helped me to obtain this opportunity, through the Swiss Federal government, to persue studies in Switzerland. The conscious or spontaneous warmth,

friendship, collaboration and help of my friends and colleagues have contributed immensely during my stay here all these years. The accommodation and hospitality of Mr. & Mrs. Gem has been of unforgettable value. To them all I offer my gratitude.

Finally, my fondest appreciation to my wife Nayana for her patience and understanding and and to my daughter Karunamayi who brought a new dimension to my life. My respectful gratitude to my mother who offered me the liberty to persue my interests so far away from home.

If there is some one who feels I have left him out, it is surely not intentional. Kindly contact me and we can settle that over a dinner!